NASA / CR-2000-209342

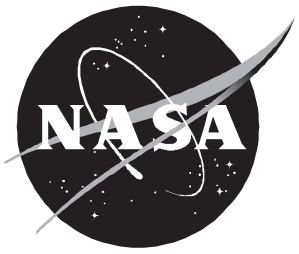

Validated Feasibility Study of Integrally Stiffened Metallic Fuselage Panels for Reducing Manufacturing Costs

R. G. Pettit, J. J. Wang, and C. Toh
The Boeing Company, Long Beach, California

May 2000

The NASA STI Program Office . . . in Profile

Since its founding, NASA has been dedicated to the advancement of aeronautics and space science. The NASA Scientific and Technical Information (STI) Program Office plays a key part in helping NASA maintain this important role.

The NASA STI Program Office is operated by Langley Research Center, the lead center for NASA's scientific and technical information. The NASA STI Program Office provides access to the NASA STI Database, the largest collection of aeronautical and space science STI in the world. The Program Office is also NASA's institutional mechanism for disseminating the results of its research and development activities. These results are published by NASA in the NASA STI Report Series, which includes the following report types:

- TECHNICAL PUBLICATION. Reports of completed research or a major significant phase of research that present the results of NASA programs and include extensive data or theoretical analysis. Includes compilations of significant scientific and technical data and information deemed to be of continuing reference value. NASA counterpart of peer-reviewed formal professional papers, but having less stringent limitations on manuscript length and extent of graphic presentations.

- TECHNICAL MEMORANDUM. Scientific and technical findings that are preliminary or of specialized interest, e.g., quick release reports, working papers, and bibliographies that contain minimal annotation. Does not contain extensive analysis.

- CONTRACTOR REPORT. Scientific and technical findings by NASA-sponsored contractors and grantees.

- CONFERENCE PUBLICATION. Collected papers from scientific and technical conferences, symposia, seminars, or other meetings sponsored or co-sponsored by NASA.

- SPECIAL PUBLICATION. Scientific, technical, or historical information from NASA programs, projects, and missions, often concerned with subjects having substantial public interest.

- TECHNICAL TRANSLATION. English-language translations of foreign scientific and technical material pertinent to NASA's mission.

Specialized services that complement the STI Program Office's diverse offerings include creating custom thesauri, building customized databases, organizing and publishing research results . . . even providing videos.

For more information about the NASA STI Program Office, see the following:

- Access the NASA STI Program Home Page at *http://www.sti.nasa.gov*

- Email your question via the Internet to help@sti.nasa.gov

- Fax your question to the NASA STI Help Desk at (301) 621-0134

- Telephone the NASA STI Help Desk at (301) 621-0390

- Write to:
  NASA STI Help Desk
  NASA Center for AeroSpace Information
  7121 Standard Drive
  Hanover, MD 21076-1320

NASA / CR-2000-209342

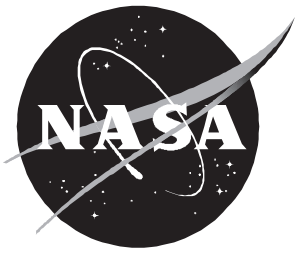

Validated Feasibility Study of Integrally Stiffened Metallic Fuselage Panels for Reducing Manufacturing Costs

R. G. Pettit, J. J. Wang, and C. Toh
The Boeing Company, Long Beach, California

National Aeronautics and
Space Administration

Langley Research Center
Hampton, Virginia 23681-2199

Prepared for Langley Research Center
under Contract NAS1-20014, Task 34

May 2000

Available from:

NASA Center for AeroSpace Information (CASI)
7121 Standard Drive
Hanover, MD 21076-1320
(301) 621-0390

National Technical Information Service (NTIS)
5285 Port Royal Road
Springfield, VA 22161-2171
(703) 605-6000

FOREWORD

This report documents work performed by the Boeing Company as part of contract NAS1-20014, Task 34, Integral Airframe Structure. Cognizant NASA/Industry representatives for this work are Joan Funk, Level III, NASA Langley Research Center, and Trent Logan, Deputy Director, Prototype Center, Advanced Transport Aircraft Development (Long Beach, CA), Boeing Phantom Works.

This page intentionally left blank.

ABSTRACT

The continual need for low acquisition cost and the emergence of high speed machining and other technologies has brought about a renewed interest in large-scale integral structures for aircraft applications. Nevertheless, applications of low cost, large-scale integral structures in damage tolerance critical areas such as the fuselage have been inhibited by a perceived lack of damage tolerance, and by cost and manufacturing risks associated with the size and complexity of the parts.

In the Integral Airframe Structures (IAS) Program, a feasible integrally stiffened fuselage concept was developed and analyses and tests were run to validate equal or better performance than conventional designs with regard to weight and structural integrity, while achieving a significant reduction in manufacturing cost. While several concepts, including isogrid and integral skin/stiffener/frame concepts were considered initially, an integral skin/stiffener concept was selected for the test study because of manufacturing risks associated with forming isogrid and integral frame configurations to complex contours. Both plate hog-out and near-net extruded concepts were evaluated, though dimensional irregularities in the extrusion precluded fabrication of large test panels from this material.

A substantial test matrix including coupons, joints, structural details, repair, static compression and shear panels, and two-bay crack residual strength panels was developed. Several of the specimens were sent to NASA Langley Research Center (LaRC) for testing. Alloys evaluated in the test matrix include 7050-T7451 plate, 7050-T74511 extrusion, 6013-T6511x extrusion, and 7475-T7351 plate. Crack turning was identified as an important phenomenon to improve the residual strength and damage tolerance of integral structure (by deflecting the crack away from integral stiffeners), and coupons and test panels were included to characterize and verify crack turning behavior. Improved methods for predicting crack turning behavior were also developed in cooperation with NASA and Cornell University.

Various cost modeling codes were evaluated, and COSTRAN (a commercial derivative of the NASA PCAD code) was chosen for cost analyses under this program. A hybrid design, made from high-speed machined extruded frames that are mechanically fastened to high-speed machined plate skin/stringer panels, was identified as the most cost-effective manufacturing solution. Recurring labor and material costs of the hybrid design are up to 61 percent less than the current technology baseline. However, there are important outstanding issues that are discussed with regard to the cost of capacity of high technology machinery, and the ability to cost-effectively provide surface finish acceptable to the commercial aircraft industry. The projected high raw material cost of large extrusions also played an important role in the trade-off between plate and extruded concepts.

Keywords: Integral Structures, Damage Tolerance, Cost Analysis
Crack Turning, Manufacturing Technology

This page intentionally left blank.

TABLE OF CONTENTS

SECTION		TITLE PAGE
1.0	INTRODUCTION	1
2.0	MANUFACTURING TECHNOLOGY ASSESSMENT	4
2.1	Applicable Manufacturing Processes	5
2.2	Processes Selected for the Feasibility Study	7
3.0	DESIGN DEVELOPMENT	9
3.1	Design Issues and Criteria	9
3.1.1	Cost	9
3.1.2	Fail Safety/Durability & Damage Tolerance	10
3.1.3	Static Strength and Repair Considerations	13
3.1.4	Corrosion Resistance	15
3.2	Biaxially Stiffened Concepts	15
3.3	Unidirectionally Stiffened Concepts	18
3.3.1	Stiffener Configuration	19
3.3.2	Frame Configuration	21
3.3.3	Integral Tear Straps	22
3.3.4	Material Selection and Sizing of Concepts for Structural Testing	23
3.3.5	Joint Design	33
4.0	COST EVALUATION	40
5.0	STRUCTURAL VALIDATION	40
5.1	Overview of Test Program	40
5.2	Materials Used	43
5.2.1	7050-T7451 Plate	43
5.2.2	Large Extrusions	43
5.2.3	7475-T7351 Plate (Seattle Lot Buy)	44
5.3	Crack Turning Characterization	45
5.3 1	Background	45
5.3.2	Crack Turning Theory	46
5.3.3	Crack Turning Test Program	59
5.4	Structural Detail Testing	80
5.4.1	Thickness Interface Specimens	80
5.4.2	Basic Stiffener Fatigue Specimens	84
5.4.3	Mechanical Joint Specimens	85
5.4.4	Friction Stir Weld Specimens	85
5.5	Panel Test Specimens	88
5.5.1	Static Compression and Shear Panels	88
5.5.2	Repair Panel	89
5.5.3	Circumferential 2-Bay Crack Panels	91

5.5.4 Longitudinal Crack Panel 95

6.0 CONCLUSIONS AND RECOMMENDED FUTURE WORK 96
6.1 Manufacturing Development 96
6.2 Structural Mechanics 97

7.0 REFERENCES 98

A.0 APPENDIX
A.1 Description of Analysis Methods for EXCEL Panel Optimizer 102
A.2 Lot Release Data for 7050-T7451 Plate 104
A.3 R-Curve Data Reduction Using DCB Specimen Results 108
A.4 Mechanical Joint Specimen Drawings 109

1.0 INTRODUCTION

The U.S. aerospace industry is critical to the economic stability and growth of the nation as the largest manufacturing export and the greatest single positive contributor to the balance of trade. Significant foreign national industry investments to produce high technology aerospace products and services for the global market continues to impact U.S. sales and exports. At the same time, the retiring of the aging global fleet of transports, combined with an overall increase in passenger demand will require delivery of some 13-17 thousand aircraft in the next twenty years valued at over $1.2 trillion dollars [1,2]--a tremendous opportunity to increase the U.S. export market.

As shown in Figure 1, about a third of the airlines' direct operating cost (DOC) of an airplane is associated with the manufacturing cost, which is probably the most critical competitive parameter with regard to market share.

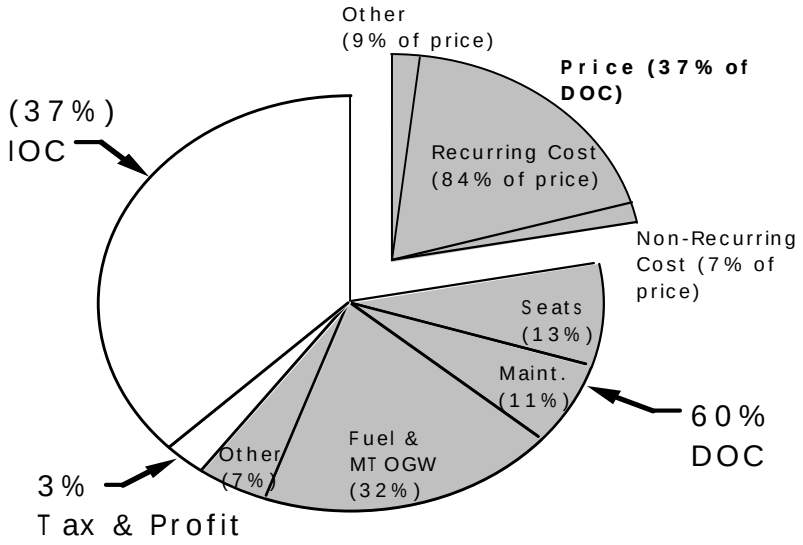

Figure 1. Representative Breakdown of the Operational Cost of Commercial Transports [1]

In the past, the airframe design process in the U.S. has been focused on riveted aluminum-skin and stringer construction, a structural concept dating from the 1940's. This process, with associated construction details and fabrication processes, has become highly refined and mature, and therefore difficult to reduce in cost dramatically without significant deviations from conventional design practice. Nevertheless, metallic structure is well proven, and the industry already has, and will likely retain extensive metallic production capability and skills for the foreseeable future.

[1] Cost breakdown shown is given as typical scenario. While it is believed to be representative of commercial transports in general, actual values will vary with model, airline, and market conditions.

The continual need for low acquisition cost and the emergence of high speed machining and other technologies has brought about a renewed interest in large integral metallic structures for aircraft applications. Integrating skin, stiffeners and doublers into larger pieces of structure offers inherent savings and flexibility, which is made increasingly more attractive as the labor required to machine the parts is reduced by faster machines. Nevertheless, application of low-cost integral structures in damage tolerance critical members such as the fuselage has been inhibited by a perceived lack of damage tolerance, and by cost and manufacturing risks associated with the size and complexity of the parts.

The purpose of the Integral Airframe Structures (IAS) Program was to study these risks by developing a feasible design concept with equal or better weight and strength compared to conventional structure, which could be produced at significantly lower cost, and which would exhibit acceptable damage tolerance and fail-safe behavior. To the degree possible, the structural and cost savings aspects of the design were to be validated by test or manufacturing demonstration.

As will be described in more detail in Sections 3.1.2 and 5.3, an important technical aspect of the program with regard to the damage tolerance and fail-safety of integral structure in general is the ability to turn or deflect cracks away from integral stiffeners as shown in Figure 2 (or the equivalent two-bay longitudinal crack). This improves the residual strength of the structure with large damage such as a two-bay crack, and can potentially improve the inspectability of the crack by making it more visually evident, and prolonging the period during which the two-bay crack fail-safe condition is satisfied. With or without consideration of crack turning, the resolution of the damage tolerance and fail safety issues for integral structure was viewed as the single most important technical aspect of the program.

An overview of the program is set forth in Figure 3. The overall project was carried out by a NASA/industry team including Boeing components in Long Beach (formerly McDonnell Douglas) and Seattle, Northrop-Grumman, Lockheed-Martin, and Alcoa.

The present document will be laid out more or less in the same order as the tasks depicted in Figure 3 with a few exceptions. The cost evaluation report is documented under separate cover [3], and includes inputs from both Boeing Seattle and Boeing Long Beach components as a unified document, since our efforts were combined at the end of the program. The theoretical work with regard to crack turning will be documented in the structural validation section

along with test data from the crack turning specimens. Also, since no direct follow-on program appeared forthcoming, the Phase II plan took the form of a more general discussion of what remains to be done with integral fuselage technology.

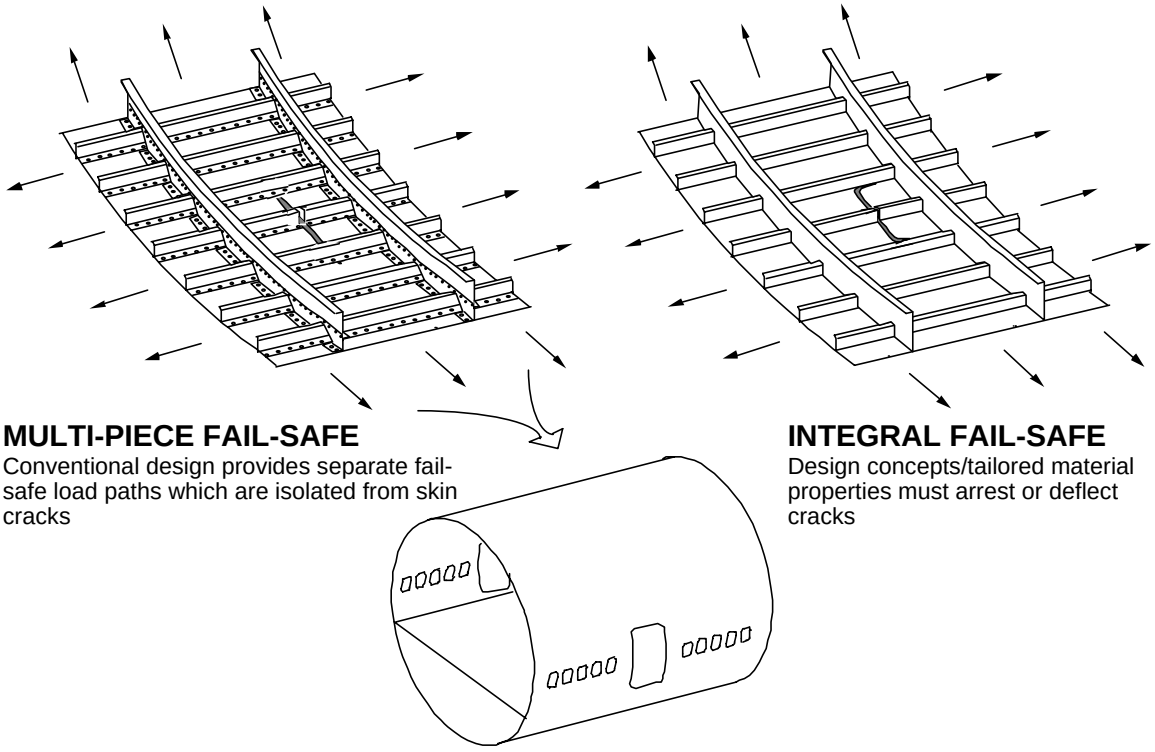

Figure 2. Fail-Safety Scenarios for Conventional and Integral Structure

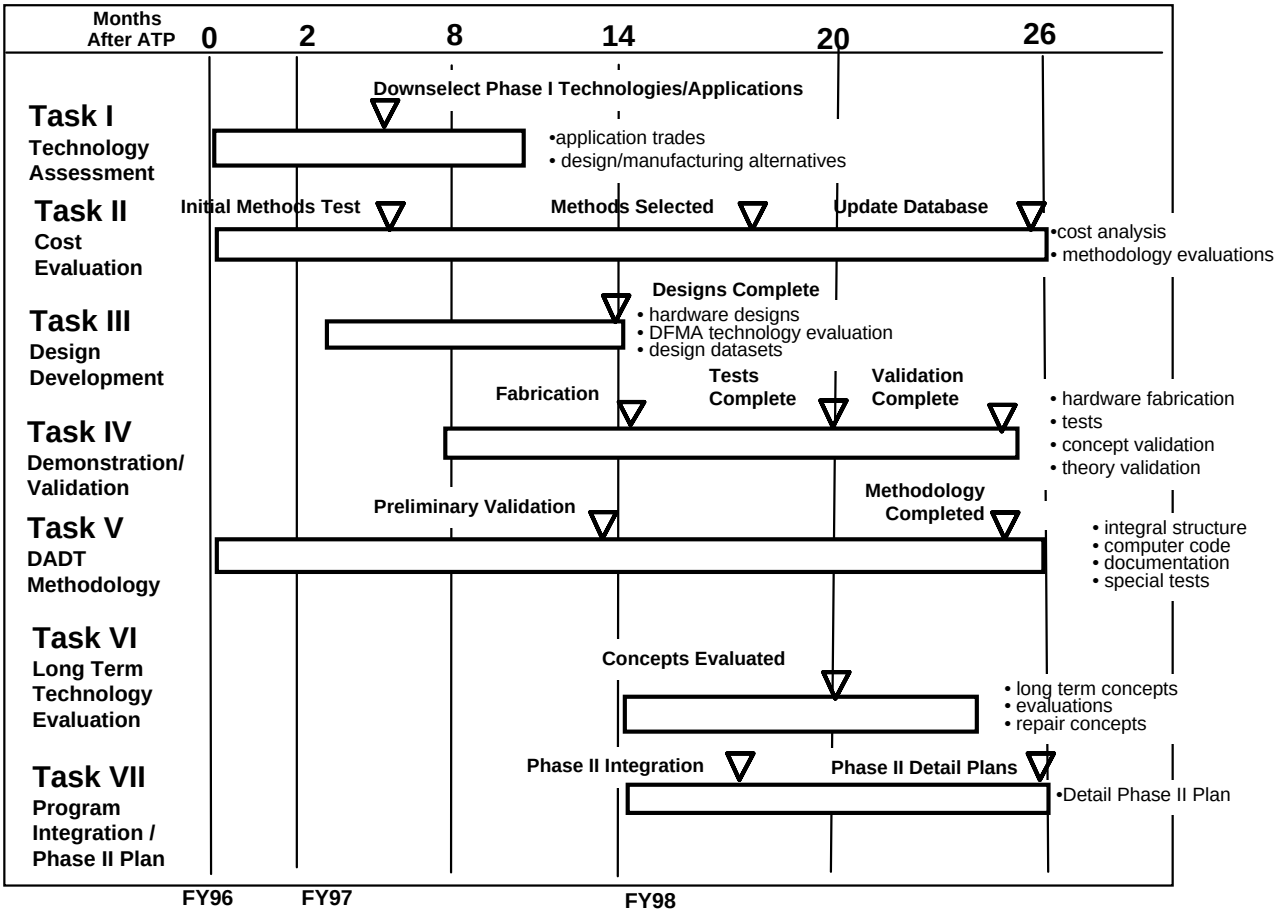

Figure 3. Integral Airframe Structures (IAS) Program Summary

2.0 MANUFACTURING TECHNOLOGY ASSESSMENT

Early in the program, an assessment of existing and emerging manufacturing technology was performed to gain insight into how integral structure might most efficiently be made in the future, what technology development might be needed, and what particular level of technology might be attainable during the course of this program for specimen fabrication.

IAS team members met April 15-16, 1997 to discuss available and emerging manufacturing technologies, and select those technologies that would be evaluated under the present feasibility study. For completeness, this section describes the outcome, and briefly highlights issues discussed and decisions made. A more in-depth discussion will be provided under the Boeing Seattle Contract NAS1-20268.

2.1 Applicable Manufacturing Processes

A matrix of possible manufacturing processes/scenarios is shown in Table 1. The table illustrates how applicable processes are to some degree driven by the design configuration and raw material product form. Not shown here is the fact that some processes, such as age/creep forming and laser welding, are only applicable to certain alloys or tempers. Note that some processes such as painting and sealing are not included in the matrix since they are virtually the same for all configurations, and equivalent to current practice for built up structure (though some savings are obtained via part consolidation). Also, some of the more exotic product forms, such as shear formed or roll-forged tubes, and very large forgings, were discussed to some extent, but are not included in the table either due to lack of maturity, or due to lack of applicability to program objectives.

Most of the processes listed are familiar, with the possible exceptions of shrink forming and friction stir welding. Shrink forming is a method of forming stiffened panels developed in Germany in which jaws grasp the stiffeners at intermediate points and bend the panel to shape. This method is little known in the U.S., and domestic production facilities are not available. Friction stir welding is a fairly new solid state metallurgical joining technique in which a rotating tool develops sufficient frictional heat as it is moved through the joint interface to soften (without melting) and “stir” the two interfaces together. It can produce a superior joint than conventional welding techniques, and is applicable to a much wider range of materials, including otherwise unweldable aluminum alloys.

Table 1. Assessment of Manufacturing Alternatives for Integral Metallic Fuselage Structure

	Product Form			Preforming Operation		Machining Stage		Forming Stage				Joining Stage				
Configuration Class	Casting	Plate	Large Extrusion	Extrusion Flattening	Plate Forming (Prior to machining)	High Speed Machine	Chem Mill	Break/ Roll Form	Creep/Age Form	Shot Peen Form	Shrink Form	Friction Stir Welding	Laser Weld	Mech. Joining	Process No.	Comments
								(Singly curved)	(Doubly curved)							
Longitudinally Stiffened (Separate frames)	x											x		x	1	Properties low for castings,
													x	x	2	weight parity unlikely.
		x				x		x				x		x	3	Longitudinally stiffened hog-out is
													x	x	4	most producible with current tech.
									x			x		x	5	High speed machining can far reduc
													x	x	6	cost. Would require strong, tough
										x		x		x	7	material for weight parity with
													x	x	8	baseline.
					x	x						x		x	9	Requires 5-axis mill. Thickness
													x	x	10	tolerances likely looser.
			x	x		x		x				x		x	11	With near net, high precision
													x	x	12	extrusions, could be extremely cost
									x			x		x	13	effective. Extrusion flattening needs
													x	x	14	development. Poor as-flattened
										x		x		x	15	dimensions could impair
													x	x	16	machinability.
							x	x				x		x	17	Similar to 11-16, but chem-
													x	x	18	milling is more robust with regard
									x			x		x	19	to skin waviness. However, masking
													x	x	20	of stiffeners is a severe problem
										x		x		x	21	which could result in high scrap
													x	x	22	rate.
Ortho/Isogrid (Integral Frames)	x											x		x	23	Propeties low for castings, weight
													x	x	24	parity unlikely.
		x				x		x				x		x	25	Forming to contour difficult for
													x	x	26	isogrid with thin gage stiffeners
									x			x		x	27	typical of fuselage structures
													x	x	28	(unlike launch vehicle structure).
										x		x		x	29	Stiffeners tend to roll during
													x	x	30	forming.
											x	x		x	31	Requires special capital equipment,
													x	x	32	experience.
					x	x						x		x	33	Requires 5-axis mill. Thickness
													x	x	34	tolerances likely looser.

2.2 Processes Selected for the Feasibility Study

The planned structural design and validation segments of the feasibility study were intended to address key aspects of structural integrity and damage tolerance of integral fuselage concepts, requiring test specimens which would have to be made during the course of the program. It was foreseen that some of the advanced manufacturing technologies desirable for consideration might not be available within the program time frame, either due to further required development, or due to the level of demand on high performance machinery. However, if a given panel configuration designed for an efficient manufacturing technology could be fabricated by alternative, but structurally equivalent processes, then test specimens could be made in that way, and cost studies could anticipate savings due to superior processing methods.

Early in the program, both longitudinally stiffened and biaxially stiffened concepts were considered. Biaxially stiffened concepts such as isogrid, however, are more difficult to manufacture, largely due to the difficulty of forming these structures to shape--even simple contours. Previous experience in the launch vehicle segment of the industry utilized break forming to create large isogrid-stiffened rocket casings. However, isogrid design concepts applicable to fuselage were anticipated to have lighter-gage stiffeners, which were shown to roll and buckle during break forming in a manufacturing demonstration by Boeing [21]. Buckling distortion of the stiffeners was considered a significant risk for age/creep forming of biaxially stiffened structures as well, and peen forming was considered risky for the combination of thin gage skin and circumferential stiffeners. A second isogrid panel showed that such a panel could be manufactured by forming the plate first, then machining with a 5-axis machine, but this approach was not favored because of the additional cost. Castings, though potentially applicable to biaxially stiffened structure, were not favored largely because existing casting alloys exhibit low strength, making weight parity difficult to achieve.

With these manufacturing risks, and without a sufficiently compelling argument in favor of isogrid or orthogrid from a design standpoint (see discussion in Section 3.1), it was decided to focus on unidirectionally stiffened concepts for the present study. Both plate and extrusion product forms were viewed as potentially cost-effective, the plate being less expensive per pound, and the extrusion nearer net. Forgings were not seriously considered within the scope of this program because size limitations could not support test panel fabrication, and would be even a more severe constraint for production size panels.

For the extruded configuration, the ideal was to extrude net stiffeners and pocket the skins. Chemical milling of the pockets was not favored because of known problems with accidental maskant damage on raised edges, such as the

stiffener edges, which would result in acid leaks and thus an unacceptable scrap rate. Thus high speed machining was left as the most likely feasible material removal process (problems with this approach will be discussed in Section 3). Another problem with large extrusions was that due to current press size limitations, increased panel width required extrusion of a curved panel configuration, followed by a flattening operation that was still not very mature. Also, the stretch straightening of wide extrusions could result in variations in the stiffener spacing due to Poisson contraction, potentially causing stiffener mismatch at circumferential joints. Despite these challenges, it was nevertheless felt that the large extrusion concept was promising enough to merit further study under the program. However, due to the poor dimensional quality of prototype large extrusions made later in the program, large panel specimens of acceptable quality could not be made (see Section 5.2.2)

The baseline process of stretch forming was not considered applicable to integral structures because the stiffeners are on the inner mold line, and would thus interfere with the tool. Also, there are other problems with respect to how to grip specimens, the unevenness of stretch, distortion due to Poisson contraction, etc. The remaining forming processes were segregated by their applicability to single and double curvatures. Bump forming to single curvatures had been previously demonstrated, and could support the fabrication of test panels. Double curvatures involved more risk, but team members familiar with the age-creep and shot peen forming processes felt that both might be potentially applicable. Of all the processes, it was believed that age-creep forming would likely result in the most accurate and repeatable final curvature, possibly enabling further cost reductions by use of precision assembly techniques. However, only alloys requiring artificial aging are compatible with age-creep forming, thus use of these alloys was considered favorable where practical.

With regard to joining processes, the favored option was to use a combination of friction stir welding for joining two or three smaller panels together, which would then be mechanically joined using more conventional techniques. This is particularly applicable to extrusions, which even when extruded curved and subsequently flattened are still narrow compared to available sheet and plate widths. Laser welding was considered a backup technology, but also had the advantage of a higher weld velocity, though limited with regard to material type and weld quality in aluminum alloys.

Based on the above discussion, the Table 1 process sequences 3 and 11 were chosen for test specimen fabrication (though conventional machining could be substituted for high speed machining as required), preferably using materials which would support age-creep forming (sequences 5 and 13) and to a lesser extent laser welding. Thus, the test data could potentially apply to any of the process sequences 3-22.

3.0 DESIGN DEVELOPMENT

The purpose of this segment of the program was to develop a feasible integral fuselage design concept with equal or better weight and strength compared to conventional structure, which could be produced at significantly lower cost, which would exhibit acceptable damage tolerance and fail-safe behavior, and which could be easily maintained and repaired. This section describes the issues facing integral fuselage structure, and design criteria to satisfy them, document design studies performed under this program, and the motivation behind various structural features finally selected for further study and validation by test.

3.1 Design Issues and Criteria

The following design criteria/goals for integral fuselage structure evolved during the course of the program.

1. Significantly lower cost than conventional structure (goal: 30% reduction). This demands attention to design for manufacturing and assembly practice.
2. Acceptable damage tolerance/fail-safe behavior
   a. Equal or better crack initiation life than conventional structure
   b. Meets two-bay crack residual strength criterion for longitudinal and transverse cracks with or without crack turning.
   c. Structure designed for crack turning and arrest to occur as cracks approach stiffeners in pressurized flight (to improve inspectability and arrest behavior of large damage) except in areas potentially subject to Multi-Site Damage (MSD) or other phenomena which could disrupt crack turning.
   d. Areas of potential MSD (i.e. joints) should be sized generously to postpone MSD development (preferably beyond the initiation lives of less critical MSD features) and to ensure fail-safe load capability for a straight growing crack (per 2b).
3. Equal or better with respect to conventional structure with regard to
   a. Weight
   b. Static Strength
   c. Repairability
   d. Corrosion resistance

3.1.1 Cost

Even before the inception of this program, there was a common belief among airframers that integral fuselage structures could likely be manufactured less expensively than conventional structure. The reader is referred to the cost study [3] released concurrently with this document, which is also summarized briefly

in Section 4.0. For the integrally stiffened skin, plate hog-out using high speed machining technology appears likely to be the most cost effective fabrication practice in the near term. Cost models predict that if large extrusion prices are reduced closer to the cost of sheet and plate materials, then extrusion might become the least expensive option. However, significant metallurgical and producibility problems are associated with the utilization of large near-net extrusions, and are not reflected in these cost studies.

Much of the cost is in the details. Effort was made to avoid part flips and tool changes where possible for machined parts, to keep assembly interfaces to a minimum, but to avoid troublesome interface combinations which demand unnecessarily tight tolerances or are prone to assembly mismatch. Reference to these and similar principles will be made as the description of the design development continues.

3.1.2 Fail Safety/Durability & Damage Tolerance

Properly designed integral structures with attention to fillet radii and other potentially life-limiting features, can potentially achieve very long fatigue lives. Nevertheless, damage tolerance has long been a concern for integral structures [4], which have been particularly shunned in critical areas like the fuselage. This concern was largely based on NASA fatigue crack growth tests [5,6] which showed that a skin crack slows more when crossing a mechanically fastened stiffener than an integral stiffener. Multi-bay panels were seen to crack through considerably faster in integral construction, compared to multi-piece designs.

However, if one assumes an externally inspectable damage which includes a combination of a broken stiffener and a skin crack (Figure 4), then the fatigue crack interval from this inspectable size to a two-bay crack would be identical for either case (if one assumes no difference in material properties--the likelihood is that there will be a difference in material properties, which will be discussed later). Because residual strength typically drops below limit load for cracks beyond two bays length, the benefit of slowed growth in this regime is seldom if ever considered in design or analysis because the aircraft is already unsafe (yet this is the regime where most of the benefit occurred in the NASA tests). Once a crack reaches this length, it is generally considered “walk-around inspectable” before the next fight. Clearly, integral structure must satisfy fail-safe loads (generally limit load) with a two-bay crack (either longitudinal or circumferential), just like their built-up counterparts.

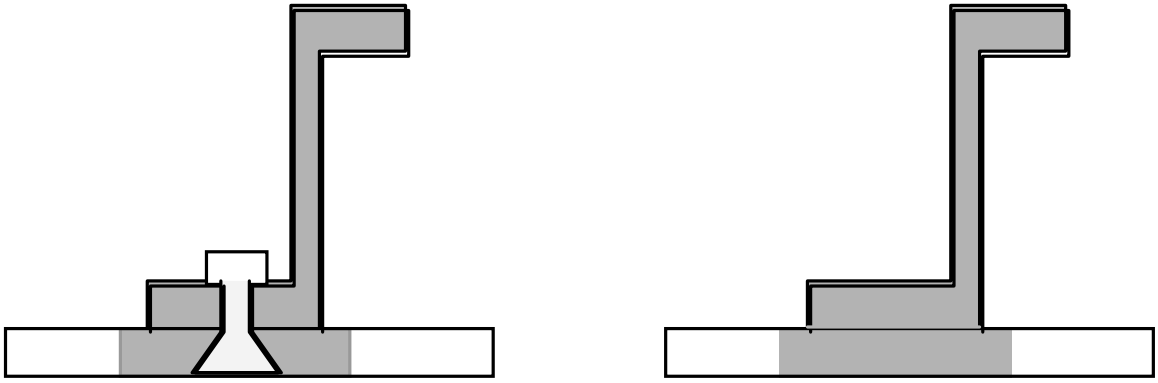

Figure 4. Equivalent Inspectable Damage Scenario for Conventional and Integral Fuselage Construction (Cracked Region is Shaded)

Crack turning has long been known to occur in pressurized aircraft fuselages, typically resulting in crack arrest and containment [4,7,8,9,10]. In general, this behavior occurs for longitudinal fuselage cracks in narrow-body thin-skinned fuselages (less than 0.040 thick per reference [9]), and the crack turns and flaps, relieving the pressure, as shown in Figure 5. Because this behavior typically results in crack arrest and damage containment,

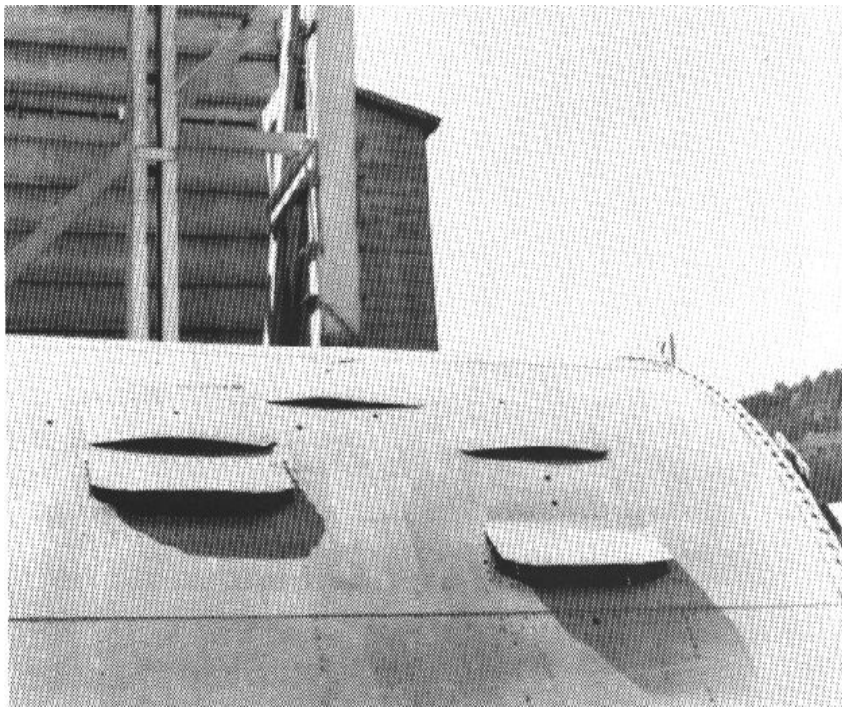

Figure 5. Crack Turning and Flapping in Boeing 707 Test Panel [9]

it was viewed favorably as an arrest phenomenon for many years, and is a typical design criterion for regions excluding the joint areas. Nevertheless, the phenomenon of crack turning has not been well understood, and therefore has been viewed as difficult to rely on. In particular, the absence of crack turning on Aloha Flight 243, in which the airplane lost a large section of its upper fuselage [11,12], underscored the fact that the likelihood of crack turning can be significantly reduced by the presence of Multiple Site Damage (MSD). The mechanism behind crack turning would have to be sufficiently well understood and demonstrated in test, and the design could not utilize crack turning for scenarios where MSD or other considerations might prevent crack turning. It was also agreed among the IAS team that two-bay crack fail safety must be satisfied whether or not the crack turns. Thus crack turning would not be relied upon for fail safety, but would provide improved arrest characteristics and inspectability for large damage.

There is evidence suggesting that crack turning might occur more readily in integral structures than in conventional structures. Boeing tests indicated that turning phenomena did not occur on widebody fuselages [9]. However, hardware tested on the Primary Adhesively Bonded Structure (PABST) program [4], showed excellent crack turning and flapping for a thick-skinned, wide-body adhesive-bonded fuselage (YC-15 geometry, 108 inch diameter). Because the stiffness of adhesive-bonded and integral construction is comparable (and much stiffer than mechanically fastened), this infers that the same behavior might well have occurred had the test hardware been of integral construction. Improvements in the ability to model crack turning behavior have also begun to shed light on the mechanism behind the phenomenon [13,14,15]. Analyses and tests of integral panels with two bay circumferential cracks [16] have also shown that crack turning in the self-similar case is due to a crack tip stress field which occurs in a narrow region (on the order of a half of an inch wide) immediately adjacent to the edge of an arresting stiffener or increasing step in thickness. It has been suggested that the concentrated nature of the turning forces in that region could not likely be achieved by attached stiffeners with the typical one-inch fastener spacing. (Note that in asymmetric cases crack turning is easier to achieve due to mode II stress intensity which is not limited to this small region, but that turning forces near the arresting stiffener still play an important part). The analyses also indicated that the turning phenomenon was driven by geometrically nonlinear behavior (pressure pillowing) which would not occur if the panels were unpressurized. The geometrically nonlinear nature of the problem also implied that increased material fracture toughness, lower modulus, reduced skin thickness, wider stiffener spacing, or higher pressures would generally enhance the likelihood of crack turning. Testing confirmed turning in the pressurized case, but also showed the need to account for the fracture orthotropy of the panels (due to the oriented nature of the grain structure).

Theory and tests to include the effects of fracture orthotropy on crack turning and to demonstrate turning and arrest of longitudinal and transverse cracks were undertaken in this program, and are presented in Section 5.3. A graduate program at Cornell University was also initiated to continue this work beyond the IAS program, and implement the improved theory into adaptive mesh fracture simulation codes FRANC2D and FRANC3D. Understanding crack turning and providing design codes will make this phenomenon more accessible for use in design.

With most any practical integral structure fabrication method, there is freedom to tailor the thickness with little cost impact. With regard to MSD, it was determined to tailor sufficient bulk into the joint regions to extend their life beyond other less critical MSD sources (such as longitudinal cracks developing the end fasteners on the shear clip feet) and reduce the stress intensity of any (rogue, or non-MSD) cracks which should occur in the joint region to allow slow, readily inspectable crack growth without turning. Joint members splicing stiffeners crossing the joint may also provide separate-piece arrest capability as required for two-bay crack fail-safety. It should be noted that the baseline structure of conventional aircraft at present may well not be capable of sustaining a two-bay crack along a joint fastener row with MSD [17].

3.1.3 Static Strength and Repair Considerations

For many years, built-up aircraft structure has employed a medium strength, but highly tear resistant skin material (2024-T3), stiffened by high strength stiffeners, typically 7075-T6 or T6511, and more recently with 7050, 7150, or even 7055 alloys with high strength, corrosion resistant tempers. This choice of a tough skin with a high strength stiffener is motivated by fail safety and damage tolerance, and has reached a high degree of structural efficiency. Integral structure presents a unique challenge in that the skin and stiffeners are made of

one piece, and are therefore of the same alloy and temper[2]. Material selection under these circumstances must carefully balance the need for both strength and toughness in the same material. In order to achieve strength and weight parity with conventional structure (if the structure is static critical), the static strength of the selected material must in general be higher than the low strength skin material, and higher in toughness than the incumbent high strength stiffener material. The results of a trade study of various materials will be discussed in Section 3.3.4.

One structural advantage which is characteristic of integral structure in compression (which is critical over much of the fuselage) is that if the stiffener foot pad is twice the skin thickness or more, the effective width of postbuckled skin acting in compression is increased as shown in Figure 6. Since this section acts at the yield strength of the material, it contributes significantly to the efficiency of the structure. The stiffener foot then also serves as an integral tear

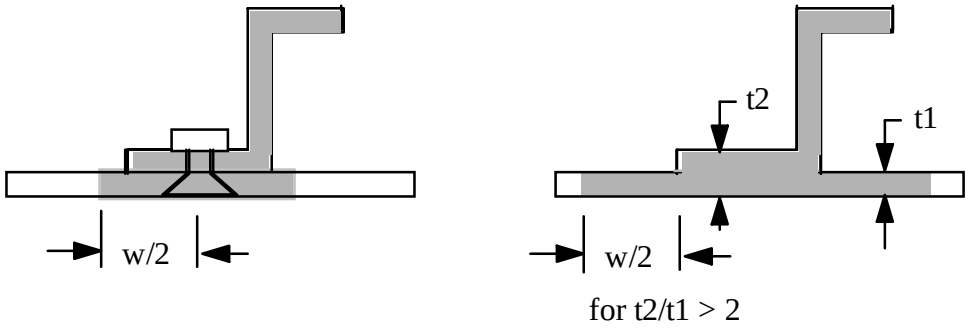

Figure 6. Effective Area (Shaded) for Compressive Strength Calculations for Multi-piece and Integrally Stiffened Structure

strap to help arrest or turn cracks, and provides a reinforced region useful for repair using mechanical fasteners. Ideally for repair of integral structure, a pattern of closed cells bounded by such reinforced regions could be utilized, enhancing repair life for patches sized to an integral number of bays. The width should then be sized (as a minimum) to accommodate a single row of fasteners. Figure 7 illustrates an internal repair scenario used to define a minimum width for the stiffener foot. An external repair is actually a more likely option for the asymmetric (Z) stiffener foot configuration shown, but requires less width. While perhaps a bit on the generous side, the 1.1 inch minimum width derived here was adopted for the upper fuselage.

[2] Actually, it is possible to friction stir weld high strength stiffeners to high toughness skin (or perhaps achieve a similar result by other means). However, the advantage of such an approach was not obvious from a cost standpoint because it still would require individual fabrication of the skin and each stiffener, followed by a joining operation. In this case, there is also the issue of the crack-tip-like faying surface crevice on either side of the friction stir weld at the skin/stiffener interface.

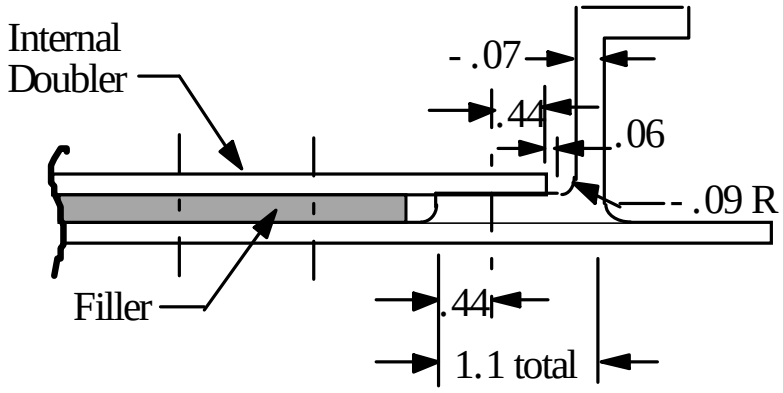

Figure 7. Minimum Sizing of Stiffener Foot for Internal Repair Scenario

3.1.4 Corrosion Resistance

Because integral structure comes presumably from other than sheet aluminum, it is not likely to be clad, thus an alloy of improved general corrosion resistance over conventional 2024-T3 would be favored. From a cosmetic standpoint, the prospect of an uncoated, specular, integrally stiffened (and therefore unclad) airplane does not appear to be likely. Like composite parts, integrally stiffened parts would probably have to be painted for good corrosion resistance.

With regard to stress-corrosion, plate hogout concepts, if implemented, will almost certainly have fasteners--possibly interference fasteners--installed at some point in the short transverse grain orientation, such as through the web of an integral stiffener. If this is not required by the manufacturer for mechanical joining, then it will likely occur during a repair. Alloy selection should consider whether the stress corrosion threshold of the material can tolerate the possibility of fastener induced short transverse stresses.

3.2 Biaxially Stiffened Concepts

The discussion now turns to the performance attributes of various design concepts, and individual design features within each concept. As described in

the Manufacturing Technology Assessment section above, orthogrid and integral frame concepts were eliminated early in the program, largely because of manufacturing challenges beyond the scope of this program associated with forming such biaxially stiffened concepts into curved panels. Nevertheless, this report would be incomplete without a brief discussion of biaxially stiffened concepts, which were considered in the early stages of the program. The remainder of the discussion will then focus on the unidirectionally integrally stiffened skin concept with attached frames, which was selected for further study and testing.

From a developmental standpoint, perhaps the coarsest starting point for an integral design concept would be to hog out skins, stiffeners and frames complete to a geometry otherwise identical to conventional structure. A major drawback of this approach is the tremendous inefficiency associated with machining plate 5-6 inches thick down to comparatively light gage fuselage structure. As a next step, one might leave only an integral blade running circumferentially, to which the upper frame could later attach. The longerons could be simplified at least to zee's and possibly to blades (simpler to machine, but with somewhat less structural efficiency). A blade stiffened orthogrid concept with attached frames was used on the Concorde upper fuselage at very low operational stresses.

Realizing that the best configurations for integral fuselage structure might well differ in geometry from the familiar skin/stringer/frame arrangement of conventional airframes, alternative concepts were also considered. In particular, since the sidewalls of the fuselage are loaded principally in hoop and shear, it appeared that orienting the stiffeners at an angle, rather than longitudinally, might be advantageous using an isogrid arrangement. In Figure 8, the stiffeners on the crown and lower fuselage are shown as longitudinal, corresponding with the principal loading, and various sidewall isogrid geometries are shown.

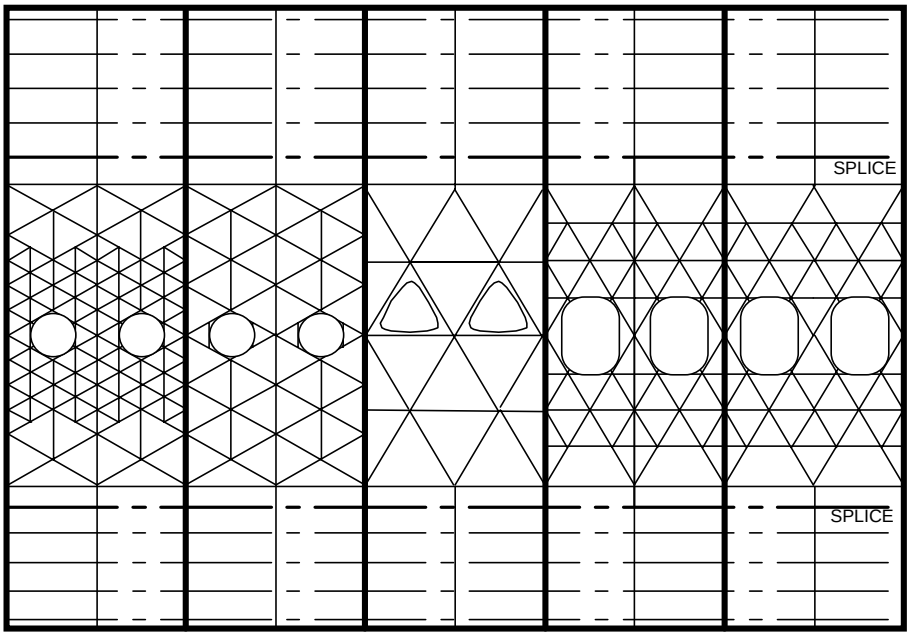

Figure 8. Isogrid Window Belt Design Concepts

These sketches represent very preliminary concepts, but merit some discussion. Note that the window configuration has a heavy interaction with the isogrid configuration, as well as the inherent assumption that the isogrid must transition to a frame spacing of approximately 20 inches on center at the upper and lower fuselage. Since the space between the windows must bear full hoop load, in most cases the frame was carried through the window belt. In concept d, this was done probably to some disadvantage, since it adds an additional member to the isogrid, and results in sharp angles between integral stiffeners, which adds significant amounts of dead weight in the fillets between the members. Of these, concept (e) seemed perhaps the most sensible, but no analysis was run.

Isogrid structures have been claimed potentially more weight efficient than conventional fuselage structures [19] (though in this reference the analysis method is not clearly described), and are used extensively in rocket skins. Considerable design literature exists with regard to isogrid launch vehicle structure that need not be reviewed here. Characteristic of launch vehicle design, the standard design practice is a buckling resistant structure (ultimate load equates typically to the onset of buckling). Fuselage structure is typically very light gage, and is therefore generally of post-buckled design. Short of nonlinear finite element analysis, there is no standard method for post-buckled design of isogrid structure to the authors' knowledge.

Isogrid structure for launch vehicles is typically bump formed to cylindrical contours. However, these structures have relatively thick, short blades

compared to what would be expected for fuselage design. As part of the Boeing Seattle IAS effort, forming trials of an isogrid panel considered more representative of fuselage structure was bump formed, and resulted in tool-marks and buckling in the web. It was clear that lightweight, biaxially stiffened panels in general would have this problem if bump formed. Team members familiar with age/creep forming admitted that very likely web buckling would occur for isogrid or orthogrid structure using this process as well. Peen forming was not believed capable of obtaining the contours required.

Remedies were conceived, such as filling the bays with plastic fillers or the like to suppress web instability during forming. Nevertheless the development required, and risk inherent in such approaches led the team to postpone work on biaxially stiffened concepts to follow-on programs, thus protecting the immediate objective of finding a feasible concept within the scope of the present program. A predominantly unidirectionally stiffened approach with attached frames was seen as a much more producible option, and it was felt that developments in manufacturing, cost prediction, and damage tolerance which would come with pursuing such a concept could later benefit biaxially stiffened concepts, should it ever become clear that they were more advantageous.

3.3 Unidirectionally Stiffened Concepts

By allowing the frame to be mechanically fastened, the forming problem associated with web buckling is eliminated for the axis of primary curvature, allowing bump forming of singly curved skins. The secondary axis of curvature for compound contours would be much less severe, believed within the capability of age creep forming and/or peen forming for most fuselage applications[3]. Also, the stiffened skin can in principle be extruded nearly net if desired, so long as the stiffeners are parallel.

An upper fuselage concept in keeping with the foregoing discussion in Section 3.1 is illustrated in Figure 9. A detailed description of geometric features follows.

[3] This statement is based on information from vendors who perform age/creep forming. Unfortunately, fabrication of a doubly curved fuselage demonstration panel was out of the scope of the current program, and thus the ability to form double contours in integral fuselage structure remains unproven.

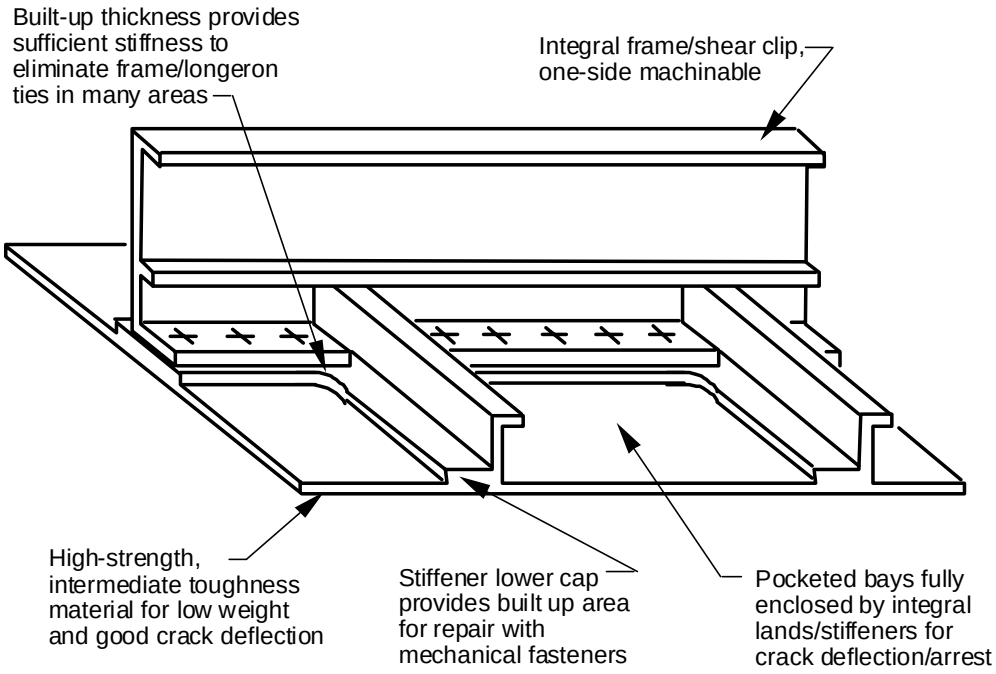

Figure 9. Integral Upper Fuselage Concept

3.3.1 Stiffener Configuration

Integral Z or J stiffeners were chosen instead of hats or blades for various reasons. First, manufacturing cost for machined details is a strong function of the part surface area, and thus Z's, channels or blades would be less expensive than hats. Blades, while less expensive to machine than Z's or channels, would be less structurally efficient because they have less moment of inertia, and as one-edge free members have less resistance to crippling under axial compression. In the highly compression critical areas, J's are more structurally efficient, and are also favored in the lower fuselage for repair. Z's have a slight advantage over channels from a repair standpoint, and possibly a slight disadvantage from a torsional stability standpoint.

Another motivation for not using hats was to eliminate the need for a stringer clip at each mousehole (see Figure 10). The frame/stringer connection, because it joins two periodic and perpendicular interfaces, is not advantageous to preinstall (or integrate) to either the stringer or the frame, but must be attached last to avoid mismatch due to assembly tolerances [20]. Attachment of the clips does not lend itself well to automation, and is thus likely to remain a manual operation. There are typically several thousand clips per fuselage, representing a significant amount of cost and weight.

The stringer clip serves three main purposes--it stabilizes both the frame and stringer from rotation, and it provides a rigid connection between the frame and

stringer members which increases the shear strength of the panel by making it more difficult for shear buckles to form through the mouseholes. Torsional frame instability is naturally suppressed throughout much of the fuselage by miscellaneous structural hardware associated with cutouts or other features (where this is not the case, the frame will have to be stabilized occasionally by stringer clips or intercostals). The Z (or channel) stringers, anchored to the skin with an integral foot, and also at each frame crossing with the integral tear strap, were believed to be adequately stabilized without the addition of stringer clips (this was later supported by compression panel test data; see Section 5.5).

The rigidity of the frame/stringer connection to ensure good postbuckled shear performance is a remaining issue, but the integral design of Figure 9, given sufficient integral tear strap thickness, has inherently better stiffness than conventional structure minus the stringer clip. As illustrated in Figure 10, the end of the frame foot serves effectively as a frame/longeron clip if the end fastener is nestled up close to the stiffener web. Clearly, the proximity of the end fastener is closer for a Z than for a hat (a blade stiffener would also be good in this respect).

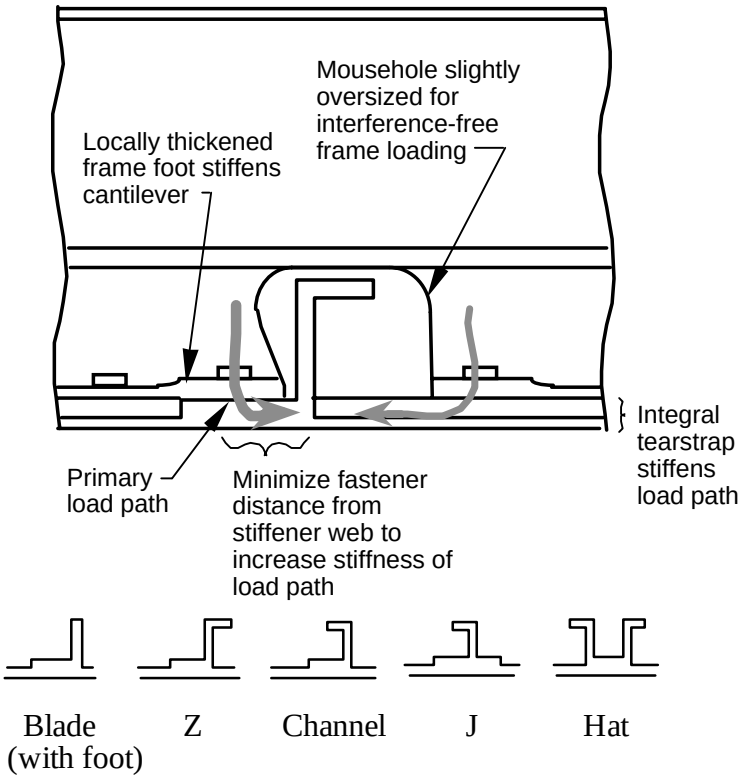

Figure 10. Strategy for Increasing Stiffness of Frame/Longeron Connection without Separate Clip

The stiffeners were sized for static strength, subject to various constraints. The stiffener foot was sized to accept a repair fastener on one side for a Z (or channel) on the upper fuselage, and on both sides of the J in the lower fuselage. The upper flange of the stiffener was also sized to accept repair fasteners (and restricted to that width to avoid excessive rolling). The height of the stiffener was restricted to match a baseline configuration (generally the frame/longeron height is limited to maximize the usable interior volume of the aircraft). The stiffener web was also restricted to at least 2/3 of the upper flange thickness to ensure that the flange was sufficiently stabilized. The thickness of the lower flange was kept ample for crack arrest/deflection (between 2-3 skin thicknesses).

Sizing of the fillet radii, particularly at the skin/stiffener foot transition, was recognized as a potentially important design variable affecting fatigue life. Because the asymmetric shoulder in tension deflects in a nonlinear fashion, determination of the true stress concentration factor in a pressurized fuselage was a nonlinear 3D problem, and was thus difficult to model reliably. A small test program to evaluate the effect of the fillet radius on life was initiated to evaluate this feature (see Section 5.4.2)

3.3.2 Frame Configuration

For the current design, the frame is not integral to the skin, thus a fairly conventional frame arrangement could likely be used. However, for potential cost savings and additional functionality, an integral frame/shear clip configuration combination was developed for use in this program.

In general, frames are attached to the stiffened skin by shear clips, stringer clips, or both. For integral construction, it was felt that the inclusion of an integral shear clip feature on the frame could improve the crack turning performance of integral structure because it would stiffen the structure near the thickness interface. The frame/skin interface, because it is a single, smooth interface with one reasonably flexible side, is inherently less troublesome than the stringer clip interfaces from an assembly standpoint. One could allow the (fairly rigid) frames to set the interior mold line, and let the skin flex to fit. Based on the previous discussion, the frame/stringer clips could be omitted throughout much of the fuselage.

Three possible frame cross-sections with integral shear clips are compared with conventional construction in Figure 11. Concept (a) has a stress concentration due to the unreinforced web around the mousehole, which could begin a

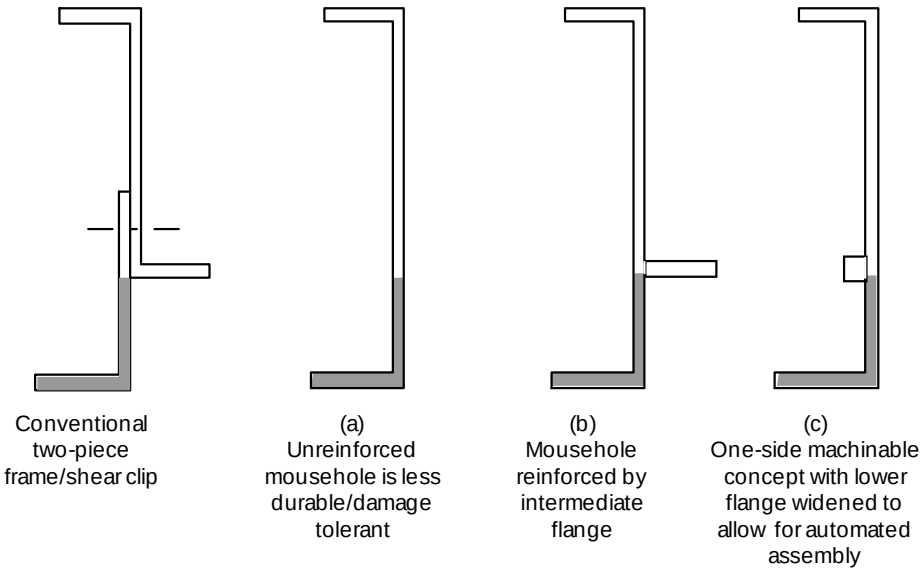

Figure 11. Integral Frame/Shear Clip Design Considerations (Mousehole Region Shaded)

fatigue crack and take out the entire frame. Also, assuming a longitudinal skin crack through the mousehole area, there is no effective lower cap to the frame. Concepts (b) and (c) each reinforce the critical region of the mousehole with an intermediate integral cap to reduce the stress concentration and provide a measure of fail safety in case of a skin crack. Concept (b) would be best extruded, but would then have to be stretch formed. Stretch forming requires high strains, and thus would likely be accomplished in a soft temper, followed by subsequent heat treat, yielding results which may not be sufficiently accurate if the frame is to define the contour of the aircraft. Concept (c) can be one-side machined to high accuracy, and was thus preferred. This concept is also pictured with the frame foot locally stiffened near the mousehole in Figure 10, a detail which may or may not be critical, but is easily accomplished during the machining operation.

Frame sizing is largely stiffness driven, and would be similar for integral and built up structure. From a material selection standpoint, note that the fasteners in the frame foot are installed in the short transverse orientation, and thus a stress corrosion resistant material should be used.

3.3.3 Integral Tear Straps

The thickened lands that ride under the frames serve as integral tear straps to turn/arrest longitudinal cracks. The lower cap of the longeron performs this role for circumferential cracks. One of the objectives of the program was to learn

how to properly size integral tear straps to arrest running cracks, and preferably to turn either running cracks or fatigue cracks.

A previous investigation had accomplished crack turning and 2-bay straight crack arrest for circumferential cracks with a three-to-one thickness increase in the stiffener pad, but at close (4.6 inch) stiffener spacing. There was also the concern that the fillet radius might affect the residual strength. Coupon and panel test programs were initiated to address these issues (see Section 5.4.1 and 5.5). In the meantime, finite element analyses were used to evaluate test configurations, typically using linear elastic fracture mechanics, and with geometrically nonlinear models where appropriate. These results are described along with the test results in Section 5 where appropriate. Integral tear strap to basic skin thickness ratios of 2.83 and 2.35 were used on this program, as will be discussed.

The integral tear strap was sized to a two inch width to accept two fastener rows for repair purposes. This was also comparable to widths used previously for mechanically fastened tear straps.

3.3.4 Material Selection and Sizing of Concepts for Structural Testing

Many aspects of what sizes the structure have already been discussed. Prior to actually performing sizing computations, load requirements must be defined. For trade study purposes, two sets of wide-body load requirements were defined, an upper-aft load set, and a lower-aft load set, as shown in Figure 12. The upper aft load set was representative of a region intermediate between the crown and the window belt, since the crown was originally considered too critical for integral construction. These loads were approximated from representative allowables of low margin panels on a wide-body aircraft, and thus the loads are given as required allowables for tension, compression and shear acting individually. This implies the assumption that the load interaction behavior of the integral structure will be very similar to that of the baseline structure.

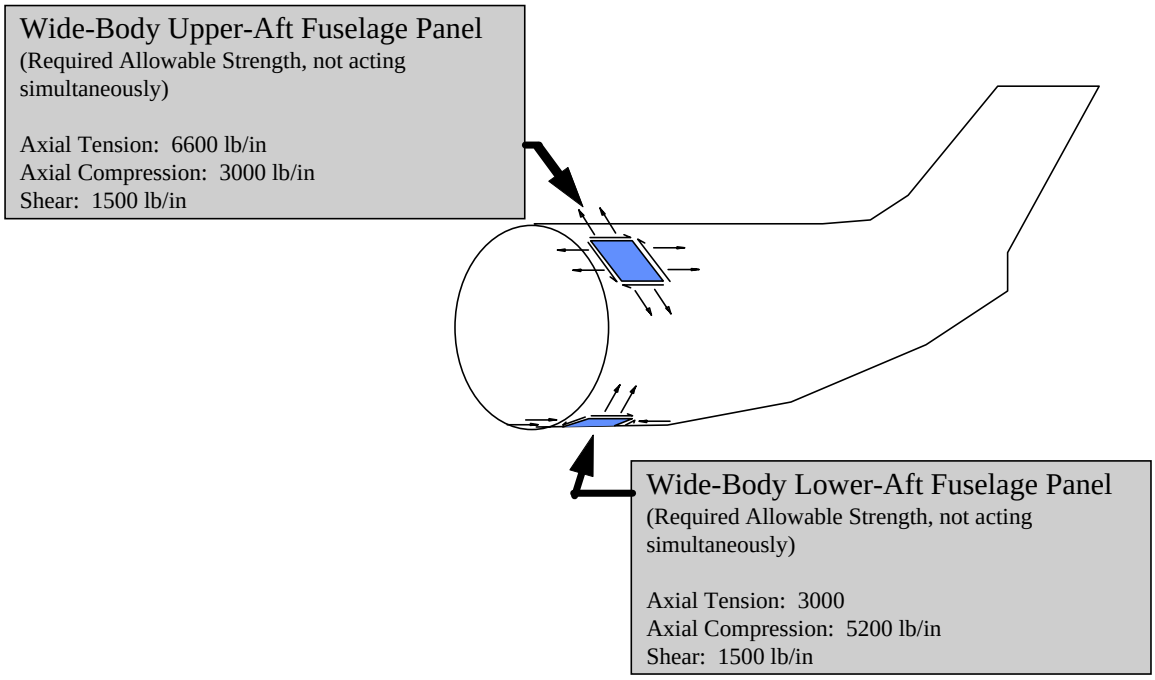

Figure 12. Load Scenarios for Material Selection Trade Study

In order to have a fair weight comparison between baseline and integral structures, and to distinguish the merits of each material, it was necessary to optimize both a baseline structural concept, with baseline materials, and various integral concepts with candidate materials. To accomplish this, an EXCEL spreadsheet was written to calculate the tension, compression, and shear allowable of a parametric representation of each structural concept. A description of the analysis method is given in Appendix Section A.1. Using the Solver function of the program, each concept was optimized to minimize weight while satisfying the required static allowables, subject to various constraints as discussed in section 3.3.1.

The integral tear strap is not analyzed nor sized in the static analysis, yet initial calculations indicated that the integral tear strap weight would exceed the weight of typical tear straps used on existing aircraft. A weight allowance of 6% of the baseline weight was added to each integral configuration to compensate for this difference, based on a preliminary sizing of the tear straps for the 7050 panel. In reality, this would be material dependent, but in the absence of accurate methods to size the tear straps, this penalty was applied equally to all integral concepts for the purposes of the trade study.

A summary of materials analyzed, and the weight change obtained for each configuration is given in Table 2. Various material properties and characteristics are tabulated which are of interest for material selection, though only the static properties were used to calculated the weight change (except in

Table 2. Trade Study Materials and Summary

Alloy/ Product Form	Ftu (ksi)	Fty (ksi)	Fcy (ksi)	Short Transverse Fastener OK?	Creep Formable ?	% Weight Change Upper Aft Fuselage Case*	% Weight Change Lower Aft Fuselage Case*
Baseline Clad 2024-T3 Skin 7150-T77511 Extrusion	62 85	45 78	37 78	N/A	N/A	0	0
2024-T351 Plate	60	45	36	NO	NO	+28	+29
2324-T39 Plate	≈10% higher than 2024			NO	NO	Approx +18	Approx +19
7475-T7351 Plate	70	59	58	YES	YES	-2	-1
7050-T7451 Plate	74	64	63	Probably YES**	YES	-6	-6
6013-T6 Plate or Extrusion (Sheet props used)	52	47	48	?	Probably YES	+25	+13
2024-T3511 Extrusion	57	42	34	N/A	NO	+32	+32
2224-T3511 Extrusion	≈10% higher than 2024			N/A	NO	Approx +18	Approx +19
C434-T3511 Extrusion	≈20% higher than 2024			N/A	NO	Approx +8	Approx +12
7050-T74511 Extrusion	73	63	63	N/A	YES	-5	-5
7175-T73511 Extrusion	69	59	59	N/A	YES	-1	-1

** Weight change is relative to baseline, and includes a 6% increase in weight for the integral tear straps.

* There was some division among the IAS team as to whether 7050-T7451 plate has sufficient stress corrosion resistance to permit short transverse fastener installation.

the case of the 6013 alloy, which has two percent less density than the other baseline and candidate alloys, which was also taken into account). Static properties, where available, were taken from Mil-Hdbk-5 [17] . In the case of 6013-T6 plate, sheet properties were used in the absence of plate values. For three proprietary alloys, the actual static properties could not be included explicitly, but are approximately referenced by ratio to 2024-T3 properties (though the best values available were used in the analyses).

Note that the baseline stiffener alloy used for the trade study was 7150-T7711 extrusion, which has higher strength than the 7075-T6 used on many existing aircraft, in order to better represent an airplane of conventional design, but up-to-date materials selection. 2024-T3 and the more modern (and tougher) 2524-T3 are of essentially the same static strength, and may be considered equivalent in that respect for the purposes of the trade study.

It should be mentioned that low weight density alloys, in particular aluminum-lithium alloys, were excluded from the studies early in the program. These were immediately ruled out for plate hogouts because of the high buy-to-fly ratio, in view of the high price of the raw material. Cost and availability were also concerns with respect to large extrusions, as well as the low plane stress fracture toughness and directional nature of these alloys in an extruded product. It was felt that it was premature to include these materials in the test program at this point, but that what would be learned from more available alloys could later be applied to more advanced alloys or alloy development.

The baseline built-up configuration optimized for both upper and lower fuselage cases was a Z stiffened skin. For the upper fuselage loads, the integral panels likewise optimized to well-proportioned Z-stiffened panels. When optimizing the lower fuselage integral panels, however, the Z stiffened concept converged on concepts with unreasonably bulky stiffeners, particularly for the lower strength alloys. Much better proportioned stiffeners, and better weight efficiency were obtained when a J configuration was used. Because this was also favorable to repair in this damage prone area, the J configuration was adopted for all lower fuselage integral panels.

All the alloys considered were known, or at least believed to possess high plane stress fracture toughness, which is important for damage tolerance. Unfortunately much of the fracture toughness data is proprietary or even nonexistent for the product forms indicated, and is thus not included in the chart. However, the 2000 series aluminum alloys in general, and 2024-T3 in particular is known to have very high fracture toughness, with R-curves approaching 180 ksi-in$^{1/2}$ for wide panels [18]. Of the 7000 series alloys, 7475-T7351 was expected to have toughness approaching that of 2024-T3. The -T73 temper was favored over the -T76 temper because it is known to retain fracture toughness better at -65°F for this alloy, and for improved stress corrosion resistance.

Based on the static strength/weight analysis, the 7050 alloy appeared to be a good choice in both plate and extrusion product forms, yielding 5-6 percent potential weight savings. In addition to high static strength, the alloy was known to have good plane stress fracture toughness in the L-T orientation (crack running normal to the grain), though less than 7475-T7351 and 2024-T3, and was age/creep formable, a potentially important characteristic for curved panel

fabrication. In the plate product form, it has sufficient stress corrosion resistance that it is likely acceptable for applications requiring short transverse fastener installation (though there was some division among IAS team on this point). 7050-T7451 plate had also performed well in a previous transversely cracked integral panel test at NASA [16].

A structural configuration representing the upper aft fuselage was sized for 7050 alloy (suitable for both plate and extrusion product forms), and is illustrated as Concept #1 in Figure 13. As documented in Section 5.0, a test matrix[4] was adopted of specimens ranging from material characterization coupons to structural panels based on this structural configuration. As work progressed, crack turning test specimens showed that the T-L fracture toughness (cracking parallel to the grain) was very low for the 7050 plate material (about 83 ksi-in$^{1/2}$), and likely inadequate for efficient longitudinal fuselage crack arrest. The crack path also favored this direction, making it very difficult to turn longitudinally running cracks in this material. Later tests showed similar problems in the 7050 extrusion as well.

No doubt the most critical test in the program plan was a 10 ft x 10 ft. pressurized longitudinal 2-bay crack panel scheduled for testing at Boeing Seattle late in the program. It became clear that this test would not likely be successful using 7050 plate or extrusion due to the low fracture toughness of the material. This issue was discussed among the IAS team, and after a check of available information showed the toughness orthotropy to be much less severe for 7475-T7351 plate (a trend later confirmed by crack turning specimens), that material was selected as the alloy of choice for the longitudinal crack test.

7475-T7351 plate had a lower static strength than 7050-T7451, and showed only slight weight advantage over baseline, but that still met the program minimum objective of weight parity. It had higher plane stress fracture toughness (including excellent T-L toughness), excellent corrosion and stress-corrosion resistance (commonly used in applications with interference fit fasteners in the short-transverse orientation), and is age/creep formable. Based on some preliminary finite element studies performed at Boeing Seattle which became available at this point in the program, it appeared that integral tear straps might be better crack stoppers than originally thought, and with the additional toughness, perhaps crown panel applications were not out of reach as previously thought.

An excellent baseline for crown panel performance was available in the form of wide-body crown panel tests performed previously at Boeing Seattle under FAA contract [18] to investigate two-bay crack arrest with and without MSD. It was decided to design an integral panel of equivalent strength and weight as the FAA panels, and to test with a two-bay longitudinal crack on the same rig at Boeing Seattle.

[4] modified from a test plan developed under an earlier study, contract NAS1-20268.

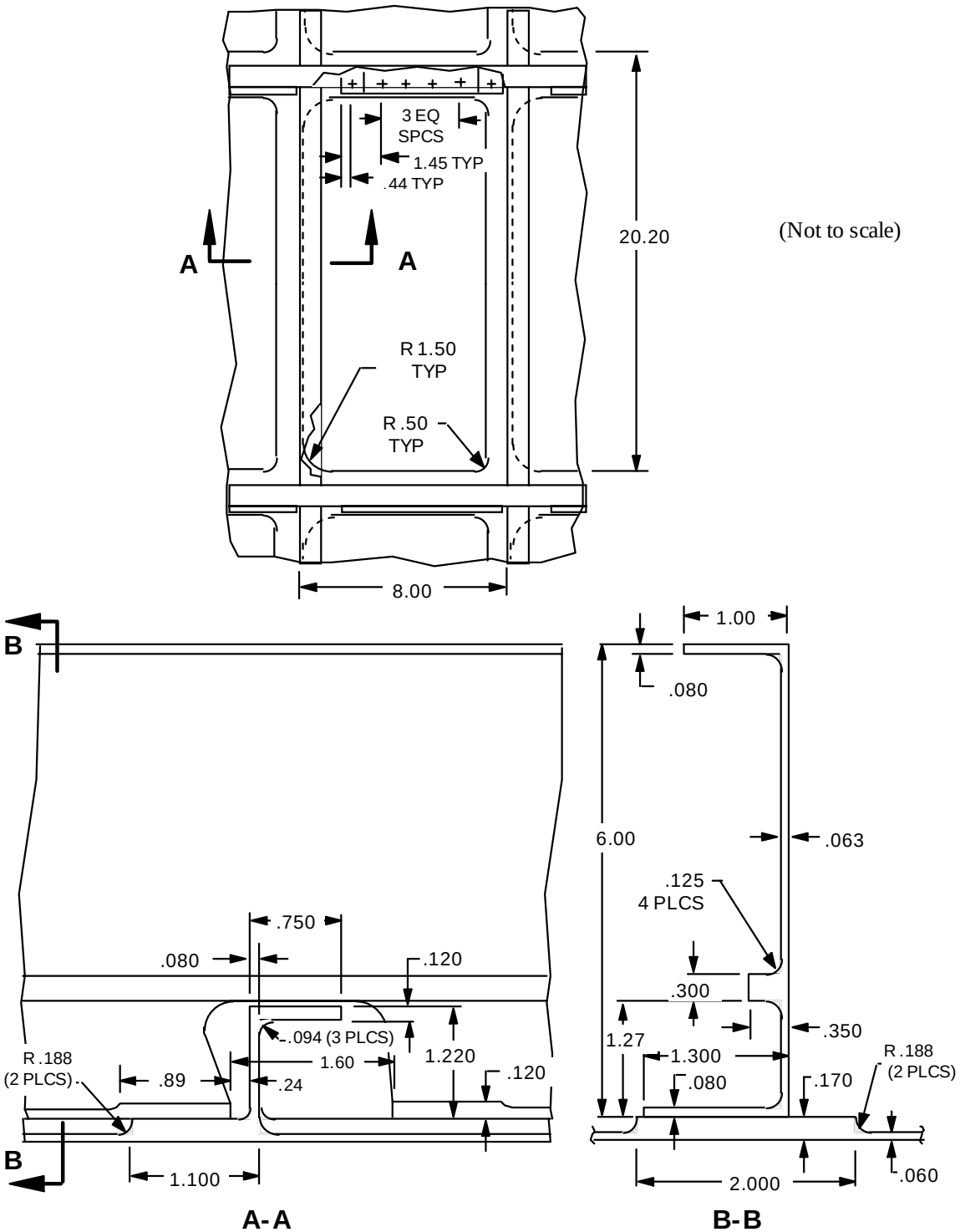

Figure 13. Integral Upper Aft Fuselage Panel Geometry (Concept #1)

In order to obtain the load capability of the baseline panel concept, the spreadsheet panel sizing tool was modified to reflect the geometry and materials of the hat-stiffened FAA panels. A Z-stiffened 7475-T7351 integral panel was then sized to equal or better strength in tension, compression, and shear (separately applied). As a refinement to previous analyses, the strength and weight associated with fillet material was accounted for, and the weights of all structural details (including frames, the baseline frame-longeron clips, and the baseline tear straps, but excluding joints) were calculated. The integral tear straps of the new design were then sized so that the weight per unit area of the two panels would be the same. A finite element analysis on this concept was performed [21], assuming straight crack growth initiating at the end fastener of a frame foot. The concept appeared conservatively adequate to sustain 9.4 psi pressure (the same as the FAA panel failure load) with a two-bay crack based on linear elastic fracture mechanics.

Table 3. Weight/Strength Comparison Between Crown Panel Baseline and Concept #2

		FAA Crown Baseline	Integral Crown (Concept#2)	% Difference	Comments	
Static Strength Comparison						
Predicted ultimate strength, loads acting separately					Assuming the crown panel is shear/tension critical, the integral concept is slightly overdesigned, and could be refined based on the actual critical loads	
		lbs/inch	lbs/inch			
	Tension	5798	6047	4.3		
	Compression	2172	2191	0.9		
	Shear	1324	1495	12.9		
Weight Comparison/Breakdown						
Effective thickness, t_{eff}, based on density of aluminum, 0.101 lb/cu in						
An attempt has been made to divide weight of integral structure up by function.						
		teff	t_{eff}			
	Skin	0.06300	0.06300	0.0	Items shown in boxes are integrated in Concept #2. Weight parity was acheived, but further refinement could likely reduce weight in integral tear straps, clips, and frame.	
	Stringers	0.03357	0.02793	-16.8		
	Tear Straps	0.00773	0.00826	6.8		
	Frames	0.02271	0.02329	2.5		
	Shear Clips	N/A	0.00809	100.0		
	Stringer Clips	0.00359	N/A	-100.0		
	Total teff	0.1306	0.1306	0.0		
Total in lb/sq ft		1.900	1.899	0.0		

The baseline and integral crown panel (Concept #2) configurations are illustrated in Figures 14 and 15 respectively. A table showing strength and weight parity is given in Table 3. The weight analysis accounted for minute structural features not explicitly detailed in Figure 14, such as lobes on the tear straps, and also fillet material with a few minor exceptions. While weight parity with baseline was achieved in the integral crown panel design, it is likely that refinement could further reduce weight without unacceptably degrading performance in terms of static strength or two-bay crack fail-safety.

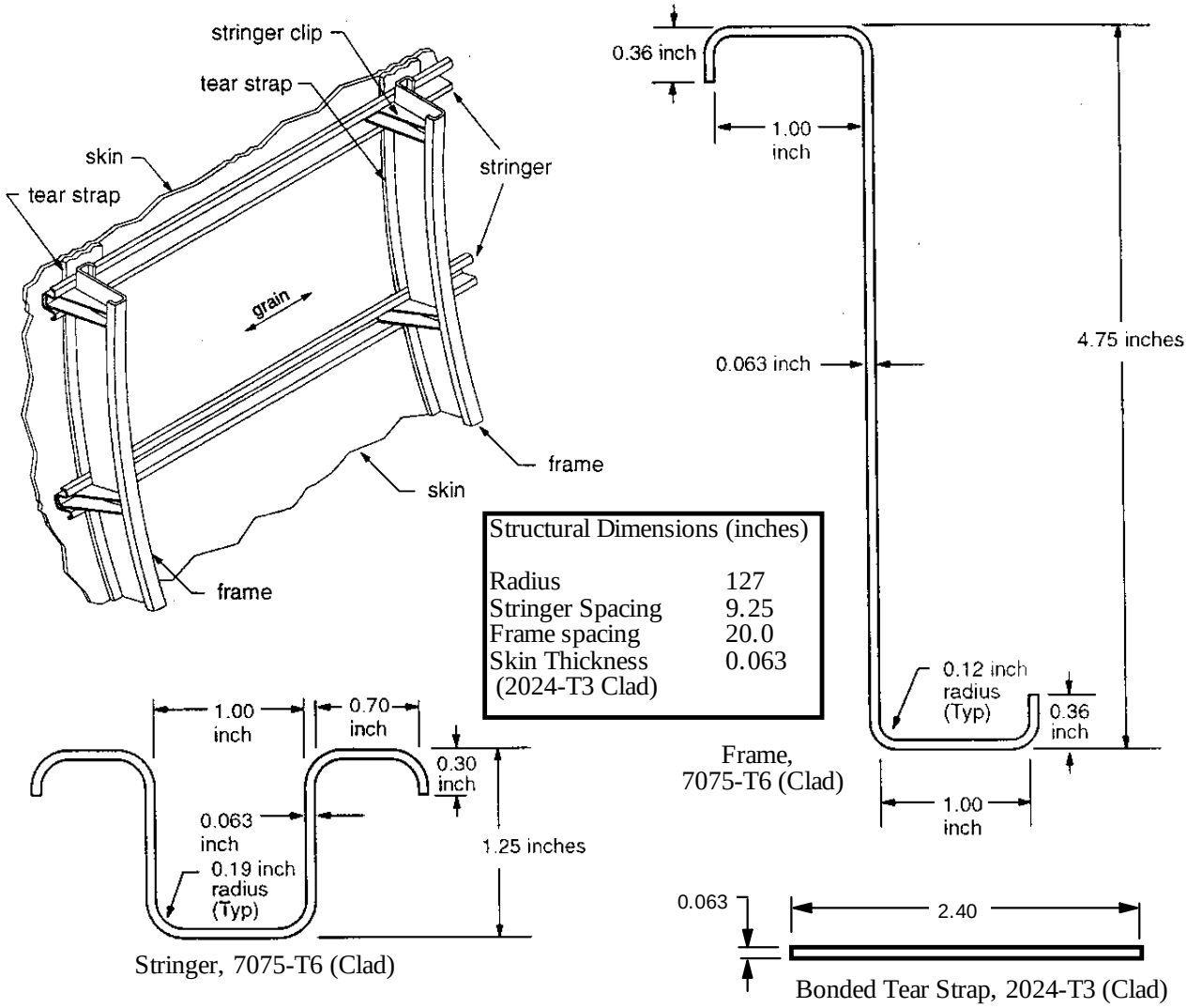

Figure 14. Baseline Crown Panel Geometry [17]

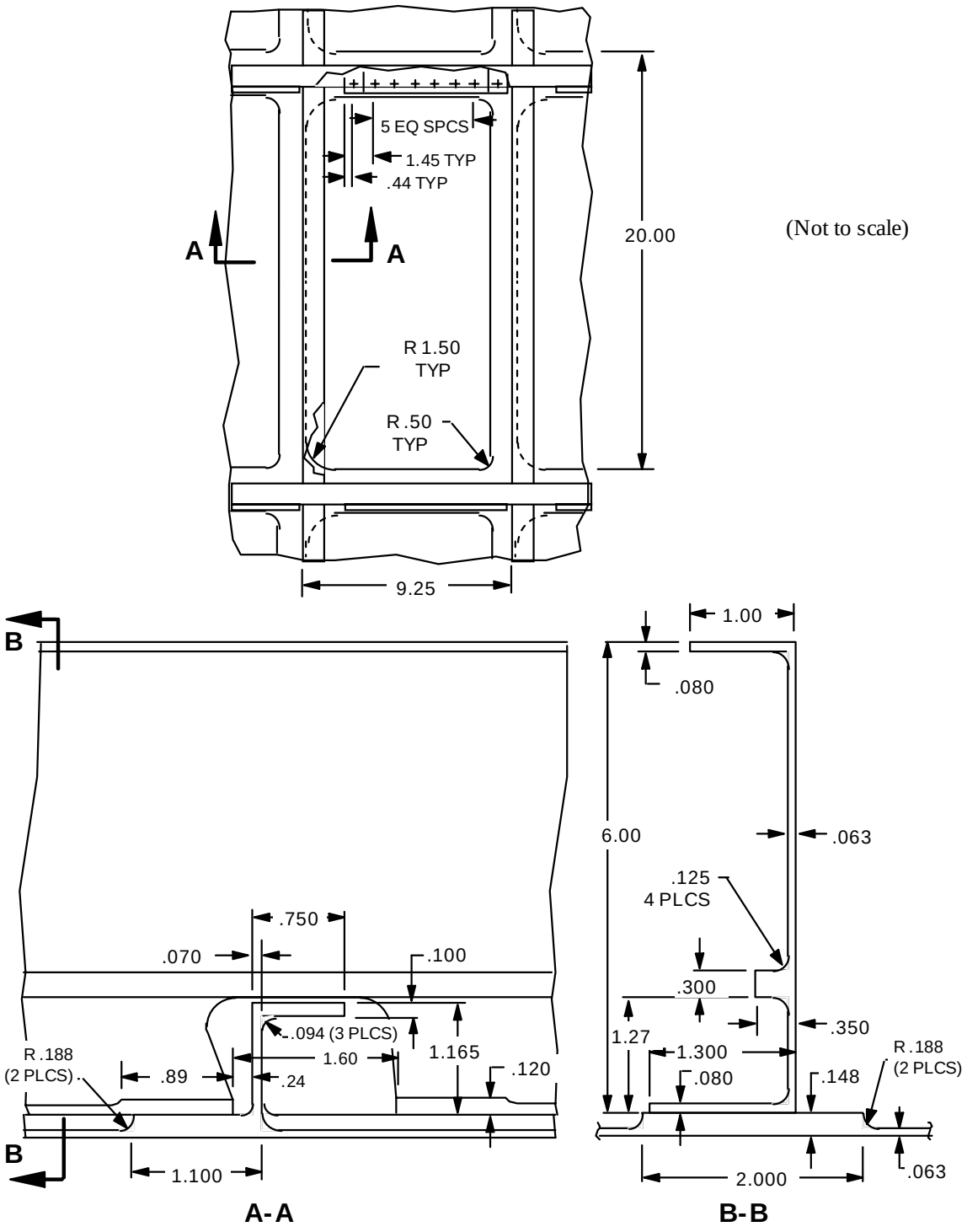

Figure 15. Integral Crown Panel Geometry (Concept #2)

In light of the fact that in order to achieve static strength equivalence and meet fail safety requirements, 7475-T7351 seems to be the best current candidate for integral structures, some discussion with regard to fatigue and crack growth

performance is appropriate at this point. The S-N fatigue performance of 7475-T7351 (and 7000 series alloys in general) is generally not considered to be as good as the incumbent 2024-T3 skin material (or 2000 series in general). Reference is typically made to Mil-Hdbk-5 data which gives (bare) 7475-T7351 plate S-N data and bare 2024-T3 sheet data, showing the 2024-T3 to have roughly 3-5 times the life of the 7475-T7351[5]. One must realize, however, that the true incumbent skin material is not bare 2024-T3, but clad 2024-T3, which has worse fatigue performance than bare material because the cladding acts as a fatigue initiator. Mil-Hdbk-5 7475-T7351 plate data compares more favorably with clad 2024-T3 S-N data given in [22]. 7475-T7351 showed better performance than clad 2024-T3 for unnotched specimens, but somewhat worse performance for notched specimens, where the data has to be adjusted to obtain matching notch values for comparison.

Even if there were a slight drop in S-N performance, or if the designer were tempted to reduce the skin gage to take better advantage of the higher mechanical properties of 7475-T7351, it would be primarily an issue for repair. The basic integral structure concept should have a fatigue life well beyond the baseline design due to the elimination of fastener holes along the stiffeners where the hoop stresses are the most severe, and the integral reinforcement of the remaining fastener locations at the frames and splices. Having provided reinforced skin regions for the most critical repair fasteners, as discussed in Section 3.1.3 (see Figures 9 and 13), the integral design appears adequate in this respect. Also, a simulated repair test panel was also designed for subsequent NASA testing to confirm the repairability of the structure (see Section 5.5.2).

A comparison of crack growth data from [22] shows that the constant amplitude da/dN vs. ΔK curves cross at around 1E-5 inches/cycle, with the 7475-T7351 performing better in the upper ranges, and the clad 2024-T3 performing better in the lower ranges, which represent most of the fatigue crack growth life of actual components in service.

Without any compensation for this difference in crack growth behavior, there might be a trade-off between the value of extended aircraft life and the cost of reduced inspection intervals. However, taking advantage of the tailorability of integral structure--the ease with which extra material can be placed precisely where it is needed in the vicinity of a life-limiting feature, without adding more fastener holes--it is possible to compensate in many cases by local reinforcement (integral doublers). The increased thickness in these areas not

[5] Another interesting piece of data, though more relevant to wing loading, is given in [23]. Riveted lap joints made from 0.2 inch thick 2024-T351 and 7475-T7351 plate tested with versions of the FALSTAFF load spectrum (limit stress = 21.7 ksi), showed approximately 25 percent lower life for 7475-T7351.

only increases the average fatigue life of the feature, but also slows crack growth in the early stages when the crack is growing very slowly.

3.3.5 Joint Design

At this point in the discussion, having downselected materials and structural concepts for further evaluation, a discussion of joint design for integral structure is appropriate. Mechanically fastened joint concepts were developed for longitudinal and transverse joining applications, and a friction stir welded longitudinal joint configuration was also considered. Because of the timing of the joint design process in the program, the joints are designed for use with panel concept #1 (Figure 13). As mentioned previously, a long life joint design can reduce the threat of MSD if it moves the fatigue life of the joints out beyond the fatigue lives of other, less MSD prone (more widely spaced) features, such as the end fasteners of the frame feet. A slow crack growth joint design is also important so that non-MSD cracks that might appear early in the life of the structure due to a manufacturing flaw or incidental damage will propagate slowly for good detectability. The two-bay crack must also be satisfied in this region for cracks parallel to the joint, which pass near where the stiffeners or frames are also likely spliced.

All of these objectives are aided by appropriately increasing the bulk of the splice through the thickness. Integral structures can tolerate more rapid thickness transitions than can be achieved with riveted doublers, but still one must be careful about eccentricity. Since the part is presumably machined on both faces (even the flush surface must be cleaned up to obtain a flat surface to suck down to a vacuum table) fairly complex detail features such as stepped interfaces can be machined into the joint with little cost impact, so long as the design does not require an excessive number of tool changes.

3.3.5.1 Mechanically Fastened Longitudinal Joint Concept

The longitudinal joint concept chosen for evaluation is a stepped-lap configuration shown in Figure 16 (for full geometric detail, see Appendix Section A.4), which achieves a more favorable distribution of the fastener loads than the simple lap configuration also shown.

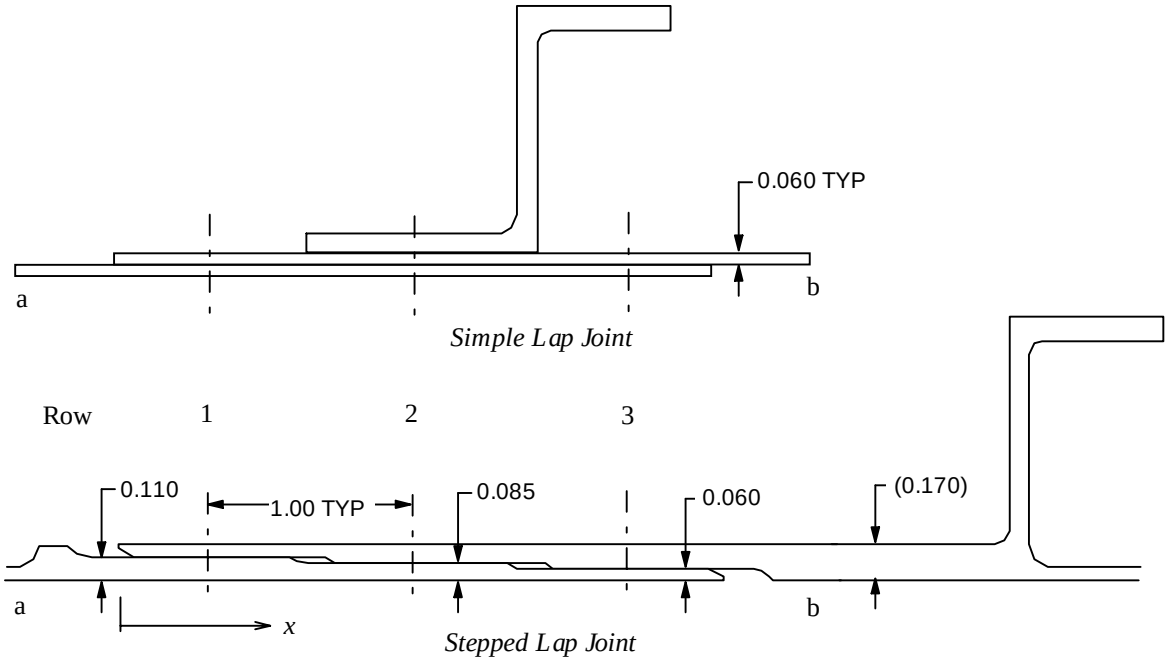

Figure 16. Longitudinal Joint Concepts

The simple lap is similar in concept to commonly used joints[18]. Ample (0.15 inches) space was left between stepped interfaces to take up slack on assembly (use of the gray or silver gap seal on the exterior recommended for cosmetics). The thickness of the overall lap was made to match the pad thickness under the stringer, which also matches the integral tear strap pad thickness. This results in a flush exterior configuration, which has a small aerodynamic benefit, but also potentially improves fit by eliminating the imprecision of the unlofted section typically associated with a lap joint. The joint concept also has a flush transition along the interior, simplifying frame configuration and attachment.

An analysis of the joint is given in Table 4, with comparison to a conventional lap joint configuration with three fastener rows of the same pitch, but a constant skin thickness of 0.06 inches. Fastener joint allowables are interpolated from Mil-Hdbk-5G values for 1097-E6 rivets in clad 7075-T6 sheet, which is comparable in bearing strength to 7050-T7451 plate. The stepped lap joint has only about 8 percent higher static strength[6], but nearly 42 percent more bearing area. Based on a displacement compatibility [25] and in-plane stress concentration analysis [24] (neglecting eccentricity), the stepped lap has an effective gross stress concentration about 46 percent less than the constant thickness lap. A rough fatigue life estimate was calculated for a skin stress of 17 ksi, R=0 for each of the concepts, based on available fatigue data [17,22]. However, because the

[6] Both joints are easily adequate for the ultimate hoop load of (8.6 psi) (1.15) (1.5)/(118.5 in) = 1758 lb/in. Conservatively high static joint strength is common for longitudinal joint design, because fatigue life is typically more critical than static strength, requiring a large bearing area. Some designers might argue that softer rivets should be used to obtain better hole fill, even though that would result in lower static strength.

analysis neglects eccentricity, interference, and the effects of countersink, fretting, and faying surface sealant, a reliable analytical estimate of the fatigue life is not possible. Nevertheless, assuming the trends are correct, the life of the stepped lap would be anticipated to far exceed that of the simple lap joint (even if the simple lap were of clad 2024-T3 material). Also, though the analysis predicts a slightly higher stress concentration at the center fastener row of the stepped lap, it seems likely that failure will occur at one of the outside rows (probably on the countersunk side) due to bending at the ends of the joint.

The increased weight associated with the stepped lap is small when spread over the overall panel, and should be viewed in the context of improving the joint inspectability and MSD resistance of the aircraft. Also, it can be offset by joining some of panels together first with a low-cost, low-weight, structurally efficient friction stir welded concept.

Table 4. Results of Joint Analyses

Simple Lap							
		Fastener Pitch (in) =	1.04		Gross Stress		
		Basic skin thickness (in) =	0.06		Concentration	Bearing Area/	
Row	t (in)	Ult Load (lbs)/rivet	Jlt Load (lb/in)	Load fraction	Kg eff	Gross Area	
1	0.060	944	907	0.340	4.214	0.184	
2	0.060	944	907	0.320	3.114	0.184	
3	0.060	944	907	0.340	2.222	0.184	
		Total Joint Strength (lbs/in):	2722		Total:	0.551	
						Reference S/N data*	
		Estimated life of 7050-T7451 joint at 17 ksi basic skin stress:			3.5E+04	[17], Fig. 3.7.3.2.8 (c)	
		Estimated life of clad 2024-T3 joint at 17 ksi basic skin stress:			6.5E+04	[22], Fig. 2.1.1.3 (b)	
Stepped Lap							
		Fastener Pitch (in) =	1.04		Gross Stress		
		Basic skin thickness (in)=	0.06		Concentration	Bearing Area/	
Row	t crit	Ult Load (lbs)/rivet	Jlt Load (lb/in)	Load fraction	Kg eff	Gross Area	
1	0.110	1094	1052	0.328	2.274	0.337	
2	0.085	1033	993	0.344	2.287	0.260	
3	0.060	944	907	0.328	2.141	0.184	
		Total Joint Strength (lbs/in):	2952		Total:	0.781	
						Reference S/N data*	
		Estimated life of 7050-T7451 joint at 17 ksi basic skin stress:			393018	[17], Fig. 3.7.3.2.8 (c)	
		*Reference data adjusted for Kt, Kg					

3.3.5.2 Friction Stir Welded Longitudinal Joint Concept

Friction stir welding is a relatively new process for creating metallurgical joints. As illustrated in Figure 17, it involves forcing a spinning mandrel into the workpieces in the vicinity of an interface, thereby softening the workpiece material locally, and

mechanically mixing it together. Friction stir welded joints are virtually absent of porosity, have no melt zone, and can be used to join metals which are not readily weldable with conventional welding processes.

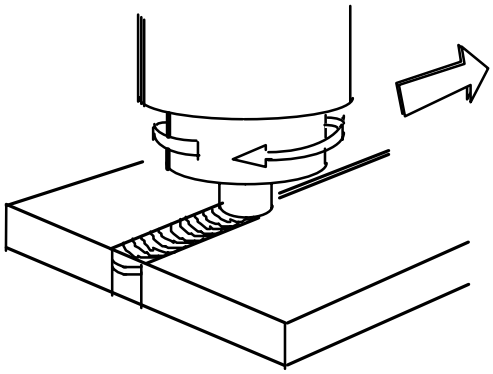

Figure 17. Friction Stir Welding Process

The 7000 series alloys of interest for this program are among the materials which have been friction stir welded with success, but which are not practical to weld by conventional means (including laser welding). Coupon specimens for static, fatigue, and corrosion evaluation of friction stir welded 7050-T7451 plate are described in Section 5. It is anticipated that the as-welded material may experience a static strength reduction of as much as 20 percent, and some loss of fatigue performance compared to the parent material. Nevertheless, the expected performance is still favorable compared to other joining methods.

Due to weld thickness limitations, it would appear that the welding process would occur after the panels are machined, thus accurate location of the panels during the welding process would be important. To compensate for the reduced properties, a friction stir welded joint should be located in a reinforced region, possibly integrated with a stiffener as shown in Figure 18. A pad thickness 1.3 to 1.4 times the basic skin would probably suffice, but co-locating the pad with a stiffener makes the weld of constant thickness as it crosses though the integral tear straps, which simplifies (if not enables) use of this process. Cleanup machining in the joint region may be necessary to remove the slightly irregular surface left by the process, but there may be merit in leaving some visible evidence of the weld process for later inspection/repair.

The integrated concept shown in Figure 18 enlarges the stiffener foot to allow manufacturing access for clamping during the welding operation, and provides room to locate the weldment between fasteners where the frame attaches (which also allows room for reinforced repair without piercing the weldment).

3.3.5.3 Circumferential Joint Concept

Butt joints are typically used circumferentially because the orientation of the airstream demands an aerodynamically flush joint. In principle, a flush lap such as that described for the circumferential joint could be employed, but such a course would mean that when assembling barrels, one would have to insert the end of one barrel inside the end of the mating barrel, which is not likely to be practical. With a butt joint, the barrels are brought adjacent to one another and

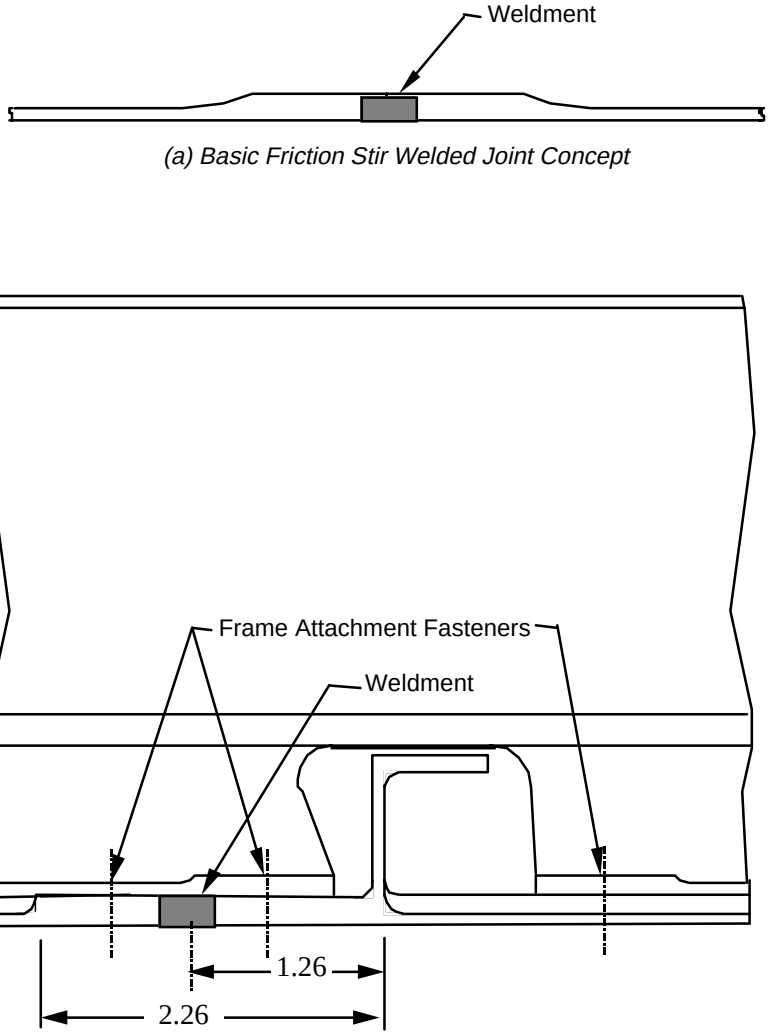

(a) Basic Friction Stir Welded Joint Concept

(b) Welded Joint Concept Integrated into Integrally Stiffened Skin Panel

Figure 18. Longitudinal Friction Stir Welded Joint for Integral Structure

joining is achieved by adding additional detail parts that bridge the gap and fasten to each side. In conventional designs, internal joint straps are used almost exclusively, thus maintaining exterior flushness, but creating undesirable eccentricity at the center of the joint. Circumferential joints in conventional

structures also tend to be many fasteners wide to provide sufficient bearing area to transfer the required load, which also helps reduce the effect of the eccentricity. Most airframers prefer to splice at a location midway between frames to avoid unnecessary complexity.

Taking advantage of the ability to locally reinforce integral structure, we have the ability to deploy more bearing area per hole, thus requiring fewer fasteners, reducing the width of the joint, and loading the fasteners more evenly--all of which is good. The shorter the joint, however, the greater the effect of the eccentricity will be.

With these factors in mind, the joint concept of Figure 19 was developed (see Appendix Section A.4 for full geometric detail). The external doubler helps alleviate joint eccentricity, but is inlaid for aerodynamic flushness. The external doubler also helps seal the aircraft, since the internal doublers are discontinuous due to the integral stiffeners (splicing the stiffeners over the joint is possible to allow a continuous internal doubler, but adds unnecessary complexity).

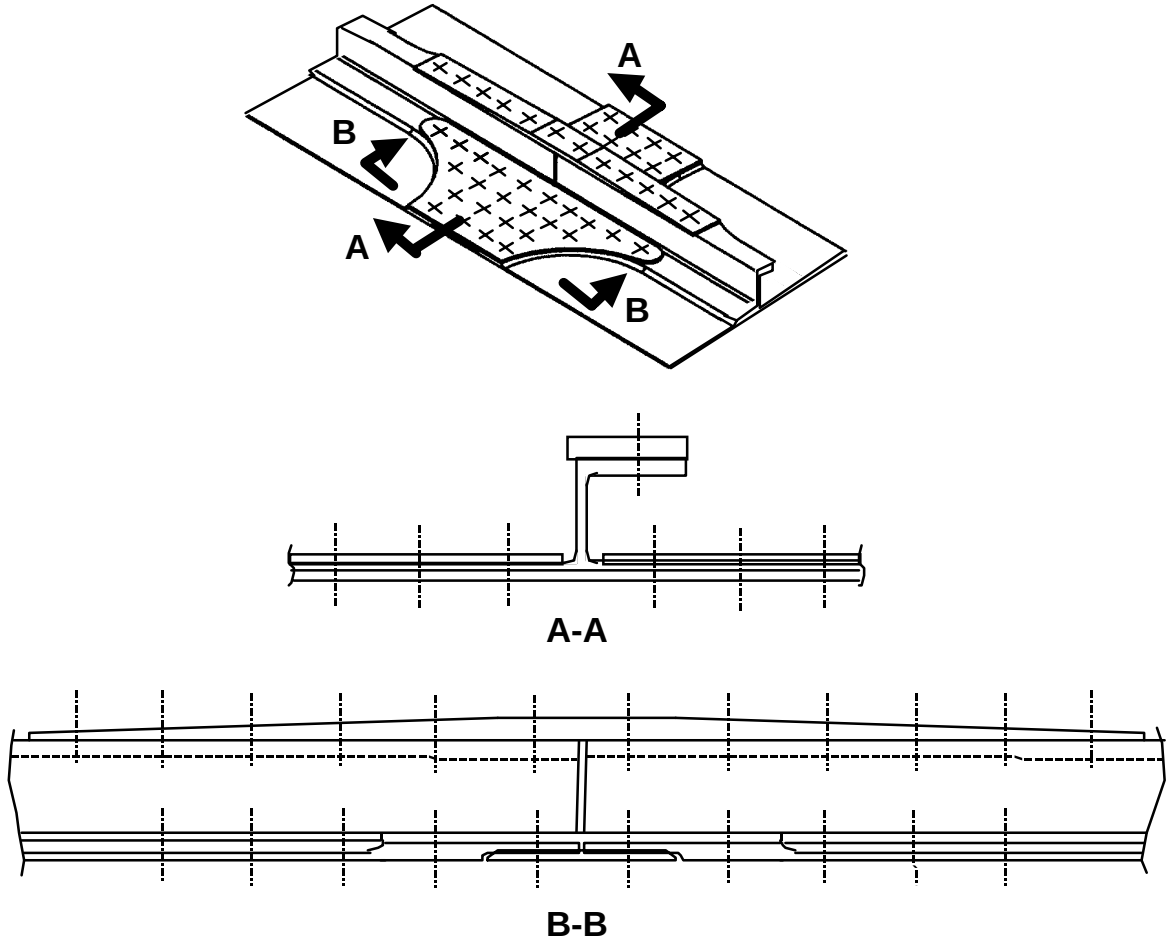

Figure 19. Circumferential Splice Concept

Another concern with regard to integral stiffeners is that in the conventional design, the stringers are left unattached for several inches on either side of the joint to allow some flexibility in case they don't match up. Once the stiffener ends are joined together, the fasteners leading up to the joint are installed. In the integral case, the stiffeners are very rigidly attached to the skin, making stiffener line-up a potentially difficult interface (actually, even with the flexibility in the conventional design, stiffener line-up and joining is often a problem interface). Most of the difficulty of this interface has to do with tangential, or "in plane" stiffener mismatch. For integral panels, even if they are precisely machined to match, some in-plane shifting of the longerons may occur as the panels are formed to contour--particularly complex contour. Also, if the panels are extruded, they must generally be stretch-straightened longitudinally as part of the heat treatment process, resulting in Poisson contraction. Some of this could be compensated for in the die design, but the contraction would vary between the grip lines. The wider the panels, the more significant the problem will be.

In order to alleviate this problem in the integral concept, the circumferential joint has been designed to eliminate the tangential component of the interface. The stiffener caps are built-up in both thickness and width in the vicinity of the joint so that all the stiffener load can be transferred through the cap via a tapered strap, which can accommodate ample in-plane manufacturing tolerance.

A static analysis of the joint is given in Table 5, estimating an ultimate strength of 49 ksi based on the gross area of the basic skin/integral stringer cross-sectional area. The ratio of bearing area to gross area is a very high 0.926, which should ensure long fatigue life. Because of the complexity of the joint, and the uncertainty of fatigue life predictions for joints, no further analysis was run.

Table 5. Static Analysis of Circumferential Joint Concept

				Fastener DIA =		0.19		
				Stiffener Spacing (in) =		8.00		
				Gross Area, incl. fillets (in) =		0.798		
Row	t crit	Critical Material	Fastener Type	Fastener Count/Bay	Ult Load (lbs)/Rivet	Ult Load (lb)	t 7050	Bearing Area/Gross Area
1	0.080	7075-T5	NAS1097E6 100° Flush 7050 rivet	8	1020	8160	0.09	0.171
2	0.080	7075-T6*	100° Flush Ti 6-4 Pin	8	2250	17997	0.17	0.324
3-5	0.080	Fastener Shear	NAS1097E6 100° Flush 7050 rivet	5	1175	5875	0.17	0.202
Stringer Cap	Various	Fastener Shear	MS20470E6 100° Flush 7050 rivet	6	1175	7050	0.16	0.229
			Total Joint Strength (lbs/bay):			39082	Total:	0.926
		*Critical in pin bearing		Ult Stress (ksi):		48.98		

4.0 COST EVALUATION

Because of the highly integrated cost evaluation and prediction efforts under the Boeing Long Beach and Seattle IAS contracts, documentation of the cost evaluation effort is combined under separate cover [3]. Several cost analysis tools were evaluated, and COSTRAN, an improved commercialized version of the Boeing/NASA developed code PCAD, was selected for the IAS program.

A 10 x 10 foot panel representative of design concepts developed in Section 3.4 was utilized as a component for cost modeling purposes. For comparison, an equivalent conventional (mechanically fastened, multi-piece) panel of z-stiffened geometry was also identified. Cost models were run based on various combinations of assumptions with regard to manufacturing technology.

A hybrid design, made from high-speed machined extruded frames that are mechanically fastened to high-speed machined plate skin/stringer panels, was identified as the most cost-effective manufacturing solution. Recurring labor and material costs of the hybrid design are 61% less than a current technology baseline. This would correspond to a total cost reduction of $1.7 million per ship set for a 777-sized airplane. However, there are important outstanding issues that are discussed with regard to the cost of capacity of high technology machinery, and the ability to cost-effectively provide surface finish acceptable to the commercial aircraft industry. It was also observed that application of advanced high-speed machining technology to the manufacture of the baseline built-up structural concept is projected to reduce its cost by 43 percent, thus at equal levels of manufacturing technology, the net savings due to the integral design concept is 18 percent. The projected high raw material cost of large extrusions also played an important role in the trade-off between plate and extruded concepts.

5.0 STRUCTURAL VALIDATION

5.1 Overview of Test Program

In addition to the design and cost work described in the previous sections, the IAS program included formulating a development test plan, and to the degree possible within the funded scope of the program, validating a feasible design concept. Development of the test plan drew upon work from previous efforts related to integral structures [16, 26], and was undertaken as a combined effort by members of the IAS team, under the coordination and leadership of NASA Langley Research Center.

Table 6. Integral Aircraft Structure Test Matrix

	Test Group	Type		Configurations	No Specimens Per Lot: Plate 7050-T7451, 1.5"	Plate 7050-T7451, 2.5"	Plate 7475-T7351, 1.5"	Extr. 7050-T74511	Extr. 6013-T651X	Other	Assignee (d=design, f=fab, t=test): MDC	BAC	LM	NG	NASA
Material Properties	1	Static Tensile		L	3	3	3	3	3			d,f			t
				LT	3	3	3	3	3			d,f			t
				ST	2	2	2	2	2			d,f			t
	2	Fatigue (Unnotched, R=.05)		L (flush side)	5	5		5				d,f			t
				LT (flush side)	5	5		5				d,f			t
				L (t/2)	5	5						d,f			t
		Fatigue (Open Hole, R=.05)		L (flush side)	5	5		5				d,f			t
				LT (flush side)	5	5		5				d,f			t
				L (t/2)	5	5						d,f			t
	3	Crack Growth/R-Curve flush side		CCT,24 in, t=.06 L-T	1	1	1	1	1			d,f			t
				CCT,24 in, t=.06,T-L	1	1	1	1	1			d,f			t
				CCT,24 in, t=.148,T-L			1					d,f			t
				CCT,12", T-L, t=.12	1	1		1				d,f			t
				CCT,12,L-T,t=.06	2	2		1				d,f			t
				CCT,12",T-L,t=.12	1	1		1				d,f			t
				CT, L-S, t=.06	1	1		1				d,f			t
				CT, L-S, t=.06	1	1		1				d,f			t
	4	Determination of rc flush side		DCB (L-T)	9						d,t	f			
				DCB (T-L)	9						d,t	f			
				DCB (T-L)						5	d,f,t				
				DCB/SDCB (L-T)				7			d	f,t			
				DCB/SDCB (T-L)				7			d	f,t			
Structural Details	5	Thickness Interface		-3 (24",Rfillet=.063)	2						d,f	t			
				-5 (24", Rfillet=.188)	2						d,f	t			
				-9 (18", Rfillet=.188)	4						d,f	t			
				-11 (12", Rfillet=.063)	2						d,f,t				
				-13 (12", Rfillet=.188)	2						d,f,t				(1)t
	6	Basic Stiffener Fatigue		Rfillet=.063	10						d,f				t
				Rfillet=.120	10						d,f				t
				Rfillet=.188	10						d,f				t
	7	Mechanical Joints	Static	Longitudinal	1						d,f				t
			Fatigue		4						d,f				t
			Static	Transverse	1						d,f				t
			Fatigue		4						d,f				t
	8	Friction Stir Weld	Static	LT	6						d,f				t
			Fatigue	LT	10						d,f				t
			Corrosion		2						d,f				t
Panels	9	Flat Repair Panel (Fatigue)					1				d			f	t
	11	Unpressurized Circ. Crack		Panel #1	1						d			f	t
		(FCGR/Res Strength)		Panel #2					1		d			f	t
	12	Pressurized Circ. Crack		Panel #1	1						d			f	t
		FCGR/Res. Strength		Panel #2				1	1		d			f	t
	13	Tens., Press.: FCGR/Res Stren		Long. Crack #1			1					d,f,t			
	14	Compr.: Static unnotched		Curved long.#1	1						d			f	t
		Static unnotched		Curved long.#2					1		d			f	t
	15	Shear: Static unnotched		Curved shear#1	1						d,f,t				
		Static unnotched		Curved shear#2					1		d,f,t				
	16	Demo Panels		Singly curved				1				d,f			
				Doubly curved		1					d		f		

Shaded boxes indicate tests not completed under this phase of the program

*For description of specimens made from material s in the "other" category, see Table 9

The plan is largely embodied in the test matrix presented in Table 6, which was negotiated as a team, and evolved somewhat through the course of the program. Planned tests include characterization of static, fatigue, crack propagation and crack turning behavior for various alloys of interest, from the same lots of material as larger specimens. Structural detail tests include specimens to evaluate the development and behavior of cracks at thickness transitions, as well as joining concepts, including friction stir welding. Larger tests include static, repair, and damage tolerance panels to validate the performance of integral fuselage structure, and our ability to predict this behavior. A large portion of the test matrix is related to the damage tolerance of integral structures, including the effects of pressure pillowing and crack turning.

Materials included in the test program included both 7050-T7451 plate and 7050-T74511 extrusion, which were identified as potentially promising materials for integral structures early in the program. 6013-T651X extrusion was also included as a more damage tolerant and slightly lower density alternative (the X designation denoting that this alloy is not a standard extrusion product). As R-curve and crack-turning data became available indicating that 7050 suffers from low T-L fracture toughness, a small group of crack turning tests of various alloys was initiated. These tests (see Section 5.3.3) indicated that 7475-T7351 plate does not suffer from excessive toughness orthotropy, and could thus be made to arrest or turn cracks more uniformly in all directions. This material was selected for the longitudinal crack panel (specimen group 13), and the repair panel, as well as a few material characterization tests, all of which were timed late in the program.

Problems were encountered with dimensional variation in the extruded shapes that made it impractical to fabricate the large panels out of the material procured. Only material coupons were completed out of the extruded products.

As indicated in the test matrix, responsibility for the design, fabrication, and testing of the specimens was divided between the various contractors and NASA Langley Research Center. In this section, the different tests will be described, with emphasis on the work performed under the Boeing Long Beach contract. Test groups 15 and 16 were not tested under the present phase of the contract, though design work was completed for the 7050-T7451 plate shear panel of test group 15. Group 16 was comprised of large demo panels of integral construction, which was intended to be built and tested as part of a barrel test in a follow on program.

5.2 Materials Used

5.2.1 7050-T7451 Plate

Twelve 7050-T7451 plates were procured consisting of six 1.5 inch plates all from the same lot, and six 2.5 inch plates from another lot. All 7050 plate specimens tested in the program come from these lots. Average lot release data from both lots is summarized in Table 7. A copy of lot certification paperwork including additional information is provided in Appendix Section A.2.

As indicated on the test matrix, numerous additional material coupons were supplied under the Boeing Seattle contract [21] for testing at NASA.

Table 7. Average Lot Release Data for 7050-T7451 Plate Material

Stock Size (inches)	Manufacturer (Lot No.)	Property	L (Sample count)	LT (Sample count)	ST (Sample count)
48.5x144x1.5	Pechiney	TUS, ksi	77.4 (1)	76.9 (1)	
	(75394/011)	TYS, ksi	68.0 (1)	68.3 (1)	
48.5x144x2.5	Pechiney	TUS, ksi	74.7 (14)	75.7 (14)	73.0 (14)
	(75436/011)	TYS, ksi	66.0 (14)	66.2 (14)	62.9 (14)
		K_{IC}, ksi$\sqrt{in}$	33.3 (L-T) (1)	27.9 (T-L) (1)	26.9 (S-T) (1)

5.2.2 Large Extrusions

Eleven extruded 7050-T74511 panels and eleven 6013-T6511X extruded panels were procured from Alcoa, with the exception that some of the 6013 panels were not artificially aged, so that they could be age/creep formed if desired. No lot release data was provided by Alcoa, though NASA material property testing of these materials is included in the test matrix.

The as-received panels measured 30 x 96 inches, and were integrally stiffened with the shape specified by Alcoa Drawing No. 470722. In order to achieve the 30 inch panel width, Alcoa extruded the panels in a “V” shape, as shown in Figure 20, and afterwards axially roll flattened, solution treated, stretched, roll flattened again, and aged the panels to the specified temper. Unfortunately, the roll flattening process is not mature, and did not produce sufficiently flat material for subsequent machining to the panel dimensions required for stiffened test panels.

Both at Long Beach and in Seattle, attempts were made to further flatten the panels by bump forming, which improved the flatness observably, but the dimensional quality was still deemed inadequate to machine large test panels. Material property characterization work continued at Boeing Seattle and NASA, but the large panels were dropped from the program.

5.2.3 7475-T351 Plate (Seattle Lot Buy)

The lot of 7475-T7351 plate shown on the test matrix was purchased under the Boeing Seattle contract.

Figure 20. As-Extruded Shape of IAS 7050-T74511 and 6013-T6511X Extrusions

5.3 Crack Turning Characterization

In this section, a second order crack turning theory is presented which includes the effects of fracture orthotropy. The fracture orthotropy is defined as the ratio of the transverse crack growth resistance to the longitudinal crack growth resistance, and varies depending on the regime of crack growth. Crack turning test data developed from Double Cantilever Beam (DCB) specimens is presented for 7050-T7451 plate, 7050-T76511 extrusion, 2324-T39 plate, and 7475-T7351 plate.

Coupon testing reveals a distinct difference in fracture paths resulting from stable fracture, as opposed to fatigue crack propagation, in a region of high positive T-stress. This is partially due to noted differences in fracture orthotropy in the fatigue and stable tearing regimes. Also the theoretical characteristic length pertaining to the second order theory, is postulated to be on the order of da/dN in the fatigue regime, and to reach a constant maximum value, r_c when fully developed stable tearing is reached. Thus the influence of the T-stress on the crack path tends to increase as the crack approaches the regime of stable tearing.

Crack paths predicted using the FRANC2D adaptive mesh finite-element code are compared to selected specimens, and correlation with observed crack paths is very encouraging.

5.3.1 Background

Crack turning has been identified as a potentially important crack arrest mechanism for aircraft structure [4, 9,10], and particularly integral structures [16] which are desirable from a low-cost manufacturing standpoint. This study is part of a larger program that addresses the feasibility of integral fuselage structure, and is intended to evaluate and characterize crack turning in candidate materials.

In integrally stiffened fuselage applications, a hypothetical crack centered on a stiffener can be made to turn as it approaches the adjacent stiffeners as shown in Figure 21, thus blunting and arresting the crack to provide fail safety. It is further believed that a turned crack will be inhibited with regard to fatigue crack growth through the adjacent stiffener when subsequently fatigue loaded. In order to take advantage of these behaviors, it is critical to understand and be able to predict crack trajectories in realistic structural environments.

As described in [16,27] crack turning in these situations can result from the presence of high T-stresses developed as part of the nonlinear response to internal pressurization. The Double Cantilever Beam (DCB) specimen has also been demonstrated capable of providing a K_I and T-stress environment comparable to that produced adjacent to stiffeners in a pressurized fuselage, and sufficient to turn a crack in isotropic materials. However, as will be shown,

the way a material is processed can result in a fracture toughness (particularly the plane stress fracture toughness) which is a strong function of crack orientation. In particular, metals tend to tear easiest parallel to the primary rolling direction (the T-L crack orientation). Because this fracture orthotropy can aid or inhibit crack turning phenomena, and because it was observed in candidate materials for integral fuselage structures, it is a key focus of this investigation.

The theories described are valid where the crack trajectory is dominated by the in-plane stress intensities, and propagation is dominated by mode I stress intensity, though the effect of mode II stress intensity is included. The effect of plate-bending stress intensities are beyond the scope of the present theoretical development, but are recommended for future study.

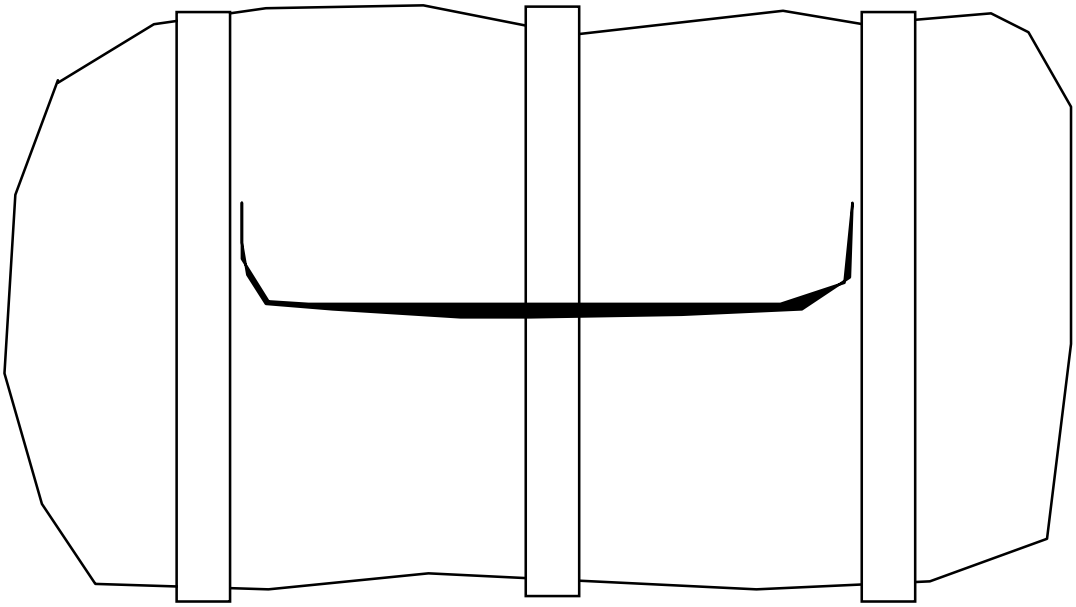

Figure 21. Crack Turning Enhanced Fail-Safety for the Two Bay Crack Case

5.3.2 Crack Turning Theory

5.3.2.1 Theoretical Development for Isotropic Case

Numerous theories have been advanced to explain crack turning behavior, but it is beyond the scope of this document to give a full history of the theoretical development. For the interested reader, an excellent survey of these theories and supporting test data is given by Zaal [28]. A more recent study by Shirmohamadi [29] classified crack turning theories into three basic approaches based on energy, stress, or stress intensity respectively. He also investigated two additional theories, a maximum strain approach, and a maximum void growth approach, but in the end, both authors favored some form of the maximum tangential stress criterion. The second-order theory potentially shows the best fit

with experimental observation, but requires an additional material parameter, the characteristic process zone width, r_c [7].

The mixed mode expression for the elastic stress field around a crack tip (Figure 22) is given by (truncating after the second term of the infinite expansion described by Williams [30])

$$\sigma_r = \frac{1}{\sqrt{2\pi r}}\cos\frac{\Delta\theta}{2}\left[K_I\left(1+\sin^2\frac{\Delta\theta}{2}\right)+\frac{3}{2}K_{II}\sin\Delta\theta-2K_{II}\tan\frac{\Delta\theta}{2}\right]+\frac{T}{2}\left(1+\cos 2\Delta\theta\right) \quad (5.3.2.1.1)$$

$$\sigma_\theta = \frac{1}{\sqrt{2\pi r}}\cos\frac{\Delta\theta}{2}\left[K_I\cos^2\frac{\Delta\theta}{2}-\frac{3}{2}K_{II}\sin\Delta\theta\right]+\frac{T}{2}\left(1-\cos 2\Delta\theta\right) \quad (5.3.2.1.2)$$

$$\sigma_{r\theta} = \frac{1}{2\sqrt{2\pi r}}\cos\frac{\Delta\theta}{2}\left[K_I\sin\Delta\theta+K_{II}\left(3\cos\Delta\theta-1\right)\right]-\frac{T}{2}\sin 2\Delta\theta \quad (5.3.2.1.3)$$

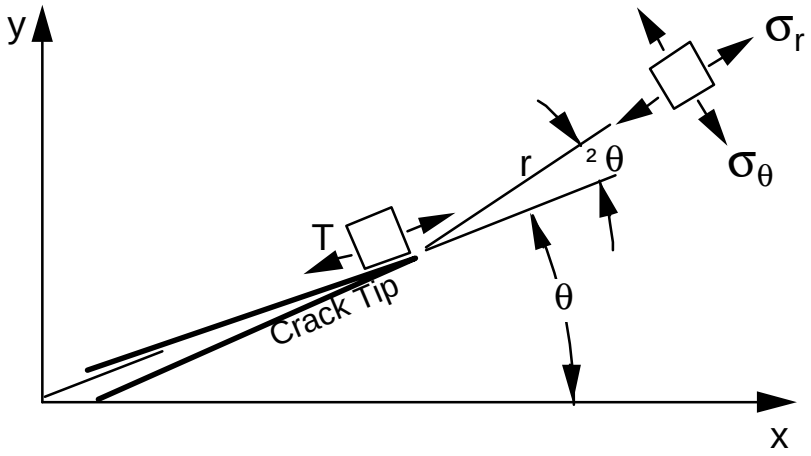

Figure 22. Crack Tip Coordinate and Stress Notation

Where K_I and K_{II} are the mode I and mode II stress intensity factors (Figure 23), and the T-stress is the far field stress component.

The classical first-order maximum circumferential stress theory, proposed by Erdogan and Sih [31] for isotropic materials, assumes that the crack would grow in the direction of maximum circumferential stress evaluated at the crack tip to obtain the crack turning angle as function of K_I and K_{II}. By differentiating the first

[7] The true physical significance of r_c is still unclear. One of the authors is presently investigating the hypothesis that r_c represents the distance ahead of the crack tip which marks the boundary of nonuniform through-the-thickness contraction (necking) for plane stress situations, and void growth for plain strain cases.

term in (5.3.2.1.2) and setting the derivative equal to zero (or, by setting $\sigma_{r\theta}$ =0) they obtained (shown slightly rearranged).

$$\frac{K_{II}}{K_I} = \frac{-\sin\Delta\theta_c}{(3\cos\Delta\theta_c - 1)} \qquad (5.3.2.1.4)$$

where $\Delta\theta_c$ is the instantaneous change in the angle of crack propagation. This expression predicts straight crack growth unless $K_{II} \neq 0$, as in asymmetric loading or in the case of a perturbed crack.

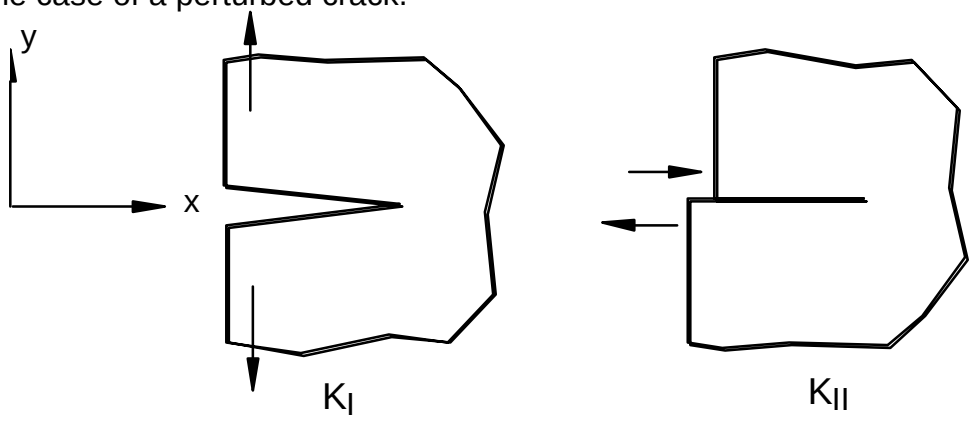

(both modes shown with positive sense)

Figure 23. Illustration of Mode I and Mode II Intensity Factors

Williams and Ewing [32] proposed that the crack would propagate in the direction of maximum tangential stress evaluated at a material specific distance r_c ahead of the crack tip. They proposed that the second term in the crack tip stress field expansion be included. Finnie and Saith [33] corrected the formulation of Williams and Ewing for the angled crack problem, and Kosai, Kobayashi and Ramulu [34] later derived a more general formulation of the same second order theory by forcing the $\Delta\theta$ derivative of (5.3.2.1.2) to zero at $r=r_c$ to obtain

$$\frac{K_{II}}{K_I} = \frac{-2\sin\frac{\Delta\theta_c}{2}}{(3\cos\Delta\theta_c - 1)}\left[\cos\frac{\Delta\theta_c}{2} - \frac{8}{3}\frac{T}{K_I}\sqrt{2\pi r_c}\cos\Delta\theta_c\right] \qquad (5.3.2.1.5)$$

Note that according to this expression, the crack may turn with sufficient T-stress even if K_{II} =0. In this case equation (5.3.2.1.5) yields $\Delta\theta_c > 0$ only if Finnie and Saith's inequality is satisfied.

$$r_c > r_o = \frac{9}{128\pi}\left(\frac{K_I}{T}\right)^2 \qquad (5.3.2.1.6)$$

where, for T>0, r_o represents the distance forward of the crack tip at which the angle of maximum tangential stress becomes non-zero. In Figure 24, equation (5.3.2.1.5) is plotted in normalized format using the dimensionless parameter

$$\bar{T} \equiv \frac{8}{3}\frac{T}{K_I}\sqrt{2\pi r_c} = \frac{T}{|T|}\sqrt{\frac{r_c}{r_o}} \qquad (5.3.2.1.7)$$

Equation (5.3.2.1.5) can be rewritten in terms of $\bar{T}$

$$\bar{T} = \frac{\sin\Delta\theta_c + \frac{K_{II}}{K_I}(3\cos\Delta\theta_c - 1)}{2\sin\frac{\Delta\theta_c}{2}\cos\Delta\theta_c} \qquad (5.3.2.1.8)$$

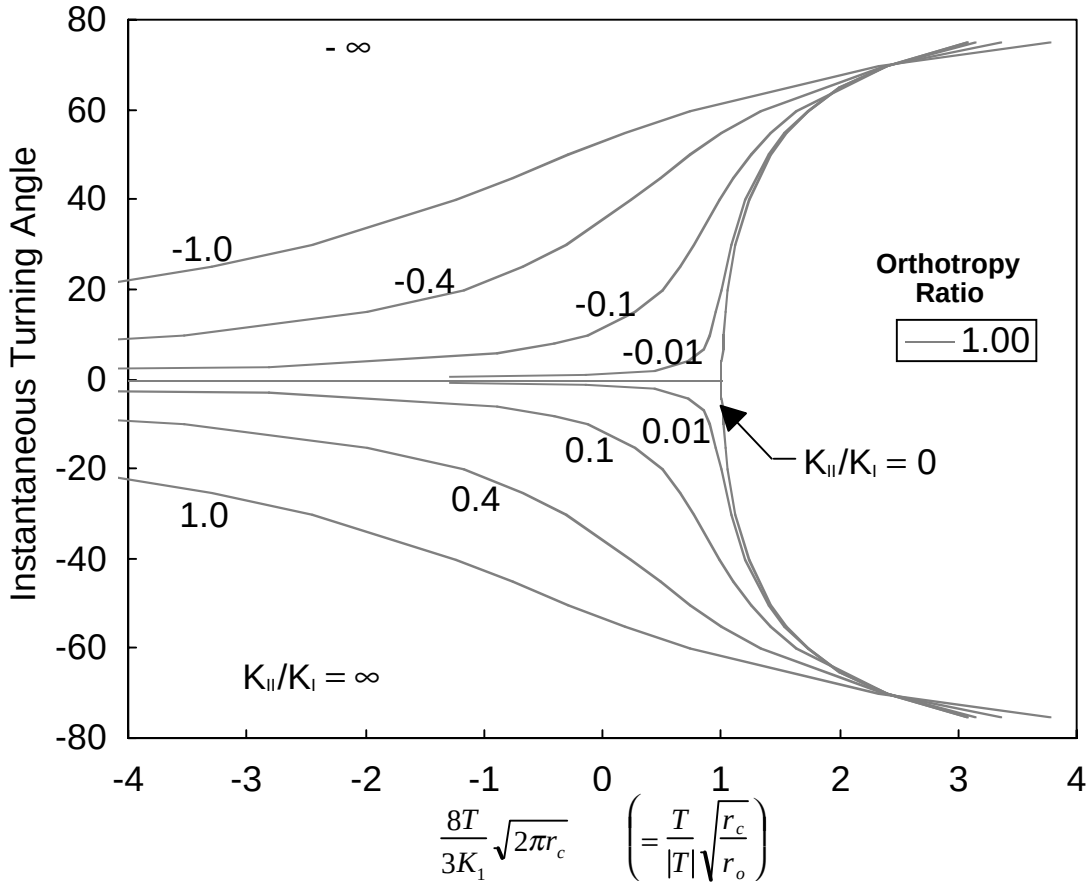

Figure 24. Normalized Crack Turning Plot for Isotropic Material Based on the Formulation of Kosai et al [31]

From Figure 24, straight crack growth is predicted only for the case where $K_{II}=0$, and $r_o > r_c$. As r_o approaches r_c, the path becomes very sensitive to small amounts of K_{II}, much in the same way that the out-of-plane deflection of a simply

supported plate in compression is sensitive to initial imperfections. The bifurcation point at $\overline{T}=1$ is analogous to the buckling bifurcation.

Note that the first order theory of Erdogan & Sih is actually a special case of equation (5.3.2.1.5) with either $r_c=0$ or T=0. The instantaneous change in crack growth direction is influenced by T only if $r_c>0$. However, Cotterel and Rice [35] showed that a perturbation in the crack path of an otherwise self similar crack directed by a first order theory would tend to diverge if T>0, and revert toward self-similar crack growth if T<0. The increased K_{II} sensitivity near the bifurcation point in the second order theory would be expected to accelerate such divergence. In the regime where $r_c > r_o$, the second order theory requires no perturbation to turn the crack. In practice, cracks growing along a self-similar path with a negative r_o gradient have been observed to turn due to natural perturbations before reaching the bifurcation point [16,27], but the turning radius gets smaller as r_o approaches r_c.

5.3.2.2 Proposed 2nd Order Theory for Materials with Fracture Orthotropy

Up to this point, the discussion has been limited to the case of isotropic materials. Many materials, such as wrought metal products, are virtually isotropic elastically, but have a preferred direction of crack propagation resulting from the manner in which the material is processed. Typically for rolled sheet and plate products, the crack growth resistance is maximum for growth across the rolling direction (90°) and minimum for growth parallel to the rolling direction (0°).

Following the work of Buczek and Herakovich and Boone et al [36, 37], we can approximate the crack growth resistance as an elliptical function[8] of θ as shown in Figure 25 in polar coordinates.

$$K_c(\theta)^2\left(\frac{\cos^2\theta}{K_c(0°)^2}+\frac{\sin^2\theta}{K_c(90°)^2}\right)=1 \qquad (5.3.2.2.1)$$

where K_c is the applicable crack growth resistance, which is a function of the orientation of the crack tip, and is a material property consistent with the regime of crack growth (more discussion on this in the next section).

[8] Actually, the form used by Buczek and by Boone for tear resistance was not a true ellipse, but replaced the square exponent on the K terms with an exponent of -1. An ellipse was chosen here, though it differs little numerically from the results obtained if an exponent of -1 were used for low levels of orthotropy. One could choose a different value for the exponent that best fits the material properties.

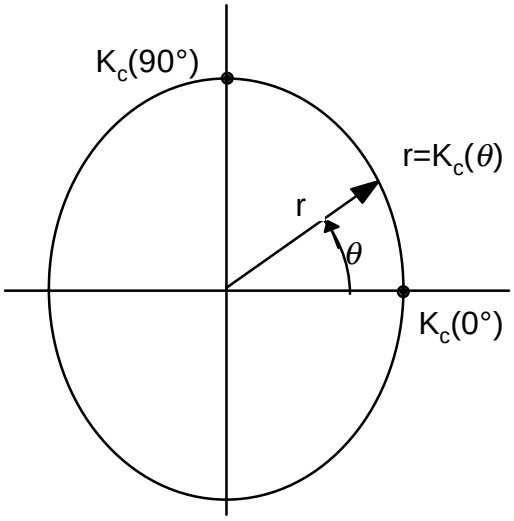

Figure 25. Assumed Elliptical Function Describing crack Growth Resistance as a Function of Orientation for Materials with Fracture Orthotropy

The elliptical assumption collocates to $K_c(0)$ and $K_c(90)$ values, and the derivatives at those points infer the orthogonal symmetry of the fracture properties, which would be expected due to the symmetry of the rolling process.

Let us define the normalized crack growth resistance as

$$\bar{K}(\theta) \equiv \frac{K_c(\theta)}{K_c(0^o)} \qquad (5.3.2.2.2)$$

which varies between 1 and $\bar{K}_m$, where $\bar{K}_m$ is the fracture orthotropy ratio defined by

$$\bar{K}_m \equiv \frac{K_c(90^0)}{K_c(0^o)} = \frac{K_{c\,L-T}}{K_{c\,T-L}} \qquad (5.3.2.2.3)$$

(The metallurgical L-T and T-L grain orientation notation is also indicated for reference). We can rewrite (5.3.2.2.1) in normalized form evaluated at the new kink orientation $(\theta + \Delta\theta)$ as

$$\bar{K}(\theta + \Delta\theta) = \sqrt{\frac{1}{\cos^2(\theta + \Delta\theta) + (1/\bar{K}_m{}^2)\sin^2(\theta + \Delta\theta)}} \qquad (5.3.2.2.4)$$

Whereas in the isotropic crack turning theory, we maximized tangential stress, Buczek and Herakovich [36] suggested that the crack path in anisotropic materials would follow the maximum of the ratio of the tangential stress to the

crack growth resistance. For our case, this ratio is given by combining (5.3.2.1.2) and (5.3.2.2.4)

$$\frac{\sigma_\theta(\Delta\theta)}{\overline{K}(\theta+\Delta\theta)} = \sqrt{\cos^2(\theta+\Delta\theta)+\left(\frac{1}{\overline{K}_m{}^2}\right)\sin^2(\theta+\Delta\theta)}\left[\frac{\cos\frac{\Delta\theta}{2}}{\sqrt{2\pi rc}}\left[K_I\cos^2\frac{\Delta\theta}{2}-\frac{3}{2}K_{II}\sin(\Delta\theta)\right]+T\sin^2(\Delta\theta)\right] \tag{5.3.2.2.5}$$

Maximizing with respect to $\Delta\theta$ we obtain in normalized form

$$\overline{T} = \frac{\sin\Delta\theta_c+\frac{K_{II}}{K_I}(3\cos\Delta\theta_c-1)-2\Psi\left[\frac{K_{II}}{K_I}\sin\Delta\theta_c-\frac{1}{3}(1+\cos\Delta\theta_c)\right]}{\sin\left(\frac{\Delta\theta_c}{2}\right)(2\cos\Delta\theta_c-\Psi\sin\Delta\theta_c)} \tag{5.3.2.2.6}$$

where

$$\Psi = \frac{\beta\sin 2(\theta+\Delta\theta_c)}{1+\beta\cos 2(\theta+\Delta\theta_c)} \quad \text{and} \quad \beta = \frac{\overline{K}_m{}^2-1}{\overline{K}_m{}^2+1} \tag{5.3.2.2.7}$$

Of potential interest is the alternate form,

$$\Psi = \frac{1}{2}\sin 2(\theta+\Delta\theta_c)\left(1-\frac{1}{\overline{K}_m{}^2}\right)\left[\overline{K}(\theta+\Delta\theta_c)\right]^2 \tag{5.3.2.2.8}$$

Note that for $\overline{K}_m$=1, Ψ =0, and (5.3.2.2.6) reverts to the isotropic theory of (5.3.2.1.8).

Equation (5.3.2.2.6) is plotted in Figures 26a-26c illustrating various fracture orthotropy ratios and crack orientations, illustrating how the orthotropy influences the location and nature of the bifurcation. As would be expected, a crack propagating in the direction of least crack growth resistance requires a higher K_{II} or T stress to alter its course. Conversely, a self-similar crack propagating along the direction of maximum crack growth resistance may turn in a compressive T stress environment given sufficient fracture orthotropy.

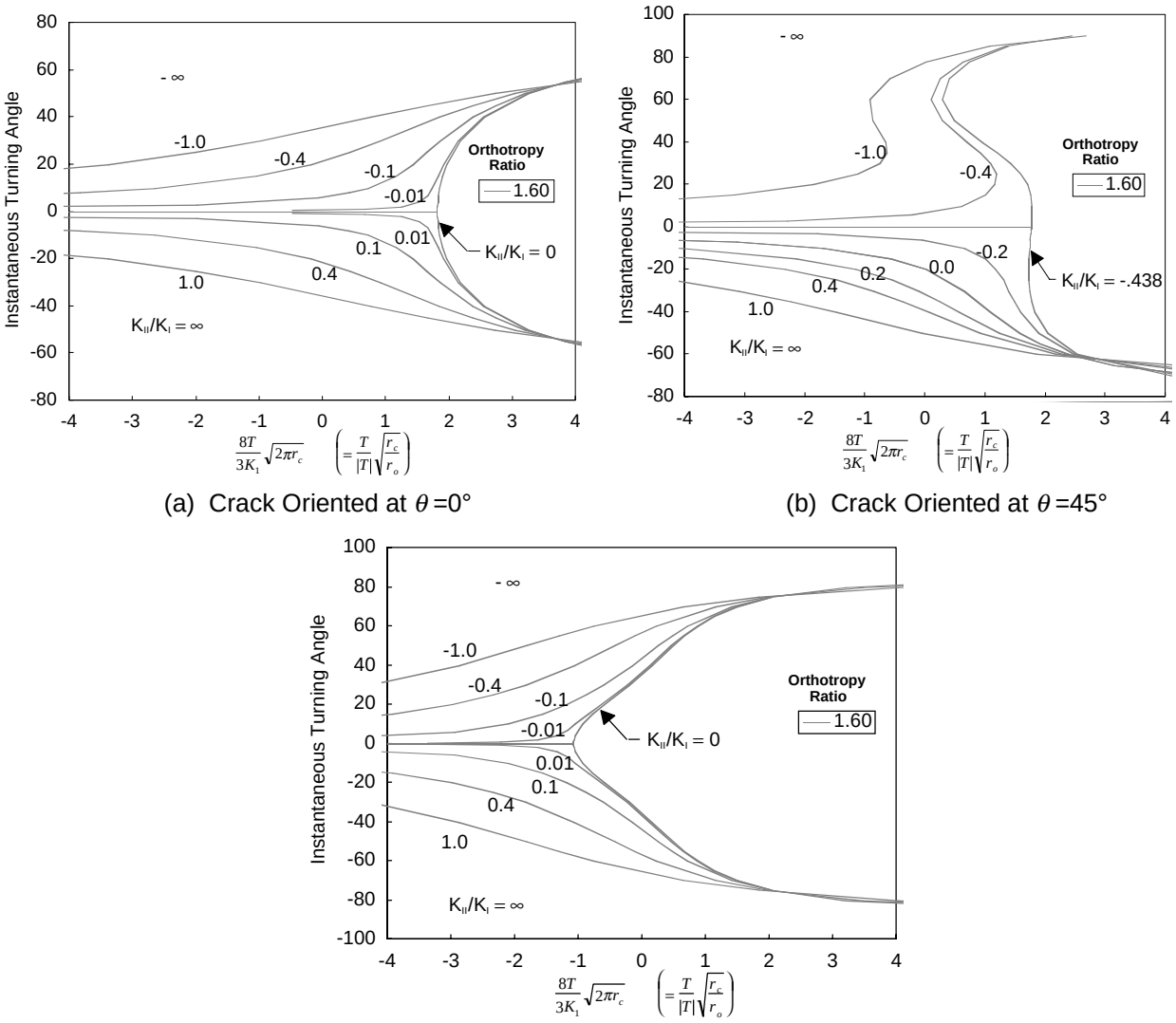

(a) Crack Oriented at θ=0°

(b) Crack Oriented at θ=45°

(c) Crack Oriented at θ=90°

Figure 26. Normalized Crack Turning Plots for an Elastically Isotropic Material with Fracture Orthotropy $\bar{K}_m$=1.6, Various Crack Orientations

In order to derive an expression for the value of $\bar{T}$ where the bifurcation occurs, we examine the limiting case of (5.3.2.2.6)

$$\lim \Delta\theta \to 0, \quad \bar{T} = \frac{2}{\Delta\theta}\left(\frac{K_{II}}{K_I} + \frac{2}{3}\Psi(\theta + \Delta\theta)\right) \qquad (5.3.2.2.9)$$

Note that the theory only predicts straight growth where $\bar{T}$ is below the bifurcation value and

$$\frac{K_{II}}{K_I} = \left(\frac{K_{II}}{K_I}\right)_{crit} = -\frac{2}{3}\Psi_o \qquad (5.3.2.2.10)$$

Where Ψ_o is defined as Equation (5.3.2.2.7) evaluated at $\Delta\theta$ =0. Note that if K_{II}/K_I exceeds this value, then $\Delta\theta_c$ <0. The bifurcation value of $\bar{T}$ is obtained when we assume that (5.3.2.2.10) is satisfied and continue with the limit, from which we obtain

$$\bar{T}_{crit} = 1+\frac{4}{3}\left(\Psi_o^{\,2} + \frac{2\beta(\beta+\cos 2\theta)}{(1+\beta\cos 2\theta)^2}\right) \qquad (5.3.2.2.11)$$

The 2nd-order theory with fracture orthotropy as given by Equation (5.3.2.2.6) has been implemented into a modified version of the Cornell University fracture simulation code, FRANC2D.

5.3.2.3 Material Fracture Parameters

In order to utilize the second order orthotropic theory, the characteristic length, r_c, and the fracture orthotropy ratio, $\bar{K}_m$, must be known for the material being analyzed. Part of the purpose of this investigation is to develop an understanding of these properties and develop test methods to determine them empirically.

5.3.2.3.1 Discussion Regarding the Characteristic Length, r_c

In the literature three approaches have been used to determine the value of the characteristic length r_c. When the isotropic 2nd order theory was first introduced [32,33], the authors merely selected a value for r_c, which resulted in a good match with crack kink angle data from Plexiglas specimens. In Reference [34], r_c was estimated for 2024-T3 and 7075-T6 aluminum alloys to be approximately equal to the length of microcrack branches observed along the crack faces (about 1.5 mm, or 0.06 inches). In references [16,27] an attempt was made to measure the r_o value at the kink bifurcation point, at which point r_c=r_o. The value obtained by this method for 2024-T3 aluminum was r_c=0.05 inches, correlating fairly well with [34]. In all cases these determinations were made for stably tearing cracks.

One of the disturbing things about the maximum stress theory, particularly in the case of stably tearing cracks, is that the applicable plastic zone sizes are typically substantially larger than the values obtained for r_c. Thus, the linear elastic basis of all the above formulations is known to be invalid. Some authors [34,38] have applied the maximum stress theory to elastic-plastic models, showing only a moderate effect of plasticity in the absence of the T-stress. One can argue that the fracture processes within the plastic zone are, within the bounds of traditional

linear elastic fracture mechanics, controlled by the surrounding elastic field parameters K_I, K_{II}, and T. The theory presented above then becomes a linear elastic surrogate for the real nonlinear process.

Consider a (quasistatically) propagating crack in a biaxially loaded infinite sheet as shown in Figure 27. Assume that the crack is long enough that the fracture is well characterized by linear elasticity, and the far field stress normal to the crack, σ_∞, which varies as required to keep the crack critical, is small compared to the transverse stress, σ_T, thus $\sigma_T = \sigma_\infty + T \approx T$. Since the crack is propagating, we assume that K_I is equal to a critical stress intensity, K_c. The effect of the T stress on K_c is generally assumed to be small so that a plot of K_c as a function of σ_T might be represented approximately as a straight line as shown in Figure 28.

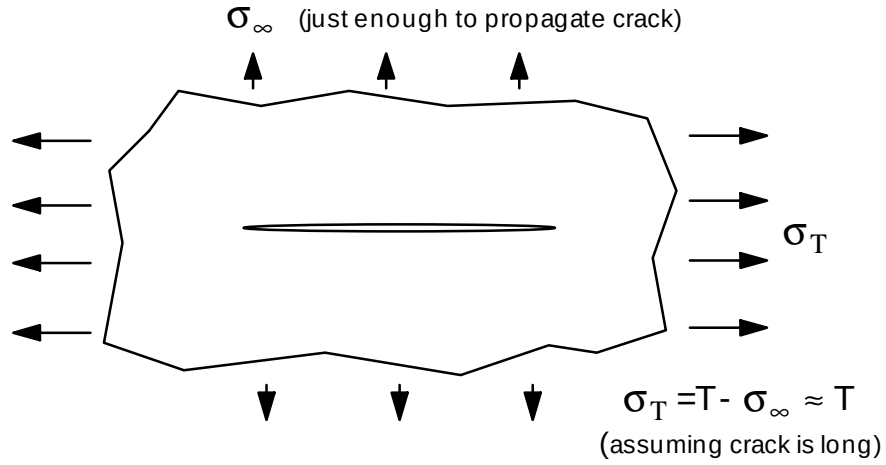

Figure 27. Unperturbed Crack Propagating in Infinite Sheet with Biaxial Loading

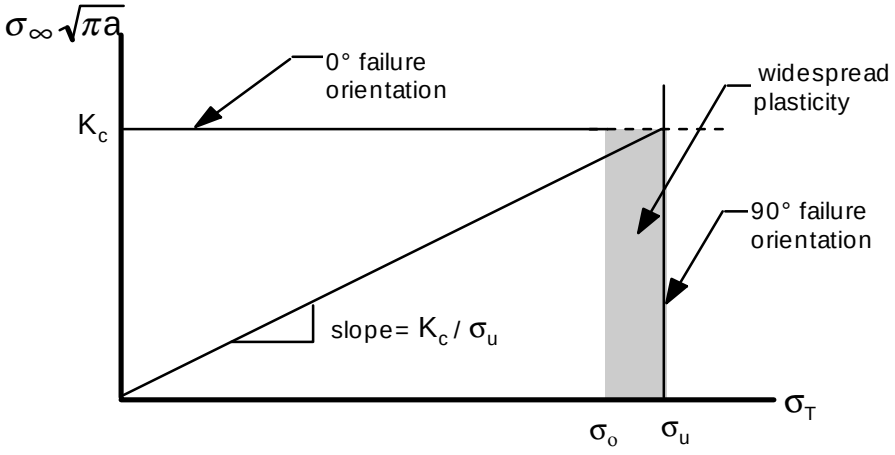

Figure 28. Critical Conditions for Crack Propagation/Failure of Unperturbed Crack Case

It is now observed that if σ_T approaches the ultimate tensile strength of the material, σ_u , the crack cannot continue to propagate along a straight path, but the panel must fail approximately perpendicular to the crack. Presumably this failure will show up as a bifurcating or turning crack. While a perturbed crack may well turn at lower transverse stress levels, even a perfectly unperturbed propagating crack must turn as σ_T approaches σ_u. As we reach this regime, K and T lose their significance as widespread plasticity develops, though for ideally elastic-plastic materials we can in principle move arbitrarily close to this point (as a--> ∞), and yet remain in the small scale yielding regime. Thus it does not seem unreasonable to consider the ratio K_c/σ_u (or K_c/σ_o) as a first approximation of the critical ratio of K_I/T at which crack turning must occur for unperturbed cracks. If we equate this to the bifurcation point in the 2nd order theory, then we can compute an estimate of r_c from (5.3.2.1.6) for isotropic materials[9].

$$r_c \approx \frac{9}{128\pi}\left(\frac{K_c}{\sigma_u}\right)^2 \qquad (5.3.2.3.1)$$

For aluminum alloys ranging from 60-160 ksi√in plain stress fracture toughness (at the top of the R-curve), and 60-90 ksi ultimate strength, this gives r_c values ranging between 0.01 inches for brittle high strength alloys to 0.16 inches for low strength, very tough alloys. Kosai [8] estimated that for aluminum alloys 2024-T3 and 7075-T6, r_c was on the order of 0.06 inches, based on measurements of crack branches on the flanks of rapid fractures. While this value falls within the calculated range, one would expect r_c values to be very different for these materials based on Equation (5.3.2.3.1) . Nevertheless, it does appear to give the right order of magnitude. One should also bear in mind that the accuracy of the literature values is also unknown.

One implication of (5.3.2.3.1) is that for materials with fracture orthotropy, r_c values are a function of crack orientation. For materials which are nearly isotropic with regard to modulus and tensile strength, but which exhibit significant fracture orthotropy (like 7050 plate, as will be described in later sections), if we assume the proportionality of (5.3.2.3.1) still holds for orthotropic materials (even if the coefficient is wrong), we can approximate

$$\frac{\sqrt{r_c(90°)}}{\sqrt{r_c(0°)}} \approx \frac{K_c(90°)}{K_c(0°)} = K_m \qquad (5.3.2.3.2)$$

$$\frac{\sqrt{r_c(\theta)}}{\sqrt{r_c(0°)}} \approx \frac{K_c(\theta)}{K_c(0°)} = \overline{K}(\theta) \qquad (5.3.2.3.3)$$

[9] The present development has obvious shortcomings, and is the object of continuing research under a NASA grant to Cornell University.

If we were to rederive the orthotropic theory with the assumption that the crack will propagate in the direction of maximum tangential stress at a distance r_c which varies per equation (5.3.2.3.3), we would obtain results comparable (though not identical) to the present theory, with r_c varying instead if K_c.

One further implication of (5.3.2.3.1) is relevant in a situation such as monotonic fatigue crack growth where the crack is propagated at low stress intensities. In this case, the equivalent to K_c in the above heuristic discussion is the maximum cyclic stress intensity factor, K_{max}, which in the slow crack growth range is typically an order of magnitude less than the fracture toughness. Based on proportionality suggested by equation (5.3.2.3.1), we can write

$$r_{cf} \approx r_c \left(\frac{K_{max}}{K_c} \right)^2 \qquad (5.3.2.3.3)$$

Thus the characteristic length, r_{cf}, for slow fatigue crack growth would be orders of magnitude smaller than the stable tearing value, and would transition into the constant r_c value as the applied stress intensity approaches K_c.

With regard to the stable tearing value of r_c, a more accurate determination than (5.3.2.3.1) is desirable, since it plays an important role in determining whether a running crack will turn or not as it approaches a stiffener or other structural discontinuity. An attempt will be made to extract it from test data in the coming sections.

5.3.2.3.2 Discussion Regarding $\overline{K}_m$

Like r_c ,it is proposed that the aspect ratio of the crack growth resistance ellipse, $\overline{K}_m$, should also be defined in accordance with the conditions of fracture. The constant value of $\overline{K}_m$ during stable tearing would be the ratio of maximum R-curve toughnesses from L-T and T-L specimens. During fatigue crack growth, $\overline{K}_m$ could logically be taken as the ratio of the ΔK values in each orientation which would result in a given crack growth rate (thus $\overline{K}_m$ is a function of the crack growth rate). For the present, we shall treat this as a hypothesis, and see if test results confirm it.

5.3.2.3.3 Calculation of the T Stress

Evaluating equation (5.3.2.1.1) at the crack flanks, we obtain in the limit

$$\sigma_r = -K_{II}\sqrt{\frac{2}{\pi r}} + T \quad \text{at } \theta = +\pi$$
$$\sigma_r = +K_{II}\sqrt{\frac{2}{\pi r}} + T \quad \text{at } \theta = -\pi \qquad (5.3.2.3.4)$$

In the absence of K_{II}, the T stress is simply the crack flank stress parallel to the crack. If K_{II} is non-zero, the T stress is the average of the upper and lower crack flank stresses evaluated in back of the crack tip. In practice, the T stress should be evaluated as close as practical to the crack tip, since higher order terms and geometry effects neglected here can contribute to the crack flank stresses as one moves away from the crack tip.

For the purpose of this study, T stresses are evaluated using a modified version of FRANC2D, a Cornell developed fracture simulation code. Following a method similar to that proposed by Al-Ani and Hancock [39], the stress along the crack flank is calculated from the relative displacements of the crack flank nodes. Because the crack flank is a traction free surface, and assuming plane stress through the thickness, the stress parallel to the crack may be calculated directly from Hook's law. For the mesh shown in Figure 5,

$$\sigma_{flank} = \frac{\Delta l}{l} E \qquad (5.3.2.3.5)$$

where l is the node spacing along the crack flank, and Δl is the relative displacement of the two nodes along the crack axis consistent with small displacement theory. We can thus rewrite the expression in terms of the nodal coordinates, x and y, and the corresponding nodal displacements, u and v, with the crack tip orientation, θ, defined as in Figure 22.

$$\sigma_{flank} = \frac{\frac{(u_2 - u_1)}{\cos\theta} + \frac{(v_2 - v_1)}{\sin\theta}}{\frac{(x_2 - x_1)}{\cos\theta} + \frac{(y_2 - y_1)}{\sin\theta}} E \qquad (5.3.2.3.6)$$

In practice, erroneous values will typically be obtained if the crack flank stress is calculated from the element immediately adjacent to the crack due to numerical errors close to the singularity. Analysis of various problems showed that for an eight-element rosette of six-node quarter point elements, the displacements from the first and second nodes trailing the crack tip generally yielded the best results. However, one other problem inherent in FRANC2D is that the meshing algorithm requires a finite initial crack-opening gap, which has been observed to adversely affect T stress calculations. A comparison of results obtained by the nodal displacement method for the DCB geometry with results from other investigators

using higher accuracy methods is given in Table 8, showing an error for this geometry of about (negative) ten percent.

Table 8. Comparison of the Stress Biaxiality Ratio, $\beta = T\sqrt{\pi a}/K_I$ for a DCB Specimen Given by Various Investigators (h/w=.2, a/w=0.5)

Leevers & Radon [40] (1976)	Cardew et al [41] (1985)	Kfouri [42] (1985)	Chen/Krause et al P-code [43] (1998)	FRANC2D Crack Flank Nodal Displ. (Present)
2.942	2.829	2.956	2.951	2.638

Recent efforts at Cornell University [43] have implemented this method and superior methods into FRANC3D, a three-dimensional fracture code, which does not have the finite gap problem, resulting in far better accuracy. However, due to the late timing of these developments, the test correlation results given herein do not reflect these improvements.

5.3.3 Crack Turning Test Program

A total of 23 crack turning tests was run in the overall IAS program[10], with fabrication and testing split between Boeing Seattle and Boeing Long Beach contracts as shown in Table 6. Where appropriate, Seattle data [21] is included in this section for completeness. A detailed test matrix of all crack turning specimens tested under the IAS program is given in Table 9.

5.3.3.1 Test Specimens

A Double Cantilever Beam (DCB) specimen (Figure 29) was chosen of dimensions h=2.4, and w=12, similar to a previous crack turning investigation [16, 27]. This geometry was sized to avoid excessive plasticity for high strength aluminum alloys, and results in high T stresses, similar in magnitude to those which may occur on a pressurized fuselage as a crack approaches a stiffener.

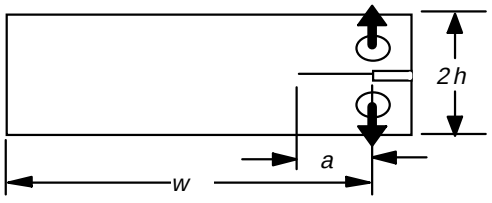

Figure 29. DCB Specimen Geometry

[10] Additional 14 specimens were also fabricated of 7050-T74511 Extrusion, and await testing. Specimen rc-TL-7050-1 showed the orthotropy of 7050 extrusion to be very high (See Figure 41).

Table 9. Crack Turning Specimen Test Matrix

DCB Specimens from 1.5 inch 7050-T7451 Plate (Pechiney Lot #75394/011)

Specimen ID	Nominal Starter Notch Length (in)	Precracking,R=.05, 5 Hz. Max Load (lb)	Comments
rc-LT-15-2	2.00	320/variable	Fatigue Crack to Failure
rc-LT-15-3	6.50	71	
rc-LT-15-4	2.00	165	
rc-LT-15-5	3.00	129	
rc-LT-15-6	7.00	65	
rc-LT-15-7	4.50	98	
rc-LT-15-8	5.00	94	
rc-LT-15-9	5.50	84	
rc-LT-15-10	6.00	78	
rc-TL-15-1	6.50	78	
rc-TL-15-2	2.00	320/variable	Fatigue Crack to Failure
rc-TL-15-4	2.00	165	
rc-TL-15-5	3.00	129	
rc-TL-15-6	4.00	106	
rc-TL-15-7	4.50	98	
rc-TL-15-8	5.00	94	
rc-TL-15-9	5.50	84	
rc-TL-15-10	6.00	78	

DCB Specimens from 2324-T39, 7475-T7351, and 7050-T76511 (Remnants)

Specimen ID	Nominal Starter Notch Length (in)	Precracking, R=.05, 5 Hz. Max Load (lb)	Comments
rc-TL-2324-1	5.00	113	cut from .95 inch plate
rc-TL-2324-2	5.00	113	cut from .95 inch plate
rc-TL-7475-1	5.00	113	cut from 1.75 inch plate
rc-TL-7475-2	5.00	113	cut from 1.75 inch plate
rc-TL-7050-1	5.00	113	cut from 1D0158B Extrusion

The stress intensity factor for the DCB specimen may be calculated using the following equation from Gross and Srawley [45].

$$K = \frac{P}{t}\sqrt{\frac{12}{h}}\left(\frac{a}{h} + .687\right) \qquad (5.3.3.1.1)$$

This equation was found to agree within 1% down to a/h=0.5 with a full range expression given by Foote and Buchwald [46], though the grip geometry doubtless has an effect at this extreme. To avoid the influence of the opposite end of the current specimen, Equation (5.3.3.1.1) should not be used for crack lengths exceeding 7.2 inches. The T stress can be evaluated in terms of r_o for the current specimen aspect ratio (h/w=0.2) using an equation given in [16]

$$\frac{r_o}{h} = .0114\left[1 + .7214\left(\frac{h}{a}\right) + .2879\left(\frac{h}{a}\right)^2\right]^2 \qquad (5.3.3.1.2)$$

for crack lengths ranging within $1 \leq a/h \leq 3$. Thus the present specimen is capable of achieving combinations of K_I and T corresponding to r_o values ranging from $0.110 \geq r_o \geq .044$.

The eighteen specimens fabricated at Boeing Seattle were made according to the DCB geometry of Figure 30 with a nominal thickness of 0.090 inches, and were made from IAS lots of 1.5 inch 7050-T7451 plate (see Tables 6, 7). The plate specimen blanks were cut through the midplane before machining to obtain two specimens per blank, and all the plate specimens were excised adjacent to the original exterior faces of the plate.

The five specimens fabricated at Boeing Long Beach were taken from remnants of non-IAS lots of various materials. The decision to run these tests was made after the adverse fracture orthotropy of 7050-T7451 plate was confirmed, in order to assess the fracture orthotropy of other candidate alloys in preparation for design of the longitudinal crack panel. These alloys included 7050-T76511 extrusion, 7475-T7351 plate, and 2324-T39 plate. The specimens were statically equivalent to the geometry of Figure 30 (h=2.4, w=12), but with modified loading and knife edge configurations as shown in Figure 31. The nominal machined thickness for these specimens was also 0.090 inches.

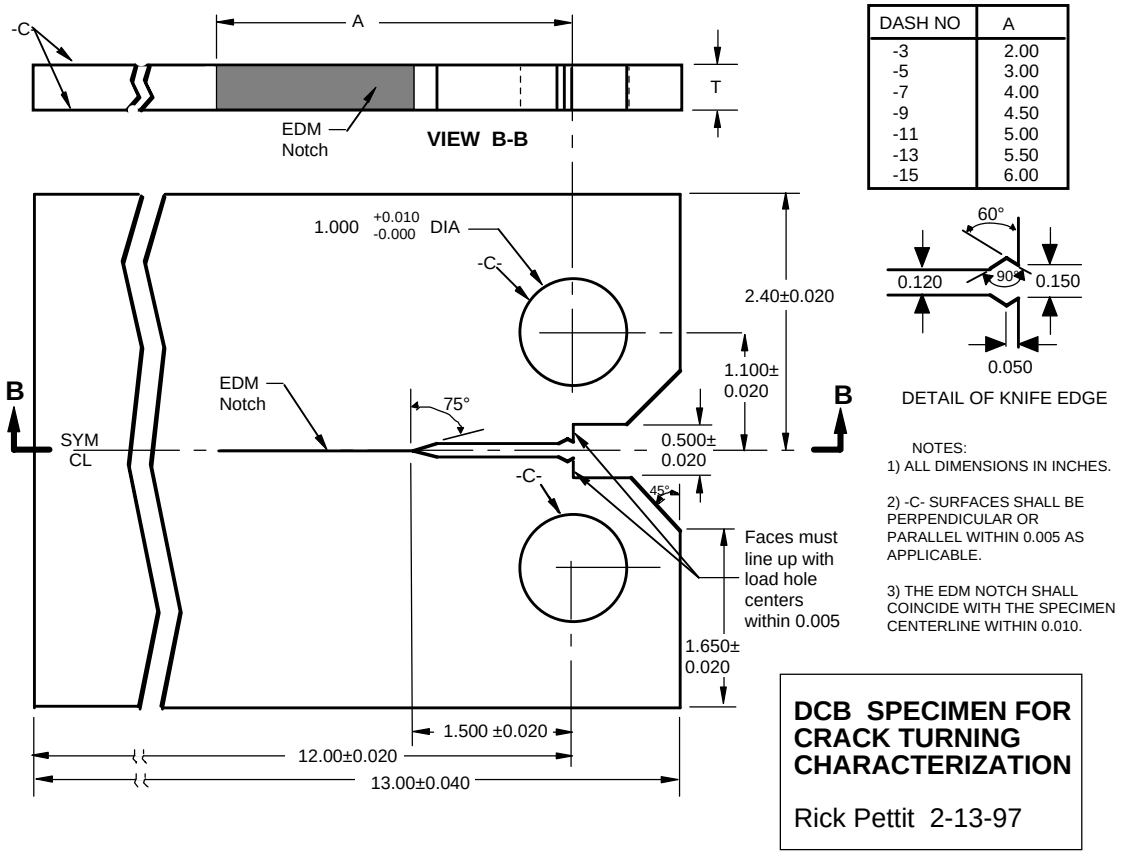

Figure 30. Double Cantilever Beam (DCB) Specimen

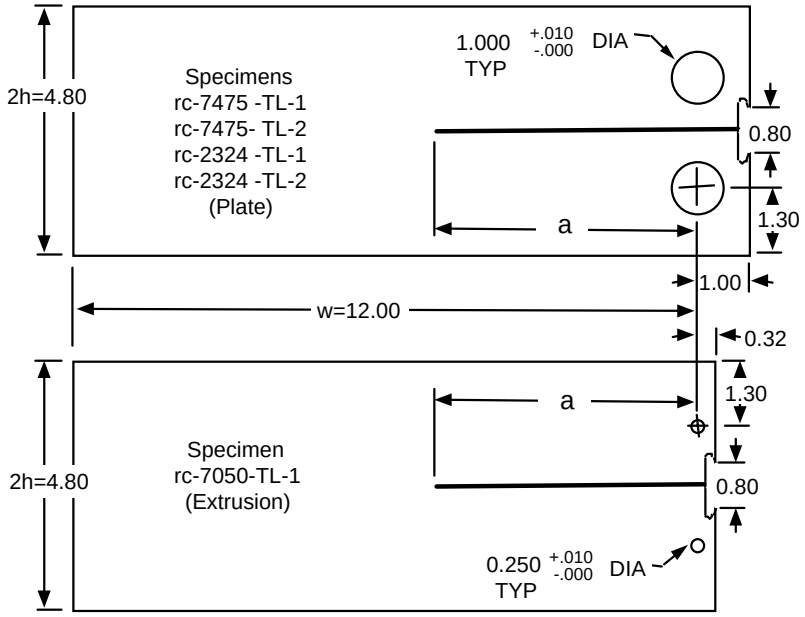

Figure 31. Modified DCB Configurations for 7050-T6511, 7475-T7351, and 2324-T39 Specimens

5.3.3.2 Test Procedure

The test procedure for DCB/SDCB specimens is as follows.

1. Wipe specimen clean. Use solvent as required, but avoid removing specimen ID.
2. Measure thickness within 0.0001, *w* within .001, and *2h* within .001 inches, and initial notch length, *a*, within .004 (specimens may be lightly scribed as required to facilitate measurements).
3. Mount specimen in MTS or equivalent test machine using 4" compact specimen grips. Fill space between clevises and specimen faying surface with shims to restrict out-of-plane movement of the specimen. Make sure shim thickness is distributed symmetrically about the specimen, and that the top and bottom clevises are shimmed to match.
4. Fatigue precrack at load indicated in table, R=0.05, 5 hz, for at least 0.04 inches growth (try 70,000 cycles). A higher starting precrack load is permissible subject to the precracking guidelines of ASTM E647-93. Total growth should be at least 0.04 but not exceed 0.10 inches. Measure and record final crack length on both sides of specimen.
5. Mount anti-buckling guide over specimen and gently finger tighten screws to achieve sliding fit. Support underside of anti-buckling guide so that its weight is not carried through the loading pins, leaving sufficient clearance at the specimen lower edge to permit specimen deflection during testing.
6. Mount Clip gage (or extensometer) at notches provided along the load line. Gage shall be calibrated to utilize its maximum range (up to 0.5 inches if possible).
7. Load specimen at 0.05 in/min, recording load, clip gage, and stroke data at 1.0 samples/sec. Continue until specimen failure or until deflection is limited by interference with the anti-buckling guide. NOTE: Continue testing even if deflection exceeds clip gage range.

5.3.3.2 Results

A detailed summary of specimen test results is given in Tables 10-12. Load/Crack Opening Displacement (COD) plots for DCB/SDCB fracture specimens are given in Figures 32-34 within the range of deflection capability of the clip gage used. Specimen photographs are presented in Figures 35-38. Crack paths for all specimens are given in Figures 39-41.

Table 10. Summary of 7050-T7451 Static Crack Turning Tests

Specimen ID	Crack Front Type After Initiation	Thickness (in)	w (in)	2h (in)	a_n (notch) (in)	a_i (precrack) (in)	Crack Length to Center of Turning Radius, a_o (in)			Minimum Crack Path Radius (in)			r_o (a_i) (in)	r_o (a_o) (in)	Max Load (lb)
							Side A	Side B	Avg	Side A	Side B	Avg			
rc-LT-15-3	slant	0.0923	11.997	4.800	6.472	6.532	6.43	6.58	6.50	0.10	0.07	0.09	0.047	0.047	879
rc-LT-15-4	slant	0.0922	11.997	4.797	2.006	2.048	2.47	2.45	2.46	0.35	0.30	0.33	0.137*	0.107	2379
rc-LT-15-5	slant	0.0924	11.996	4.799	2.989	3.031	3.18	3.18	3.18	0.30	0.25	0.28	0.084	0.080	1863
rc-LT-15-6	V shear	0.0917	11.996	4.799	6.961	7.002	6.92	6.92	6.92	0.15	0.15	0.15	0.045	0.045	896
rc-LT-15-7	slant	0.0922	11.996	4.799	4.500	4.546	4.74	4.77	4.76	0.15	0.05	0.10	0.058	0.057	1467
rc-LT-15-8	V shear	0.0926	11.998	4.800	5.007	5.054	4.99	4.96	4.98	0.20	0.20	0.20	0.054	0.055	1200
rc-LT-15-9	slant	0.0917	11.950	4.799	5.536	5.584	5.66	5.74	5.71	0.25	0.15	0.20	0.051	0.050	1178
rc-LT-15-10	slant	0.0910	11.998	4.801	5.999	6.042	6.18	6.13	6.16	0.10	0.07	0.09	0.049	0.048	1122
rc-TL-15-1	V shear	0.0925	11.997	4.800	6.492	6.536	6.53	6.51	6.52	0.35	0.45	0.40	0.046	0.047	960
rc-TL-15-4	slant	0.0931	12.000	4.800	2.006	2.050	Gradual Turning						0.137*	n/a	1858
rc-TL-15-5	slant	0.0919	11.994	4.798	3.000	3.047							0.083	n/a	1427
rc-TL-15-6	slant	0.0935	12.000	4.800	3.998	4.050							0.064	n/a	1298
rc-TL-15-7	V shear	0.0922	11.996	4.799	4.502	4.557	4.62	4.71	4.67	0.35	0.30	0.33	0.058	0.057	1254
rc-TL-15-8	slant	0.0910	11.997	4.805	4.997	5.047	Gradual Turning						0.054	n/a	1066
rc-TL-15-9	slant	0.0924	11.985	4.799	5.512	5.557	Straight Crack Growth						0.051	n/a	1003
rc-TL-15-10	slant	0.0920	11.997	4.799	6.002	6.047	Straight Crack Growth						0.049	n/a	943

* r_o values calculated slightly out of bounds of validity of Equation (5.3.3.1.2)

Table 11. Summary of 7050-T7451 Fatigue Crack Turning Tests

Specimen rc-LT-15-2	Crack Front Type	Thickness (in)	w (in)	2h (in)
	flat	0.0917	11.996	4.799

Load (lb)	ΔN	x ave (in)	y ave (in)	Curvilinear Δa avg	Δa/ΔN (in/cycle)	Curvilinear a (in)	ΔK (ksi√in)	Theta (deg)
(notch)	0	2.004	0.000	2.004		2.004		
320	5000	2.031	0.000	0.027	5.40E-06	2.031	6.99	0.00
320	4000	2.059	0.000	0.027	6.87E-06	2.059	7.04	0.00
368	6000	2.126	0.003	0.068	1.13E-05	2.126	8.20	2.12
368	6000	2.197	0.000	0.071	1.18E-05	2.197	8.36	-2.02
368	8000	2.284	-0.001	0.087	1.09E-05	2.284	8.53	-0.66
368	15000	2.475	0.007	0.191	1.27E-05	2.475	8.83	2.25
331	4000	2.512	0.006	0.037	9.25E-06	2.512		-0.77
350	10000	2.626	0.022	0.116	1.16E-05	2.627	Crack	7.71
350	10000	2.755	0.052	0.133	1.33E-05	2.760	Curves	13.30
350	5000	2.830	0.073	0.077	1.55E-05	2.837		15.39
350	5000	2.903	0.095	0.076	1.53E-05	2.914		17.13
350	5000	2.981	0.132	0.086	1.72E-05	3.000		25.08
350	5000	3.063	0.175	0.093	1.87E-05	3.093		27.80
350	5000	3.163	0.230	0.114	2.28E-05	3.207		28.59
350	5000	3.259	0.290	0.113	2.27E-05	3.320		32.22
350	5000	3.367	0.377	0.138	2.76E-05	3.458		38.82
350	3000	3.432	0.438	0.090	2.99E-05	3.548		43.20
350	3000	3.499	0.514	0.101	3.35E-05	3.649		48.63
350	3000	3.582	0.616	0.132	4.40E-05	3.781		51.00
350	2000	3.633	0.729	0.124	6.18E-05	3.904		65.61
331	1000	3.659	0.772	0.050	5.02E-05	3.954		58.84
265	4000	3.690	0.889	0.122	3.04E-05	4.076		74.99
212	4000	3.722	0.975	0.091	2.28E-05	4.167		69.48
212	2000	3.749	1.044	0.074	3.70E-05	4.241		68.99
212	2000	3.764	1.147	0.105	5.23E-05	4.346		81.75
212	2000	3.808	1.337	0.195	9.75E-05	4.541		76.96
212	500	3.853	1.471	0.141	2.82E-04	4.682		71.18
159	1000	3.855	1.507	0.037	3.65E-05	4.718		87.65
Failure		3.895	1.700	0.197	n/a	4.916		78.15
Failure		3.948	1.900	0.207	n/a	5.122		75.29
Failure		3.998	2.200	0.304	n/a	5.427		80.54

Table 11. Summary of 7050-T7451 Fatigue Crack Turning Tests (Continued)

Specimen rc-TL-15-2					Crack Front Type	Thickness (in)	w (in)	2h (in)
					flat	0.0925	11.995	4.798
Load (lb)	ΔN	x ave (in)	y ave (in)	Curvilinear Δa avg	Δa/ΔN (in/cycle)	Curvilinear a (in)	ΔK (ksi√in)	Theta (deg)
(notch)	0	2.003	0.000	2.003		2.003		
368	4000	2.035	0.000	0.032	8.00E-06	2.035	--	0.00
368	6000	2.115	0.000	0.080	1.33E-05	2.115	8.09	0.00
368	10000	2.254	0.000	0.140	1.40E-05	2.254	8.33	0.00
368	10000	2.403	0.000	0.149	1.49E-05	2.403	8.64	0.00
368	10000	2.570	0.000	0.167	1.67E-05	2.570	8.99	0.00
368	10000	2.756	0.000	0.186	1.86E-05	2.756	9.37	0.00
368	3000	2.813	-0.003	0.058	1.92E-05	2.813	9.63	-2.99
368	7000	2.969	-0.003	0.156	2.23E-05	2.969	9.86	0.00
368	5000	3.082	-0.003	0.113	2.25E-05	3.082	10.16	0.00
368	6000	3.232	-0.003	0.150	2.50E-05	3.232	10.44	0.00
368	6000	3.402	-0.003	0.170	2.83E-05	3.402	10.79	0.00
368	4000	3.522	-0.003	0.121	3.01E-05	3.522	11.11	0.00
368	5000	3.682	0.019	0.161	3.22E-05	3.683	11.41	7.68
368	4000	3.820	0.019	0.138	3.45E-05	3.821	11.73	0.00
331	4000	3.916	0.019	0.096	2.40E-05	3.917	10.78	0.00
331	6000	4.086	0.019	0.171	2.84E-05	4.088	11.04	0.00
331	7000	4.319	0.035	0.234	3.34E-05	4.321	11.44	3.93
331	4000	4.457	0.053	0.139	3.47E-05	4.460	11.80	7.66
331	4000	4.604	0.065	0.147	3.69E-05	4.607	12.08	4.67
331	4000	4.753	0.085	0.150	3.76E-05	4.758	12.37	7.65
331	4000	4.915	0.126	0.167	4.18E-05	4.925		14.20
331	3000	5.049	0.162	0.139	4.62E-05	5.063	Crack	14.84
314	1000	5.084	0.175	0.038	3.78E-05	5.101	Curves	20.11
314	2000	5.170	0.198	0.089	4.43E-05	5.190		15.06
314	2000	5.255	0.231	0.092	4.59E-05	5.282		21.40
314	2000	5.339	0.268	0.092	4.59E-05	5.373		23.77
314	1000	5.383	0.295	0.051	5.09E-05	5.424		31.35
283	1000	5.404	0.308	0.025	2.51E-05	5.449		31.16
283	3000	5.501	0.372	0.116	3.88E-05	5.566		33.62
283	3000	5.623	0.466	0.154	5.12E-05	5.719		37.73
283	2000	5.730	0.558	0.141	7.06E-05	5.861		40.69
283	1000	5.775	0.627	0.083	8.27E-05	5.943		56.60
283	1000	5.829	0.730	0.116	1.16E-04	6.059		62.44
212	1000	5.844	0.745	0.021	2.12E-05	6.080		45.00
212	2000	5.883	0.830	0.094	4.68E-05	6.174		65.35
212	1000	5.894	0.903	0.074	7.44E-05	6.248		81.11
170	1000	5.913	0.919	0.025	2.45E-05	6.273		39.21
170	2000	5.949	1.011	0.099	4.93E-05	6.371		68.90
170	1500	5.977	1.124	0.117	7.80E-05	6.488		75.90
170	1000	6.008	1.280	0.158	1.58E-04	6.647		78.90
170	276	6.014	1.375	0.096	3.47E-04	6.742		86.40
170	121	6.025	1.468	0.093	7.70E-04	6.836		82.91

Table 12. Summary of Static Crack Turning Tests of DCB Specimens of 2324-T39, 7475-T7351, and 7050-T76511 Alloys

Specimen ID	Crack Front Type After Initiation	Thickness (in)	w (in)	2h (in)	a_n (notch) (in)	a_i (precrack) (in)	r_o (a_i) (in)	Max Load (lb)
rc-TL-2324-1	slant	0.0858	12.001	4.800	4.988	5.053	0.054	1044
rc-TL-2324-2	slant	0.0915	11.999	4.792	4.995	5.049	0.054	1169
rc-TL-7475-1	slant*	0.0906	12.003	4.792	4.992	5.049	0.054	1359
rc-TL-7475-2	V shear	0.0898	11.999	4.793	4.999	5.048	0.054	1331
rc-TL-7050-1	slant	0.0985	11.997	4.804	4.993	5.054	0.054	1306

* The crack passed through a small region of V shear (about 0.08 inches) adjacent to the precrack, but completed most of the turn as a slant crack.

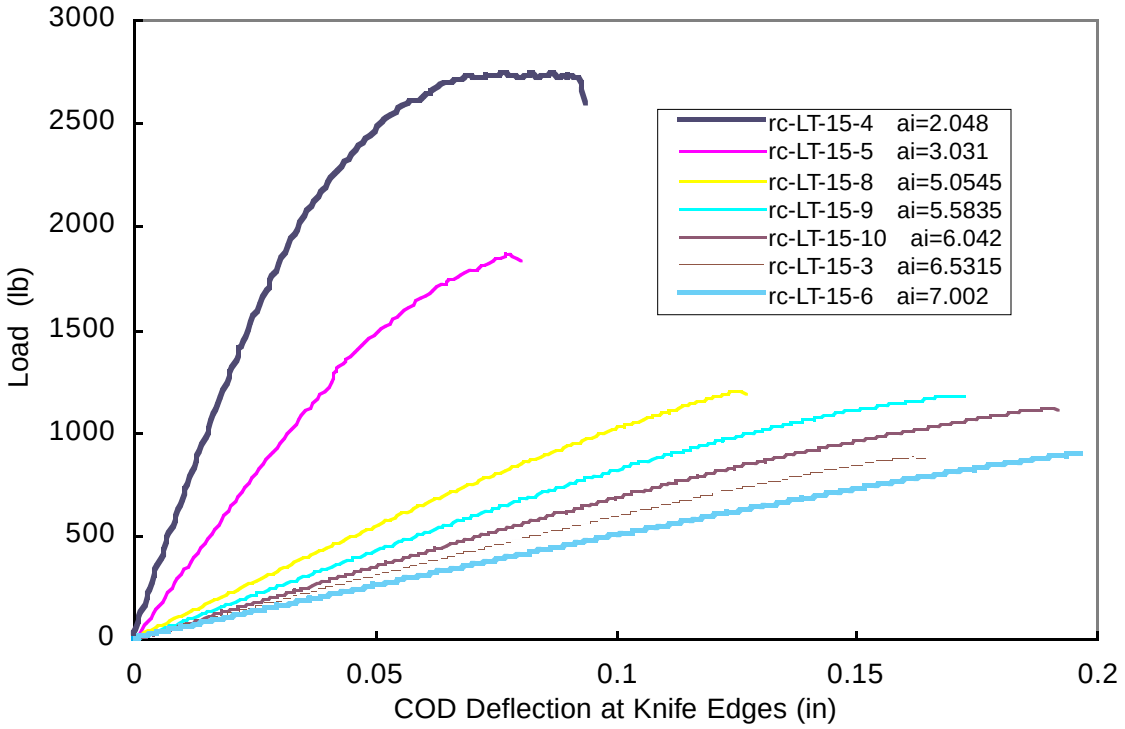

Figure 32. L-T Load/Crack Opening Deflection (COD) Curves for 7050-T7451 DCB Specimens

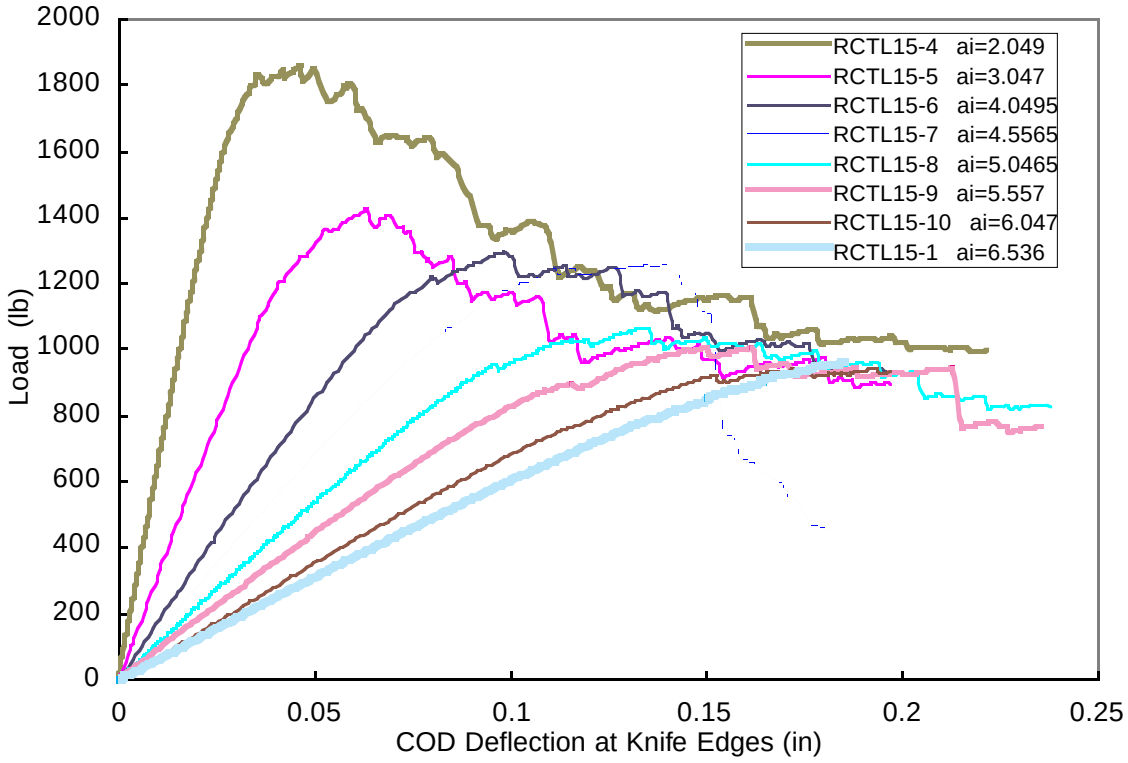

Figure 33. T-L Load/Crack Opening Deflection (COD) Curves for 7050-T7451 DCB Specimens

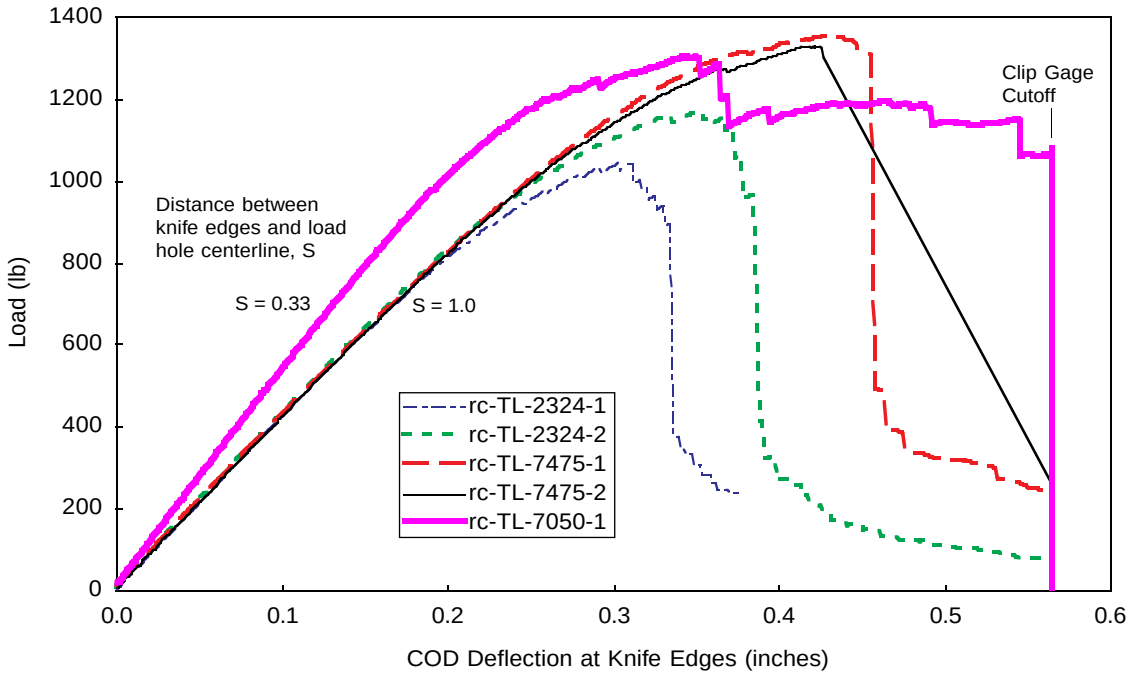

Figure 34. T-L Load vs. Crack Opening Displacement (COD) for DCB Specimens of 2324-T39, 7475-T7351, and 7050-T76511 Alloys

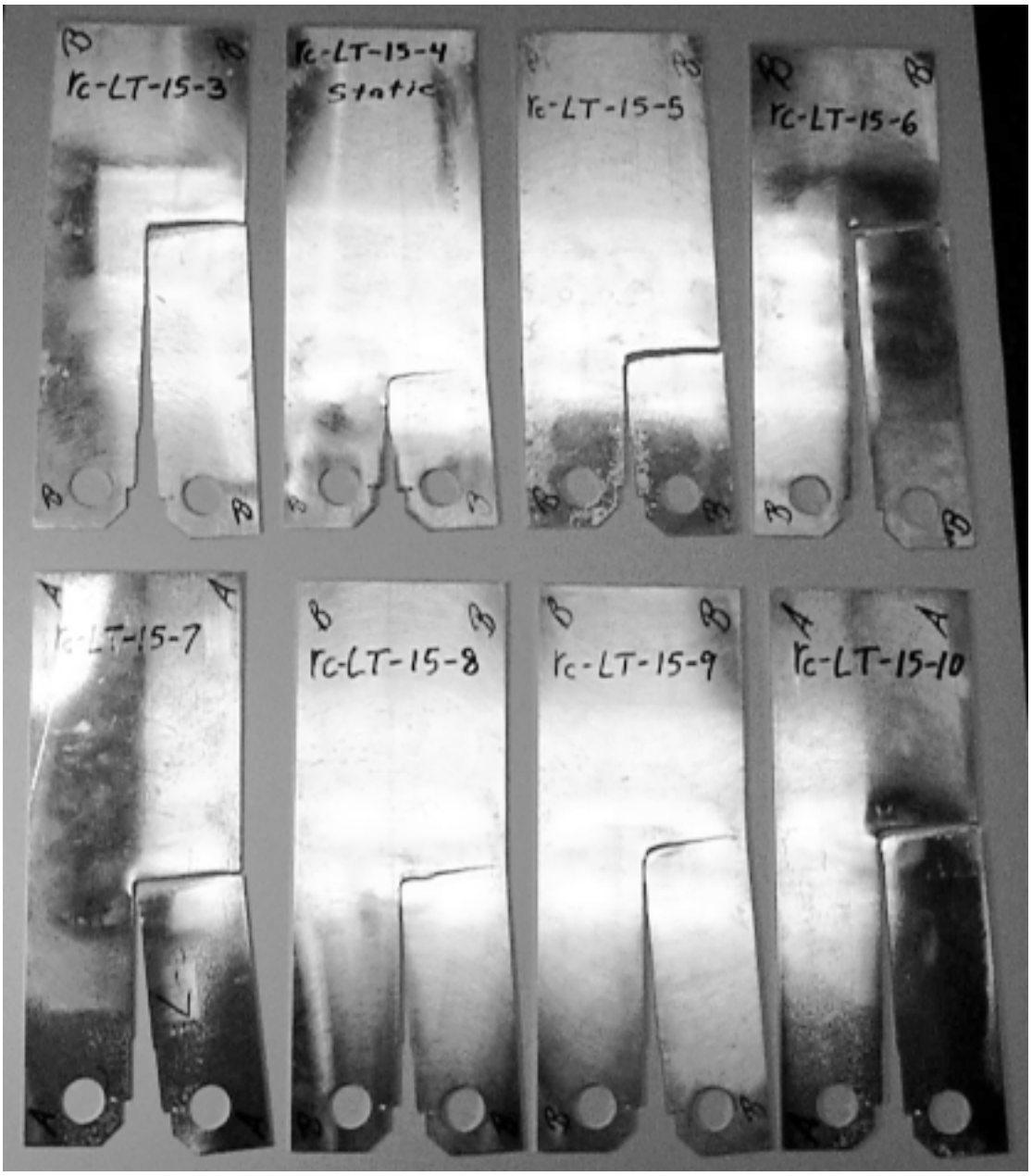

Figure 35. Specimen Photographs, 7050-T7451 Static Crack Turning Specimens, L-T Orientation

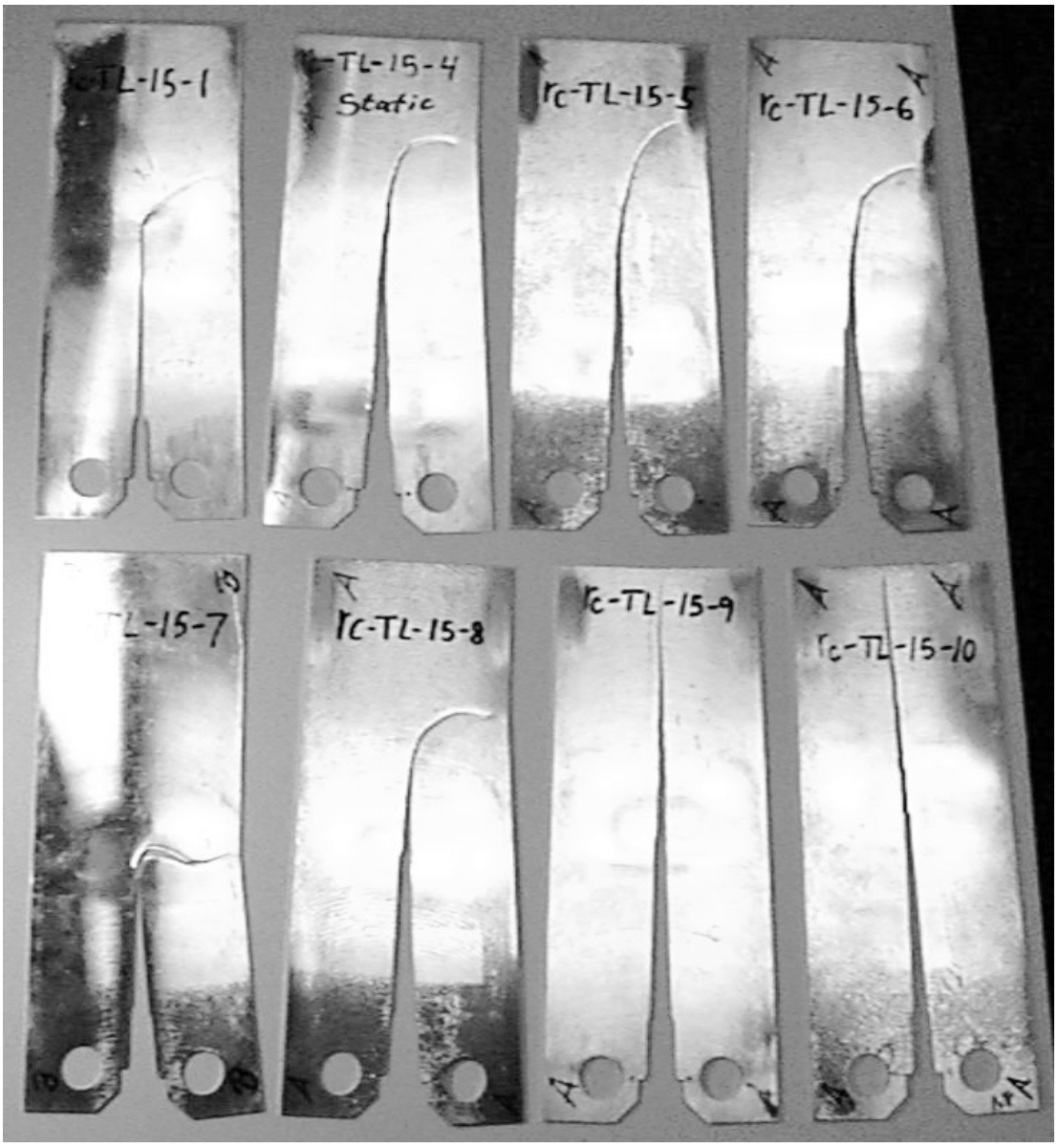

Figure 36. Specimen Photographs, 7050-T7451 Static Crack Turning Specimens, T-L Orientation

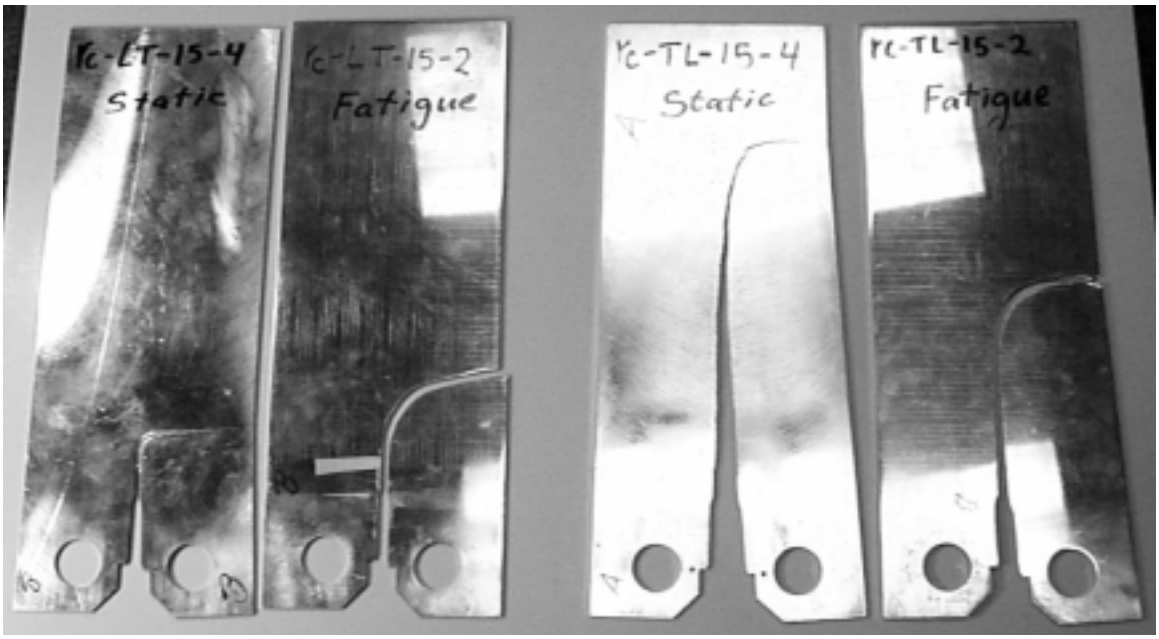

Figure 37. Specimen Photographs, 7050-T7451 Fatigue Crack Turning Specimens, Shown with Static Specimens with Same Starting Crack Length (2 inches)

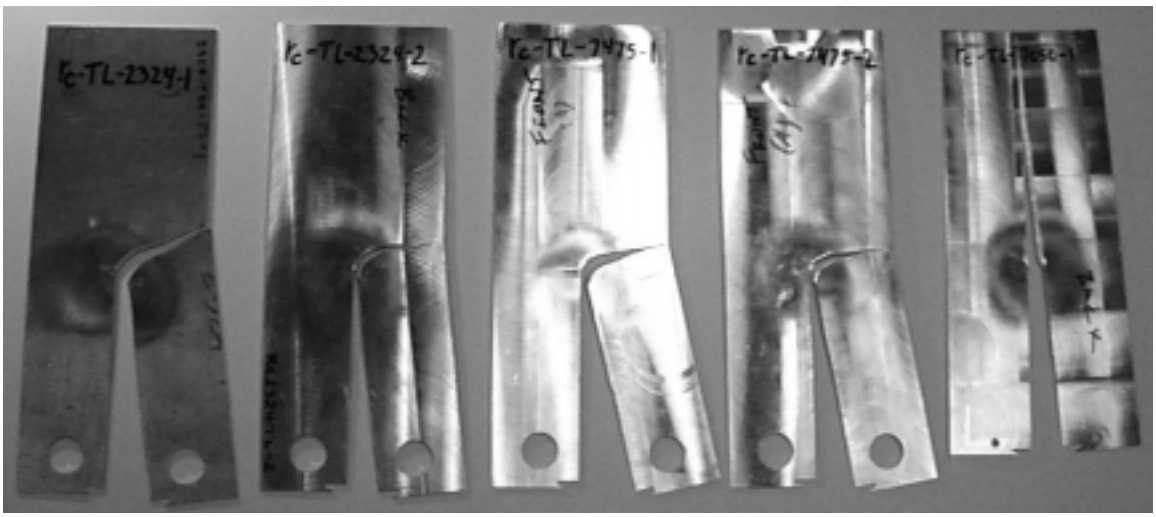

Figure 38. Specimen Photographs, 2324-T39, 7475-T7351, and 7050-T76511 Alloy Static Crack Turning Specimens (T-L Orientation)

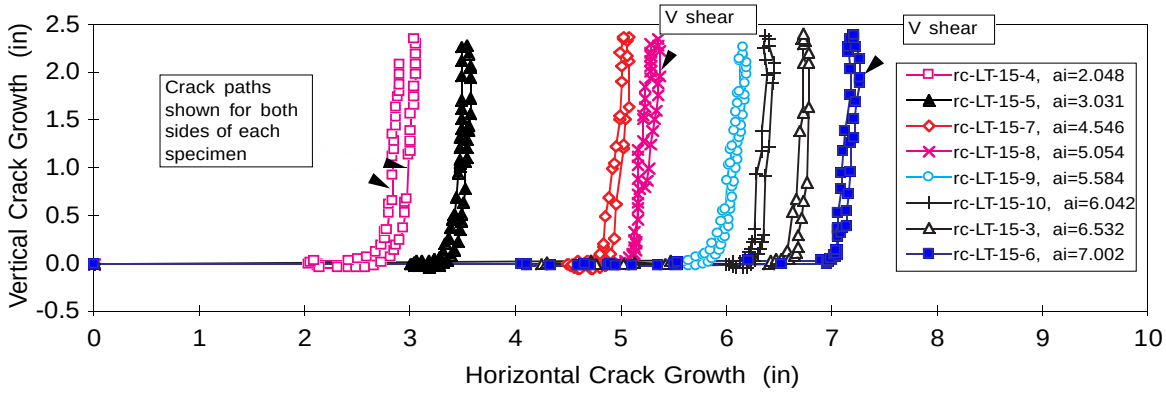

Figure 39. Crack Paths, 7050-T7451 Crack Turning Specimens (L-T Orientation)

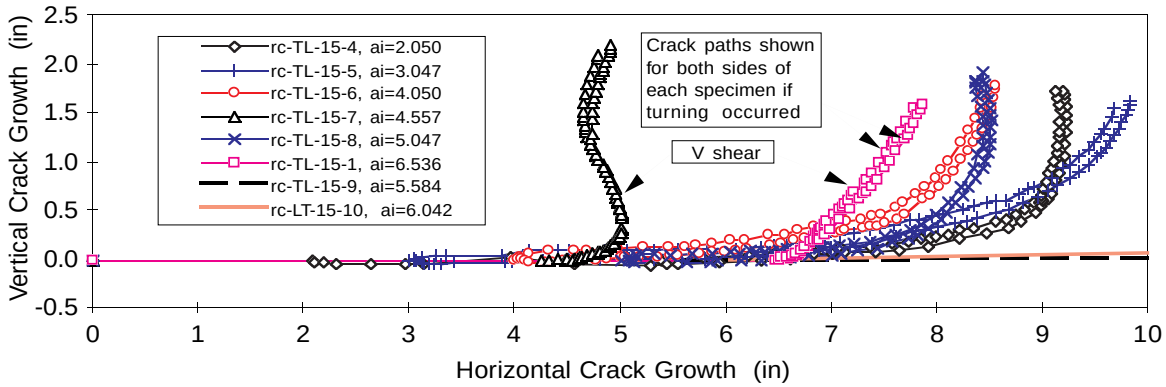

Figure 40. Crack Paths, 7050-T7451 Crack Turning Specimens (T-L Orientation)

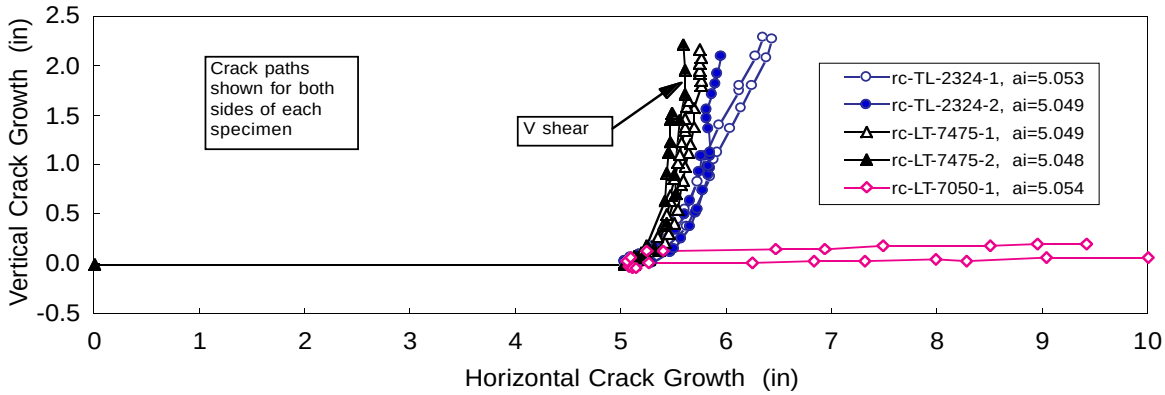

Figure 41. Crack Paths, 2324-T39 Plate, 7475-T7351 Plate, and 7050-T76511 Extrusion Alloy Crack Turning Specimens (T-L Orientation)

5.3.3.2.1 7050-T7451 Plate

A first observation is that the 7050 plate specimens behaved very differently in the L-T and T-L orientations. For static tearing, the L-T specimens transitioned from the flat notch to a slant crack, and then turned quite sharply to a nearly right angle within less than an inch of the initial notch tip. Most of the T-L specimens transitioned from flat to slant, but then took several inches to turn, if they turned at all[11]. Since the specimens were otherwise geometrically comparable except for the grain orientation, the difference in crack path could only be attributed to the orthotropy of the fracture properties of the 7050 material.

Based on NASA 24 inch wide R-curve tests [44] for the 1.5 inch plate material machined down to 0.06 inches thickness, the L-T and T-L fracture toughnesses at a crack extension of about 0.4 inches are 99 and 76 ksi$\sqrt{in}$, giving a $\overline{K}_m$ value for stable tearing of about 1.3. This was the highest toughness value obtained for the T-L testing, but the NASA L-T data continued out to a maximum value of 108 ksi$\sqrt{in}$. Because several of the T-L crack turning specimens exhibited a significant amount of straight growth, it was possible to reduce R-curve data from load/deflection data, as presented in Figure 42. Details regarding the data reduction method are given in Appendix Section A.2.

[11] A few specimens (noted in Tables 9-11) transitioned to a "V" shaped crack front instead of a slant crack, and turned more sharply than those which cracked with a slanted crack front--regardless of orientation. This "V-shear" tearing mode appears to always result in turning, and is not characterized well by the present theory. Jim Newman (NASA LaRC, Mechanics of Materials Branch) has suggested that this metallurgical phenomenon be studied and exploited as a crack turning mechanism.

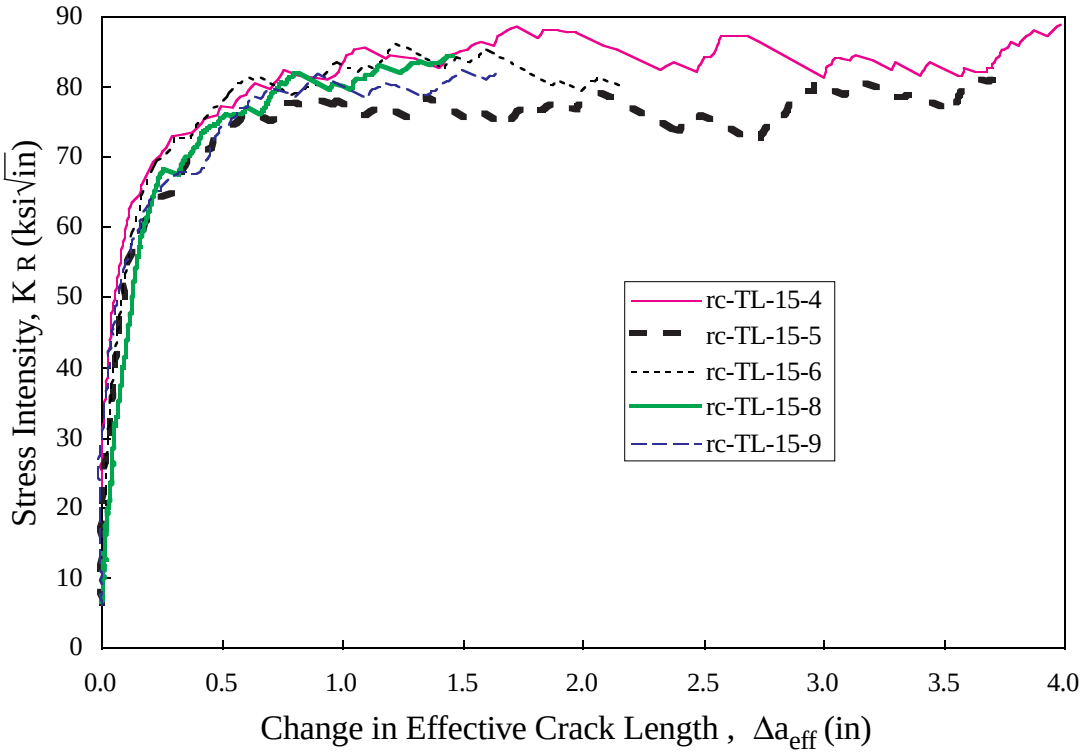

Figure 42. R-Curve Data Extracted from T-L 7050-T7451 Crack Turning Specimens in the Straight Crack Growth Region.

Since the R-curves were taken from load-deflection data, all the points were not equally critical, as the specimen tore in small finite crack extensions, thus producing somewhat rough curves as shown. The most quasi-static points were probably the peaks, which if connected would be a better representation of the true K_R curve. In any case, it appears that the curves agree well with the NASA data at 0.4 inches growth, and reach a maximum, relatively constant value after 1.5 inches of growth of about 83 ksi. Taking the ratio with the top of the R-curve L-T value, we again calculate $\overline{K}_m$=1.3. Apparently the ratio is fairly constant within this range.

Determination of the characteristic length, r_c, for stable tearing has been accomplished in a previous investigation [16] by plotting the average minimum turning radius as a function of r_o (calculated per Equation 5.3.2.1.6) . The turning radius is determined by laying a circle template over the specimen, finding the radius which best matches the radius of curvature at the turning point, and averaging the value from the two sides of the specimen. A value for r_c can be estimated for isotropic materials by extrapolation to the r_o value at which crack turning occurs with zero radius.

The test matrix was originally set up to evaluate r_c in the manner described above, and crack turning radius was determined for the 7050-T7451 specimens. However, as fracture orthotropy has become better understood, it has become apparent that the test data cannot be meaningfully reduced in this manner for

highly orthotropic materials, because the expected critical value of r_o is different in each direction, and falls out of the range of r_o values tested with the current specimen geometry. Nevertheless, literature values (of unknown accuracy) for 2000 and 7000 series aluminum alloys [8, 16] are on the order of 0.05-0.06 inches, and Equation (5.3.2.3.1) gives values in the 0.02-0.05 range depending on the orientation. It was thus desired to perform a sensitivity study for various r_c values in this range to see if the crack paths could be correlated with the 2nd order orthotropic theory using FRANC2D.

FRANC2D calculates K_I, K_{II}, and T at for a given crack configuration, calculates the new crack direction based on Equation (5.3.2.2.6), extends the crack a specified increment, remeshes the region around the crack tip, and reruns the analysis to calculate the new crack trajectory. The deformed mesh for an analysis of a DCB specimen of L-T orientation is shown Figure 43.

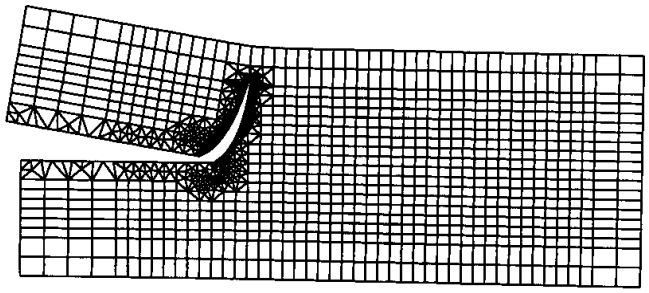

Figure 43. FRANC2D Mesh for Analysis of a DCB ($\overline{K}_m$=1.3, L-T Orientation, a_i=3.0 in, r_c=0.05 in.)

Unfortunately, the symmetric nature of the specimens is a drawback from a crack-path correlation standpoint for T-L specimens. An analysis of a DCB specimen of a hypothetical material with substantial fracture orthotropy ($\overline{K}_m$=1.67) and various angular perturbations applied at the first step is presented in Figure 44. In cases where the crack turns gradually, such as T-L specimens with high orthotropy, the perturbation sensitivity is most significant. Note that the sharply turning L-T curves plot together (independent of perturbation).

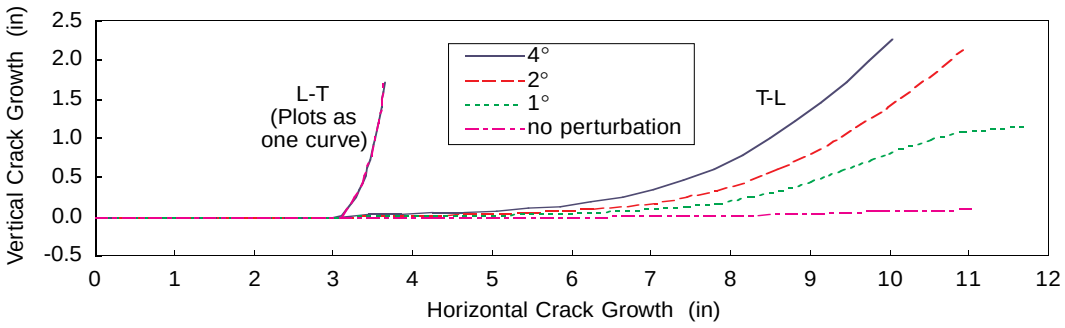

Figure 44. FRANC2D Crack Path Sensitivity Study for DCB Specimen with Various Perturbation Angles Applied at the First Step ($\overline{K}_m$=1.67, a_i=3.0 in, r_c=0.05 in.)

Modeling the specimen as if it were perfect to within the numerical precision of the computer implementation (as in the “no perturbation” case) is not physically realistic, and can be mesh dependent. Perturbation could potentially result from manufacturing imperfections in the specimen geometry, the effects of gravity on the specimen, and the natural meandering nature of the crack tip due to material inhomogeneity. Gravitational effects were largely ruled out as a major contributor, since the specimens did not all turn the same direction (up or down) in the test machine. Geometric irregularities in the specimens, while potentially significant, were small enough that they were difficult to quantify in a meaningful way, though it was evident that the precracks were sometimes observably out of alignment with the starting notches (and this varied through the thickness). Nevertheless, visual inspection of the specimens suggested that even in fairly nominally straight regions of stable tearing, the natural meandering of the crack appeared to provide a potentially significant source of perturbation.

In an attempt to quantify the inherent perturbation distribution of a meandering (stably tearing) crack in 7050-T7451 plate, a high resolution scan of a 2.5 inch length of substantially straight crack growth in specimen rc-TL-15-4 was sampled for angular slope (point to point) at various increment lengths. The data and a curve fit to a logarithmic distribution is given in Figure 45, and shows that there is about an eighty percent likelihood of an angular perturbation exceeding an angle of 1 degree over a typical 0.010 inch length of crack propagation.

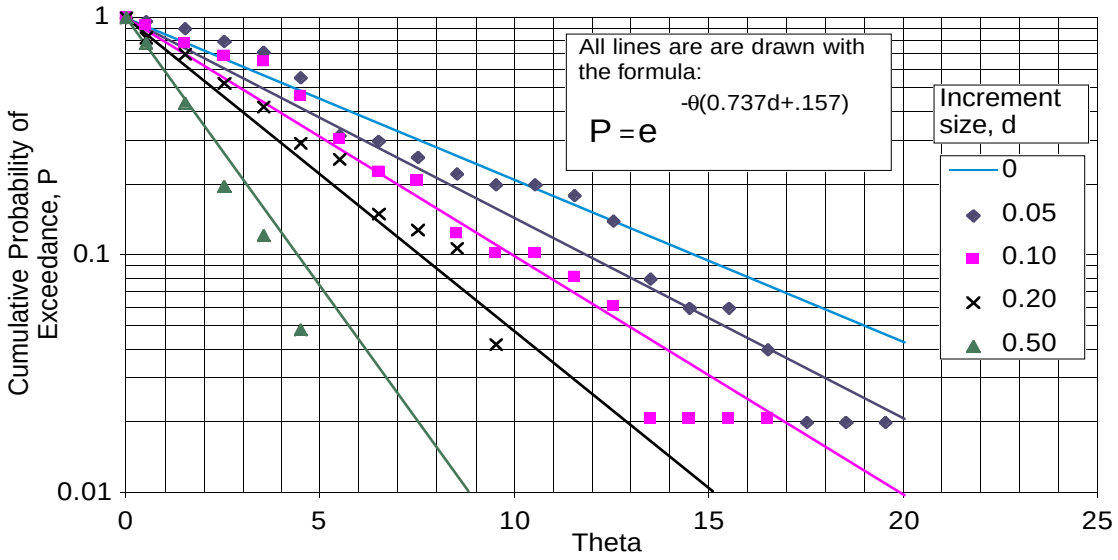

Figure 45. Perturbation Distribution for 7050-T7451 Plate, Obtained from Nominally Straight Stable Tearing Region of Specimen

With substantial random perturbation due to material inhomogeneity, and the potential for geometric imperfections, one would expect a noticeable amount of scatter in the crack paths for nominally self-similar specimens such as the DCB. However, we observe that after a finite amount of crack growth, including an amount of perturbation induced turning, the specimen geometry is no longer

symmetric. At this point its future path should be more predictable, since the nominal asymmetry is then larger compared to random perturbations[12].

Specimens rc-TL-15-5 and rc-TL-15-8 were analyzed in this manner with correlation of various analyses shown in Figures 46a and 46b. The models included the actual crack path up until the vertical (asymmetric) growth component reached approximately 0.1 inches, and the crack path was predicted analytically from that point onward. An orthotropy ratio $\bar{K}_m$=1.3, and a crack increment step size of 0.1 inches were used for both analyses.

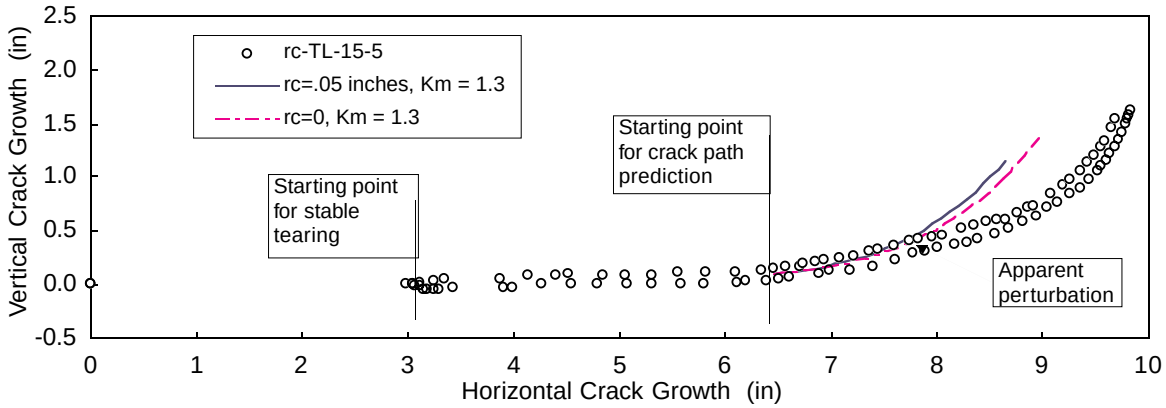

a) Specimen rc-TL-15-5

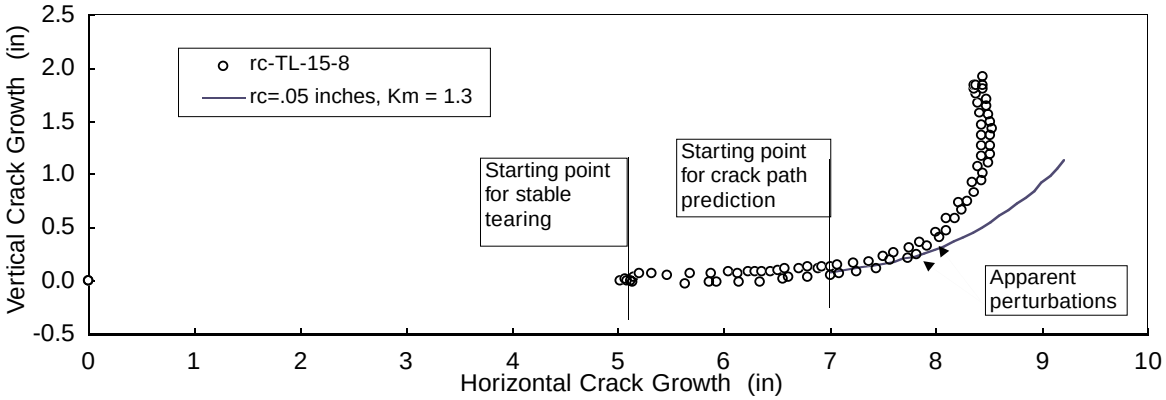

b) Specimen rc-TL-15-8

Figure 46. Correlation of Observed and Predicted Crack Paths for Selected 7050-T7451 Specimens (L-T Orientation)

[12] By the same logic, real physical problems would not be expected to be highly perturbation sensitive unless they are nearly symmetric.

From Figure 46a we observe that with the level of orthotropy present, the choice of r_c has little effect on the predicted (T-L) crack path in the regime of T stress occurring in this specimen geometry, leaving the predicted path to be primarily a function of the orthotropy ratio. The orthotropy ratio chosen from R-curve data seems to be a reasonable average value, overestimating the turning in one case and underestimating in the other. The remaining disparity in the crack paths appears to result from perturbations observed along the crack path presumably due to material inhomogeneity.

In the L-T orientation, all specimens turn fairly sharply to nearly 90 degrees, as shown in Figure 39. The FRANC2D analysis in Figure 47 illustrates that this result is predicted for an orthotropy ratio of 1.3 almost independent of the assumed value of r_c. The model is perturbed one degree in the last 0.1 inch increment of the starting crack length (though it likely made no difference, based on Figure 44), and a step size of 0.1 inches is used thereafter. The starting notch length used in the analyses is 3.031 inches, so the results could be compared to the crack path of specimen rc-LT-15-5. Clearly, the correlation is favorable.

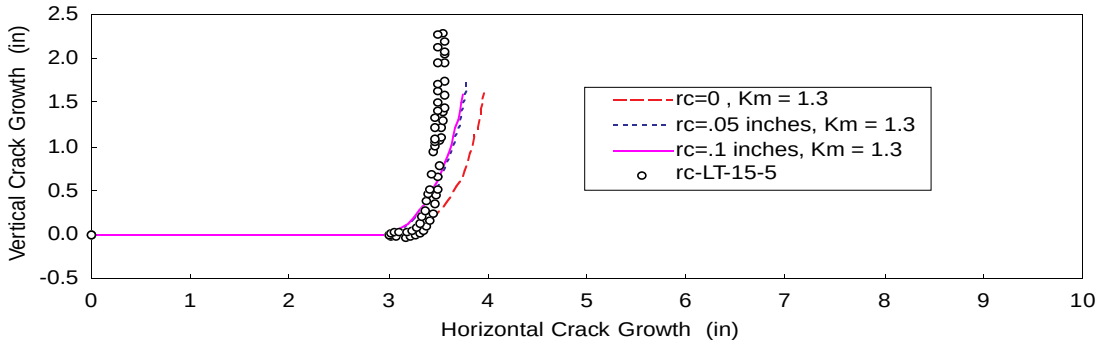

Figure 47. Correlation of Observed and Predicted Crack Paths for Selected 7050-T7451 Specimens (L-T Orientation)

For fatigue crack growth, r_c is expected to be negligible as previously discussed. The fracture orthotropy ratio can be obtained from a comparison of L-T and T-L fatigue crack growth rate data, shown in Figure 48, taken from the straight growth regions of specimens rc-LT-15-2 and rc-TL-15-2. Extrapolating the data into approximately parallel lines in this regime of growth, it is apparent that to obtain the same crack growth rate in either orientation, one would have to load the L-T crack about 10 percent more than the T-L crack, thus the orthotropy ratio is about 1.1. With r_c=0, and a nominally symmetric, gradually turning crack, a high degree of perturbation sensitivity is expected. The FRANC2D analysis thus utilized the

actual crack path up to 0.1 inches of asymmetric growth in the same manner as was done in Figure 46. The resulting correlation shown in Figure 49 is very favorable for the L-T case. Correlation was somewhat worse for the T-L case, possibly because the stress intensity for growth was getting high enough that the T-stress had an effect which was not modeled since we assumed r_c=0 for fatigue crack growth. Estimating Kmax from the da/dN data in Table 11, it would appear that starting at a crack tip coordinate of x=5.8, the value of r_c based on Equation (5.3.2.3.1) is roughly 0.005 inches, and increases to the stable tearing value at about y=1.5.

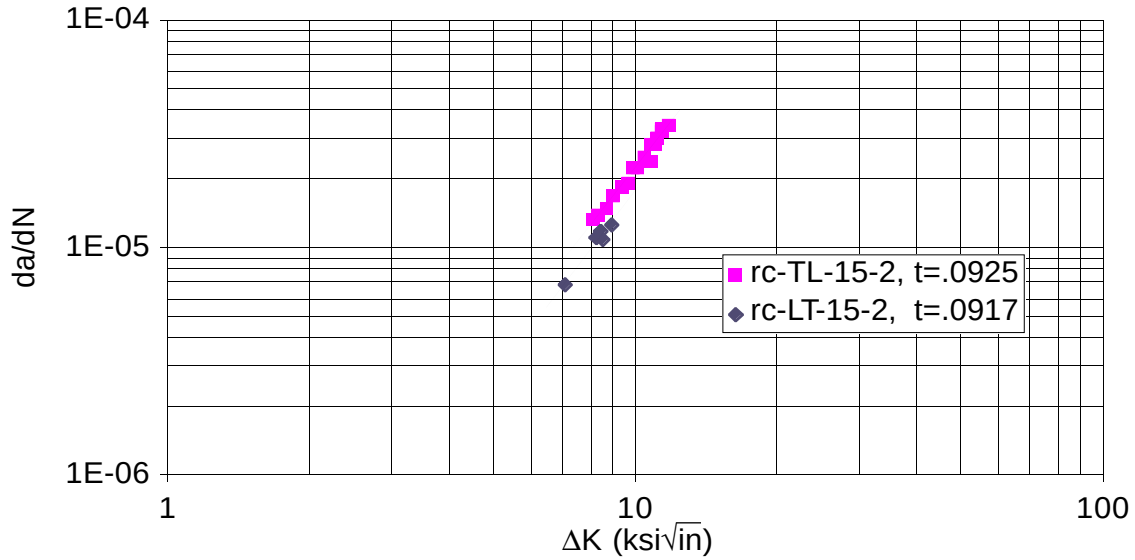

Figure 48. Comparison of T-L and L-T Fatigue Crack Growth Data Taken from DCB Specimens, Stress Ratio=0.05

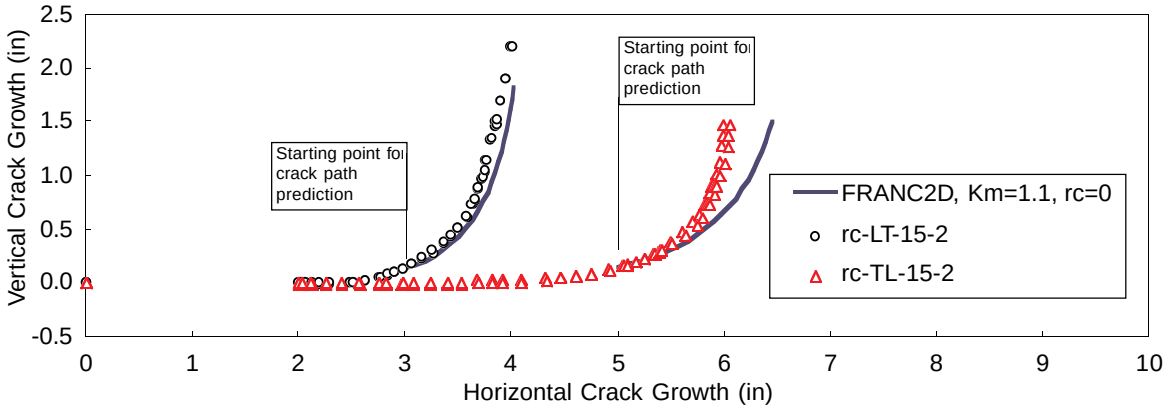

Figure 49. Comparison of T-L and L-T Fatigue Crack Paths Taken from DCB Specimens, Stress Ratio=0.05

5.3.3.2.2 2324-T39 Plate 7475-T7351, and 7050-T76511 Alloys

The primary purpose of these tests was to obtain information about the orthotropy of these alloys, and the likelihood of turning a crack from the T-L orientation. Only T-L specimens were tested with the underlying assumption that $\overline{K}_m \geq 1$. Based on results reported in [16] for 2024-T3 DCB tests, one would expect that fairly isotropic T-L specimens would turn sharply due to the high T-stress environment (note that the 2nd order theory is required to predict this behavior). From the curves plotted in Figure 41, 7475-T7351 and 2324-T9 plate clearly fall into this category, and 7050-T76511 does not.

Further crack path analysis was not performed for these alloys at this time, and would require wide panel R-curve data. Nevertheless, the turning performance of 7475-T7351 plate in particular was very favorable, supporting the decision to proceed with large panel testing of that alloy. It should be cautioned however that both 7475-T7351 specimens exhibited a small amount of V-shear behavior, though in the first specimen it was only very slight, and it appeared that the crack would have turned anyway. More DCB testing of this alloy is recommended. Also, as NASA wide panel data becomes available for the 7475-T7351 material, correlation with FRANC2D results will be possible to evaluate r_c for that material.

5.4 Structural Detail Testing

5.4.1 Thickness Interface Tests

The purpose of these tests was to evaluate the ability of an integral tear strap to arrest a straight, statically tearing crack, and provide validation data for applicable theoretical models.

Twelve thickness interface specimens were manufactured and tested. One specimen was sent to NASA Langley Research Center for testing, as indicated in Table 13. All specimens were machined out of a single lot of 48x144x1.5 inch 7050-T7451 aluminum alloy plate procured jointly for the IAS program by Boeing Seattle and Boeing Long Beach. Average lot release data for that lot of material are given in Table 7.

The specimen configuration refers to the test geometry given in Figure 50. The basic skin thickness is nominally 0.060 inches, with two integral tear straps of 0.180 inch nominal thickness. The bulky region in the center of the specimen increases the load transfer at the center of the specimen, thus increasing the stress intensity factor without widening the panel (in order to produce failure at loads well below net section yielding). It also stabilizes the specimen from out of plane movement. All specimens were designed to be geometrically similar with regard to all in-plane dimensions with the exception of the fillet radii and the loading hole diameters. The thickness of each feature of the specimen was the same for all specimens; however, panels were configured with two different fillet radii as indicated in the test matrix to investigate the effect of fillet radius on crack arrest capability.

Table 13. Thickness Interface Specimen Test Matrix

Specimen No	Configuration (Orientation)	Panel Width (inches)	Fillet Radius	Test Responsibility
THIF-3L	-3 (L-T)	23.80	.063	Boeing Seattle
THIF-5L	-5 (L-T)	23.80	.188	Boeing Seattle
THIF-9L#1	-9 (L-T)	15.86	.188	Boeing Seattle
THIF-9L#2	-9 (L-T)	15.86	.188	Boeing Seattle
THIF-11L	-11 (L-T)	11.90	.063	Boeing Long Beach
THIF-13L	-13 (L-T)	11.90	.188	Boeing Long Beach
THIF-3T	-3 (T-L)	23.80	.063	Boeing Seattle
THIF-5T	-5 (T-L)	23.80	.188	Boeing Seattle
THIF-9T#1	-9 (T-L)	15.86	.188	Boeing Seattle
THIF-9T#2	-9 (T-L)	15.86	.188	Boeing Seattle
THIF-11T	-11 (T-L)	11.90	.063	Boeing Long Beach
THIF-13T	-13 (T-L)	11.90	.188	NASA LaRC

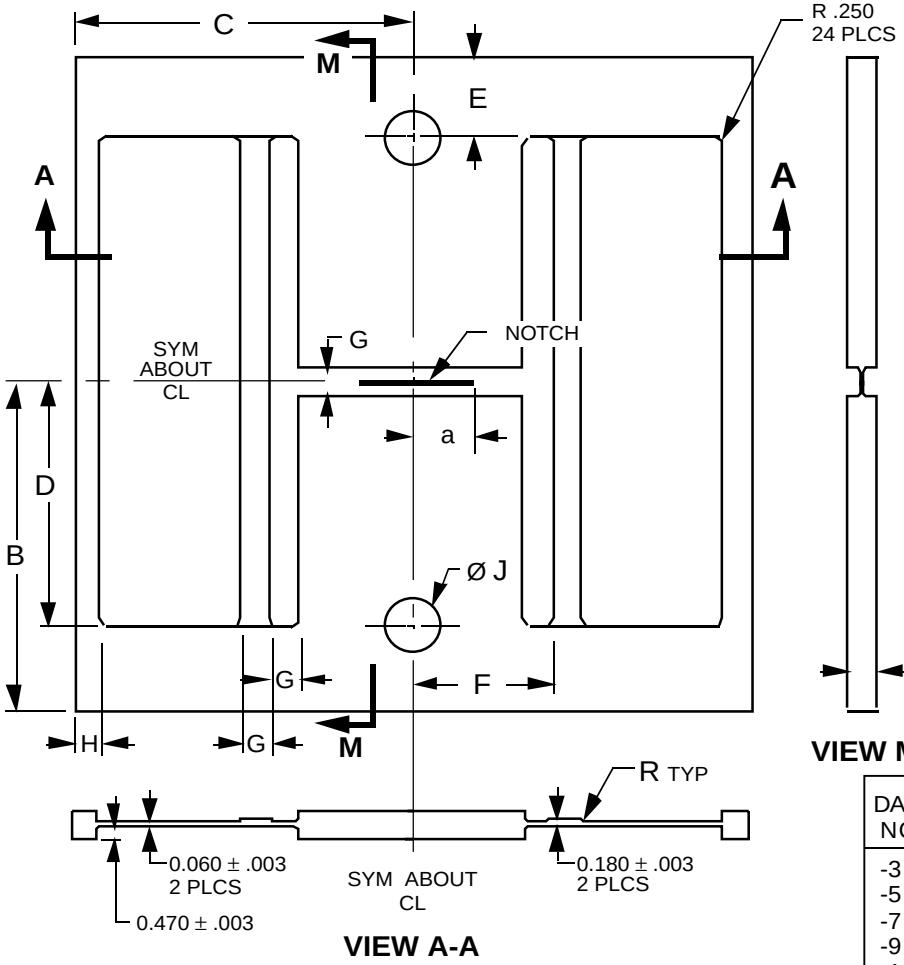

VIEW A-A

VIEW M-M

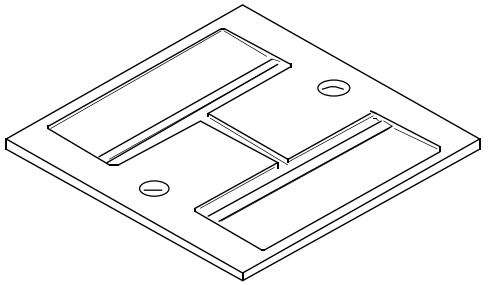

ISOMETRIC VIEW

GENERAL NOTES:

1. ALL DIMENSIONS IN INCHES.
2. DEFAULT TOLERANCES ARE AS FOLLOWS:
   .XX (2 DECIMAL PLACES, ±0.03)
   .XXX (3 DECIMAL PLACES, ±0.015)
3. SURFACE FINISH 63√PER ANSI B46-1978.
4. SPECIMEN SURFACES SHALL BE FREE OF NICKS AND GROOVES.
5. MATERIAL, GRAIN ORIENTATION AND NOTCH DIMENSIONS TO BE SPECIFIES BY ENGINEER.

DASH NO	B	C	D	E	F	G	H	J	R
-3	11.90	11.90	8.90	3.00	5.00	1.00	0.90	2.005	0.063
-5	11.90	11.90	8.90	3.00	5.00	1.00	0.90	2.005	0.188
-7	7.93	7.93	5.93	2.00	3.33	0.67	0.60	1.505	0.063
-9	7.93	7.93	5.93	2.00	3.33	0.67	0.60	1.505	0.188
-11	5.95	5.95	4.45	1.50	2.50	0.50	0.45	1.005	0.063
-13	5.95	5.95	4.45	1.50	2.50	0.50	0.45	1.005	0.188

Figure 50. Thickness Interface Specimen Concept

A detailed write-up of all test data was provided to Boeing Seattle [21]. A FRANC2D model was provided for analysis of the test specimens. A summary of the test data is included here for completeness in Table 14, and correlation with a the linear elastic analysis in Figure 51.

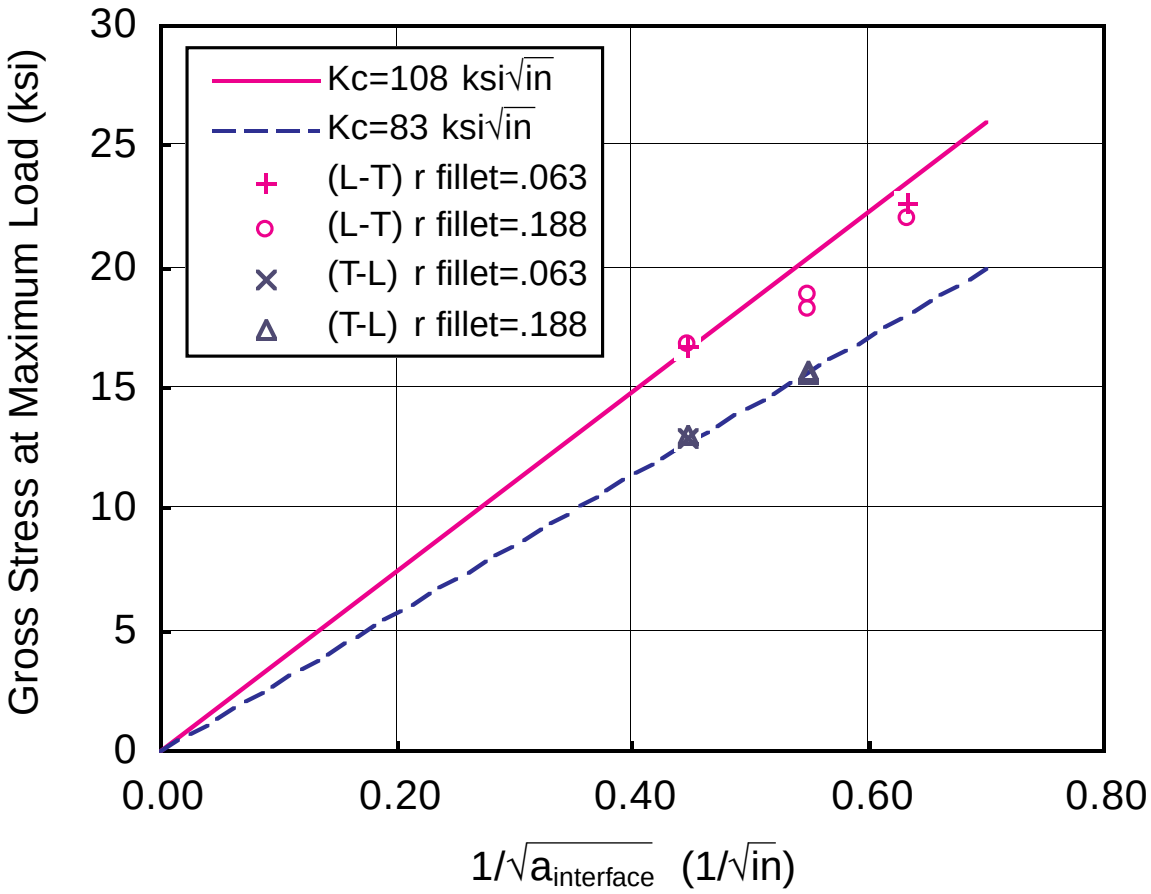

Figure 51. Correlation of Thickness Interface Specimen Data with Linear Elastic Analysis [21]

Table 14. Tabulated Thickness Interface Test Results

		$a_{precrack}$ (avg) (in)	a_{arrest}* (in)			Δa_{arrest} (avg) (in)	Measured Specimen Gross Area (sq in)	Nominal Fillet Radius (in)	Maximum Load (kips)	COD at Max Load (in)	Gross Failure Stress (ksi)	Predicted Failure Stress (ksi)
			Flush side	Stiffened side	Average of both sides							
Specimens												
THIF-3	L	3.511	5.088	4.983	5.035	1.525	3.5945	0.063	59.98	0.1059	16.69	16.62
THIF-5	L	3.500	4.971	4.922	4.946	1.446	3.5653	0.188	60.02	0.1027	16.83	16.62
THIF-9#1	L	1.833	3.297	3.255	3.276	1.444	2.3273	0.188	44.06	0.0858	18.93	20.36
THIF-9#2	L	1.834	3.294	3.240	3.267	1.433	2.2686	0.188	41.43	0.0890	18.26	20.36
THIF-11	L	1.028	2.565	2.489	2.527	1.500	1.7173	0.063	38.90	0.0942	22.65	23.50
THIF-13	L	1.033	2.596	2.466	2.531	1.498	1.7676	0.188	38.86	0.0808	21.99	23.50
Specimens												
THIF-3	T	3.553	5.002	4.970	4.986	1.433	3.7856	0.063	48.89	0.0616**	12.92	12.77
THIF-5	T	3.525	4.896	4.865	4.881	1.356	3.8254	0.188	49.83	0.0671	13.03	12.77
THIF-9#1	T	1.834	3.247	3.168	3.207	1.374	2.2657	0.188	35.38	0.0608	15.61	15.65
THIF-9#2	T	1.831	3.330	3.253	3.291	1.460	2.3087	0.188	36.19	0.0584	15.67	15.65
THIF-11	T											
THIF-13	T											

* a_{arrest} is based on the last physical crack measurement prior to maximum load, which was always in the fillet adjacent to the tear strap, but which may differ slightly from the crack length at maximum load. Flush side and stiffened side measurements are average of left and right half crack values; an overall average s also given.

** Specimen inadvertently overloaded to approx. 33 kips after precracking, but prior to test. Overload undoubtedly effected subsequent COD measurements, but should not have affected max load.

5.4.2 Basic Stiffener Fatigue Specimens

The basic stiffener fatigue specimen configuration is illustrated in Figure 52. The grain orientation for all specimens was transverse to the specimen axis, simulating a strip of material oriented circumferentially on an integral fuselage. The thickened region in the center simulates the base of an integral stiffener. Specimens were configured with .180, .120, or .060 inch fillet radii at the edges of the simulated stiffener to evaluate the notch effect of each fillet radius for fatigue loading.

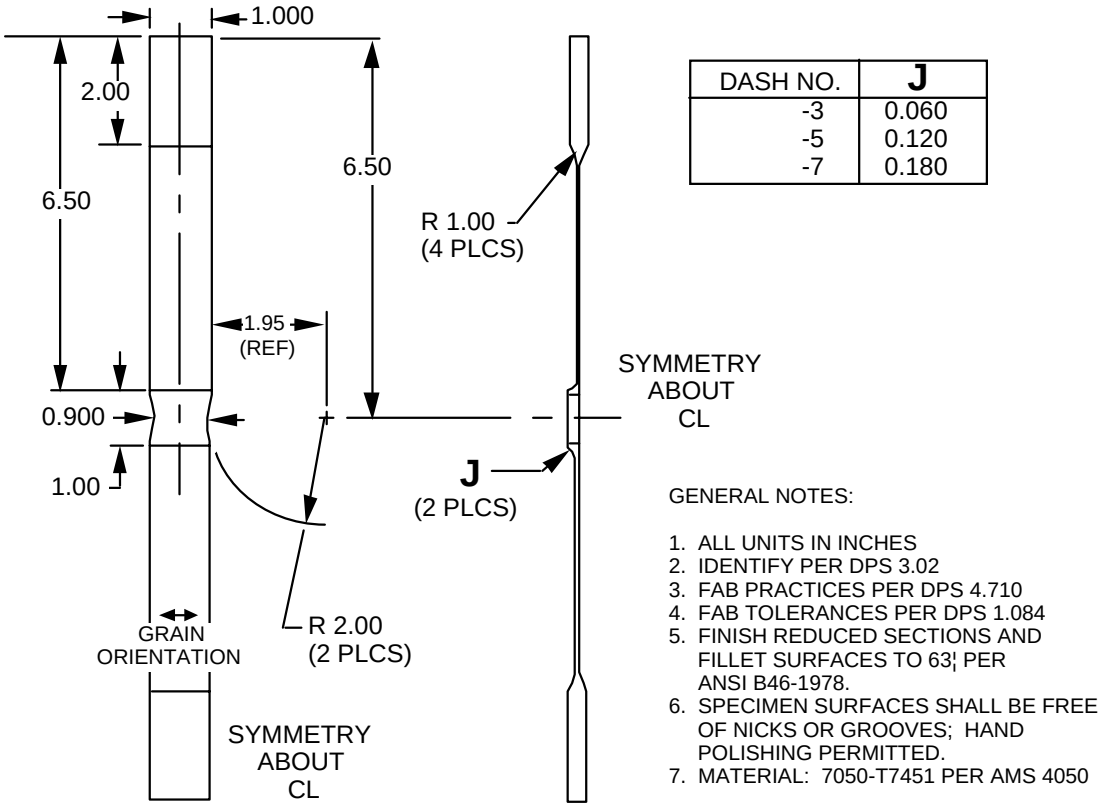

Figure 52. Basic Stiffener Fatigue Specimen

A two-dimensional finite element model of the specimen in FRANC2D showed that for straight-sided configurations, a very high notch effect not representative of the airplane would be expected where the fillets intersect the edges of the specimen. The two inch radius edge cut in the thickened region was found to eliminate this problem, though it was found to increase the stress in the center of the fillet slightly (about 2 percent).

Thirty specimens (ten of each fillet configuration) were machined out of 1.5 inch thick 7050-T745 plate from the lot described in Table 7. Specimen blanks were cut in half through the thickness prior to machining, so two specimens could be obtained from each blank.

Specimens were sent to NASA LaRC for testing. A summary of preliminary results to date [47] indicates a very mild effective stress concentration (on the order of 1.1-1.2) at the fillet. Curiously, the smaller fillet radii outperformed the larger radii. Various linear analyses have been run at NASA, Boeing and Northrop Grumman to explain this unexpected trend, and results indicated that induced bending in the specimen has a significant effect. One should bear in mind, however, that the problem has potentially significant geometrically nonlinear behavior.

It is also clear that the uniaxial tension applied to the specimen differs from the combination of hoop tension and normal pressure applied to the simulated region of fuselage. To properly capture this effect analytically would require a three-dimensional (not shell, because the fillet radii must be properly represented) nonlinear finite element model of a fuselage panel. To validate the analysis, pressure cycling of a fuselage panel to failure would be required. The stress concentration factor in this realistic load environment is expected to be higher than that observed in the coupon tests; nevertheless the mild stress concentration apparent in the coupon tests are encouraging.

5.4.3 Mechanical Joint Specimens

Longitudinal and transverse (circumferential) joint specimens were designed as discussed in Section 3.3.4 and are presented as detail specimen drawings IF-P012 and IF-P013 in Appendix Section A.3.

A total of six longitudinal, and five transverse specimens were fabricated. The skin details were taken from the lot of 1.5 inch 7050-T7451 plate described in Table 7. As shown on the drawings, the grain orientation in the skin is specified in a manner consistent with the orientation anticipated on the airplane. Other details (for the transverse joint specimen) were fabricated from 7075-T6 sheet. All details were conversion coated and primed with corrosion resistant primer, with the exception of the surfaces which represent the exterior of the aircraft, which were conversion coated, but not primed, in order to facilitate crack detection during testing.

All specimens were provided to NASA LaRC for testing. The intent is to test one specimen of each configuration statically to failure, and fatigue test the others to evaluate the performance and failure modes of the joint design concepts.

5.4.4 Friction Stir Weld Specimens

Rather than evaluating the friction stir welding joint configurations discussed in Figure 18, it was decided to take a more basic approach and evaluate the effect

of the friction stir welding process on 7050-T7451 plate material. As discussed in Section 3.3.4.2, friction stir welding typically does cause a loss of static and fatigue properties. There was also the concern that friction stir welding might alter the corrosion behavior of the material.

In order to address these concerns, a total of six static tension, ten fatigue, and two corrosion specimens were fabricated at the Boeing Huntington Beach Facility. The material was 1.5 inch 7050-T7451 plate from the lot described in Table 7, and the specimen configurations are given in Figures 53-55.

In order to fabricate the specimens, rough cut blocks of material were split through the thickness and machined to obtain 0.25 inch thick rectangular blanks. Pairs of blanks were then butted together and friction stir welded. The set marks left by the friction stir welding process were machined off, leaving smooth surfaces on top and bottom, and the specimens were excised. The final specimen thickness for the tensile and fatigue specimens was about 0.23 inches. The corrosion specimens were cut diagonally at a narrow angle (about 6.5 degrees) to evaluate the corrosion properties as a function of depth within the weld.

All specimens were provided to NASA LaRC for testing.

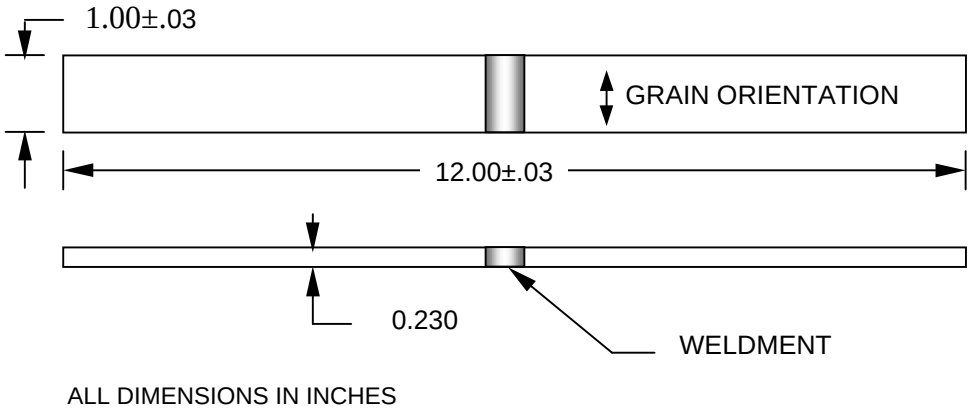

Figure 53. Friction Stir Welded Tensile Specimen

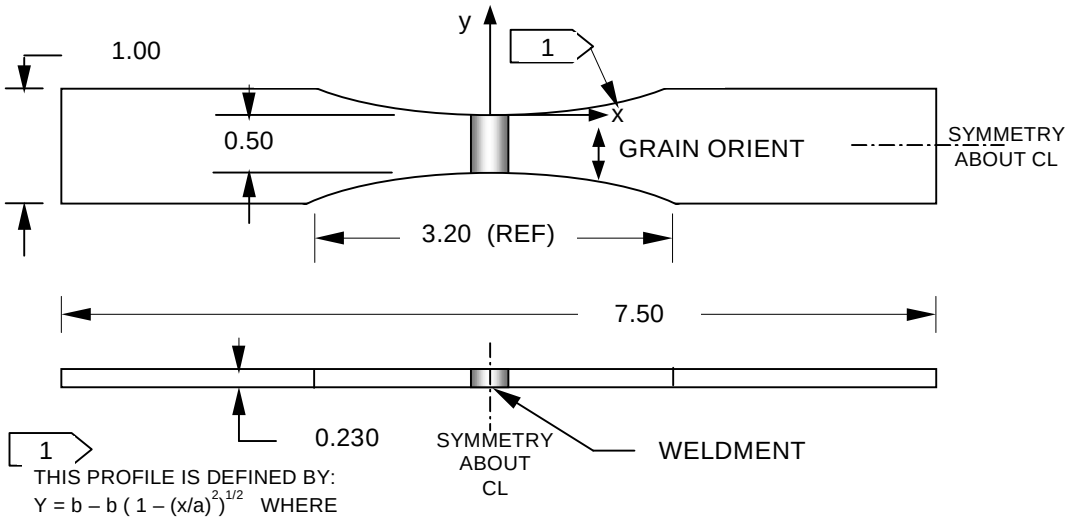

THIS PROFILE IS DEFINED BY:
$Y = b - b\left(1 - (x/a)^2\right)^{1/2}$ WHERE
a=1.6227 AND b=0.3 (SEE TABLE). THE PROFILE SHALL BE A SMOOTH CURVE WITHOUT LINEAR SEGMENTS OR SNATCHES

X±.003	Y±.003
.10	.0006
.20	.0023
.30	.0052
.40	.0093
.50	.0146
.60	.0213
.70	.0293
.80	.0390
.90	.0504
1.00	.0637
1.10	.0795
1.20	.0981
1.30	.1205
1.40	.1483
1.50	.1856
1.60	.2500

GENERAL NOTES:
1. ALL DIMENSIONS IN INCHES
2. SURFACE FINISH 63vRMS
3. TOLERANCES (UNLESS NOTED)
   X.XX ± 0.03
   X.XXX ± 0.005
4. HAND-FINISH TEST SECTION SIDES WITH DOWEL AND 320 GRIT SANDPAPER IN LONGITUDINAL DIRECTION OF SPECIMEN. FLAT DEBURR TOP AND BOTTOM SURFACES IN LONGITUDINAL DIRECTION OF SPECIMEN.

Figure 54. Friction Stir Welded Fatigue Specimen

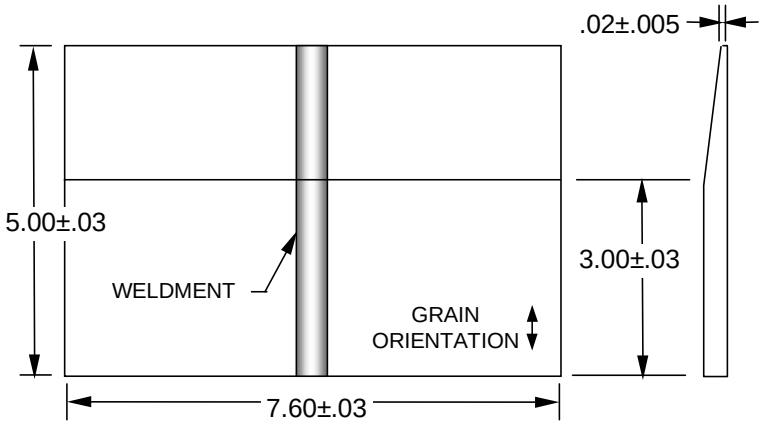

ALL DIMENSIONS IN INCHES

Figure 55. Friction Stir Welded Corrosion Specimen

5.5 Panel Test Specimens

Several panel test specimens were designed, and a summary of test panel drawings was given in Table 15. Specimen fabrication, which was under this phase of IAS program, was completed (see Table 6). The drawings were provided to NASA LaRC.

Originally, the intent was to make geometrically identical panels of plate and extrusion. However, due to current high market demand for extrusions, compromise was made to use the available extrusion geometry at Aloca. Thus, separate drawings had to be made for plate and extrusion configurations. However, as previously mentioned, the dimensional accuracy obtained on these large extrusions was found inadequate for machining of test panels (see [21] for more details). The drawings of the extruded configurations are mentioned for completeness, but were never fabricated or tested.

Table 15. Test Panel Drawings

TEST GROUP	DESCRIPTION	DRAWING NO.	INTEGRAL SKIN MATERIAL*
9	Repair Panel	IF-P015	7475-T7351 1.5 inch
11,12	Circumferential Crack Panel	IF-P001	7050-7451 Plate 1.5 inch
14 (#1)	Compression Panel	IF-P006	7050-7451 Plate 1.5 inch
14 (#2)	Extruded Compression Panel	IF-P014	7050-T74511 Extrusion
15	Shear Panel	ZJ151601	7050-T7451 Plate 1.5 inch

* Lot origin of these materials described in Section 5.2

5.5.1 Static Compression and Shear Panels

The purpose of these test panels was to validate the static strength of the integrally stiffened structural concepts developed in 3.3. The panels were configured to match fuselage concept #1 shown in Figure 13. Detail drawing numbers are given in Table 15.

The IF-P006 compression panel configuration was fabricated. The panel was 32 x 32 inches with an exterior radius of 118.5 inches. Both skin and frames were fabricated from 1.5 inch 7050-T7451 plate. Assembly using NAS1097-KE6 rivets was specified without any coatings or primer. A photograph of the specimen (after testing at NASA) is shown in Figure 56.

An Euler-Johnson compression analysis of the panel (see Appendix Section A.1) was run in using an end fixity of 2.0 to simulate the test condition (unpotted, compressed between parallel rigid plattens). The analysis assumed nominal specimen dimensions (neglecting fillets) and both actual[13] and Mil-HDBK-5 material properties. Correlation within two percent of the 97,200 lb test failure load reported by NASA[14] is summarized in Table 16.

The test load equates to 3037.5 lb/in, matching the 3000 lb/in requirement specified in Figure 12, and validating the accuracy of the analysis method for compression strength used in the design trade study of Section 3.3.4. However, it should be cautioned that the effective end fixity in a typical fuselage may differ from the value of 2.0 which simulates the test condition (typical fuselage end fixity values are more likely to be in the 1.0 to 1.5 range).

Table 16. Summary of Integral Compression Panel Analysis, 7050-T7451 Plate

Data Source	Tensile Yield Strength (ksi)	Compressive Yield Strength (ksi)	Compressive Modulus (msi)	Poisson's Ratio	Predicted Failure Load (kips)
Lot Release (Table 7.)	68	(Estimated from Tensile Yield) 68x63/65=65.9	Used Mil-Hdbk value	Used Mil-Hdbk value	99210
MIL-HDBK-5G "A" Basis	65	63	10.6	0.33	95848
Test Load					97200

5.5.2 Repair Panel

A 40x85 inch flat patch repair panel with 7475-T7351 integral skin was detail designed as Drawing No. IF-P012, and is illustrated in Figure 57. The basic structural layout of the panel followed design concept #1 (Figure 13) excluding the attached frames. Simulated damage, represented by an 8.0 inch diameter cutout, was centered on a stiffener. A 0.063 inch thick clad 2024-T3 exterior doubler (shown dashed) had a large rectangular footprint covering the two bays affected by the damage, and ending with the outer row of fasteners in the built-up regions formed by the intersecting stiffener and frame pads. This concept, completely surrounding the patch by an integrally reinforced region, makes the splice longeron and internal doubler details less critical, and promotes long patch life.

Detail parts were specified without surface coatings or primer, but with faying surface seal applied on assembly. The completed specimens are scheduled to be under fatigue test at NASA LaRC.

[13] Only the compressive yield strength, modulus, and Poisson's ratio were required for the analysis. The actual value of the compressive yield strength was estimated from the tensile lot release data using the ratio between the tensile and compressive yield strengths from Mil-Hdbk-5.
[14] Reported at the April, 1998 IAS meeting by Dawn Jegley. Formal report yet to be published.

Figure 56. Photograph of 7475-T7451 Compression Panel (DWG #IF-P006) After Testing at NASA LaRC

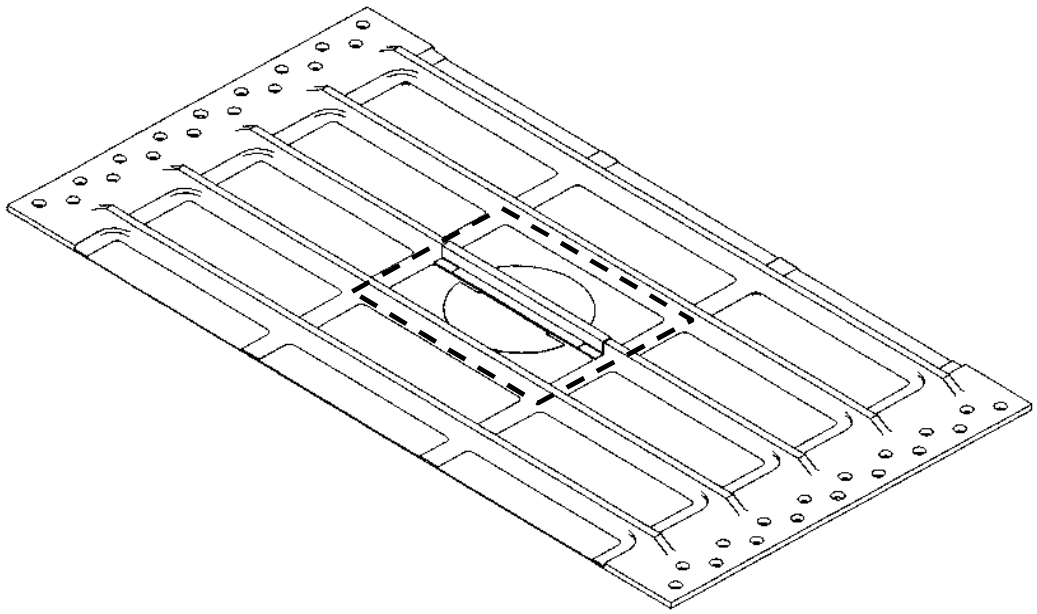

Figure 57. Repair Panel

5.5.3 Circumferential 2-Bay Crack Panels

The intent of the circumferential 2-bay crack tests was to evaluate the residual strength and crack-turning behavior of realistically sized integral structure with circumferential cracks. Previous work on smaller panels was previously reported in [16], where crack turning and high residual strength was observed in pressurized integrally stiffened panels. However, crack turning was not observed in unpressurized panels due to the absence of tensile T-stresses as the crack approached the stiffener. Thus both pressurized and unpressurized panels were specified in the test matrix for the IAS program (Table 6).

The 7050-T7451 plate specimen design, Drawing No. IF-P001, measured 78x48 inches, and was curved to an exterior radius of 118.5 inches, and configured to simulated the design concept #1 (Figure 13) excluding the attached frames. The center stiffener was altered to be symmetric, but equivalent with regard to area and moment of inertia, and the other stiffeners were arranged symmetrically with regard to the center of the panel, as shown in Figure 58 (end grips and other hardware omitted). In order to accommodate a truss plate to restrain the

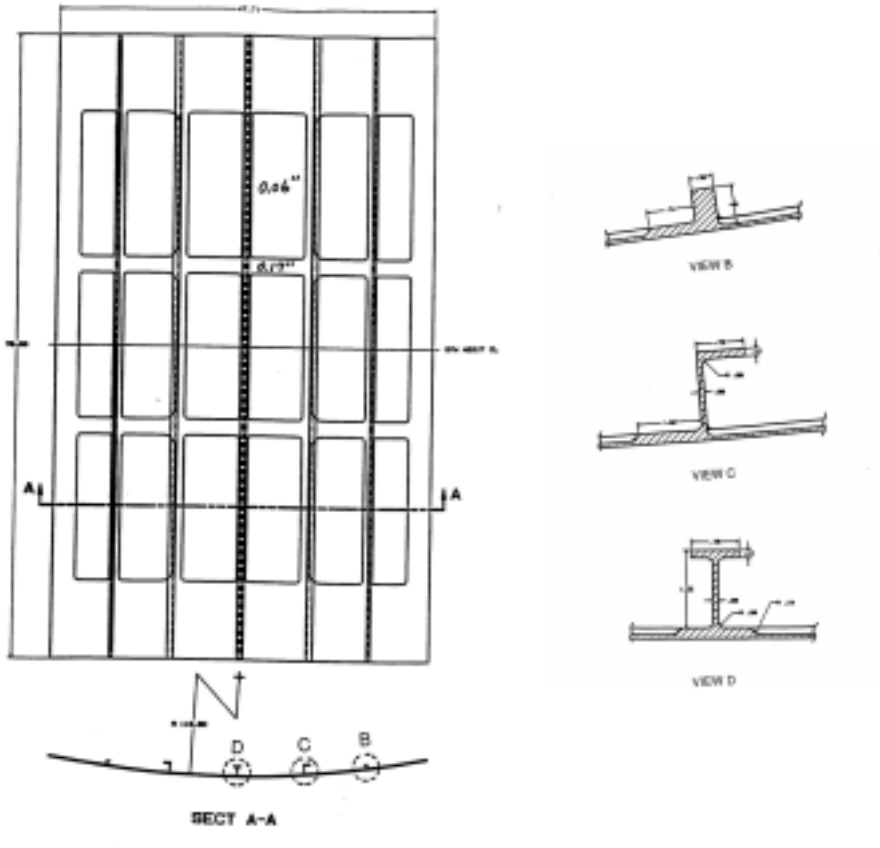

Figure 58. Integral Fuselage Panel for Circumferential 2-Bay Crack Test

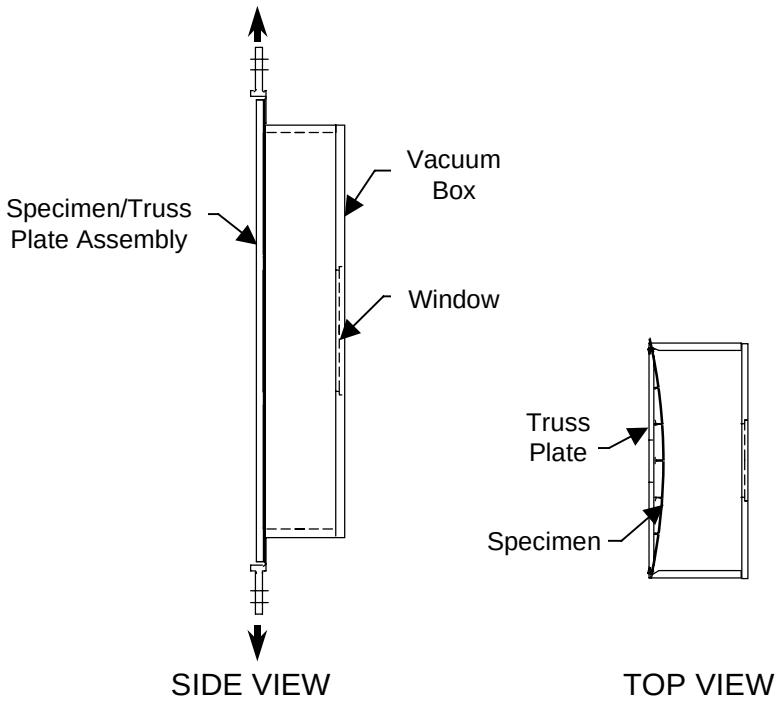

Figure 59. Test Setup Schematic

specimen during pressurization (simulated by application of an exterior vacuum), the outermost stiffeners were shortened. They were also increased in bulk to maintain equivalent cross sectional area (but not equivalent moment of inertia) compared to the other stiffeners.

A schematic of the intended test setup, showing the vacuum box and truss plates is shown in Figure 59. The vacuum box detail design was provided separately as Drawing No. IF-VB01.

Linear elastic finite element modeling of the test panel with a circumferential crack was performed using NASTRAN and STAGS. Stiffeners and the pad-up region were all modeled in detail using the shell elements, neglecting fillets. Young's modulus and Poisson's ratio for the material are 10.3 Msi and 0.33, respectively. An isometric view of the finite element model is shown in Figure 60. Along the left edge indicated, no axial displacement or rotation was allowed. A boundary condition of no tangential displacement or rotation was prescribed along both top and bottom edges. Along the right edge, a uniform displacement was specified constrained to a point at the center of the panel where axial load was applied. A uniform surface pressure of 8.6 psi was applied to the panel surface. Figure 61 shows the detailed mesh in the crack insertion region.

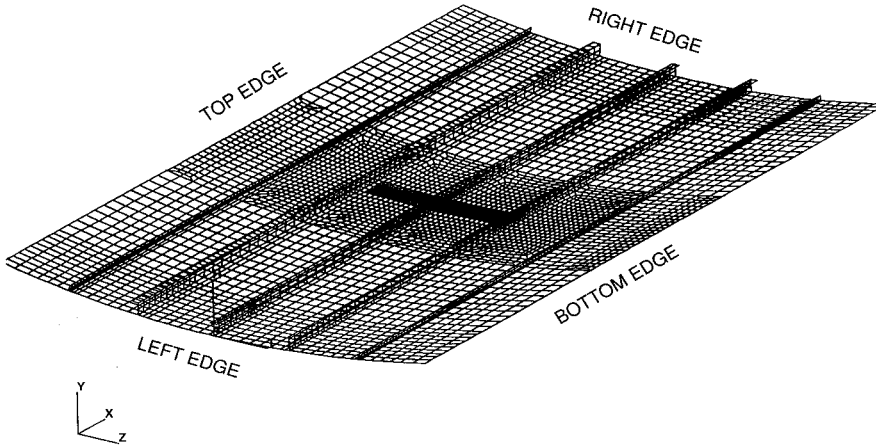

Figure 60. Isometric View of Finite Element Model of Circumferentially Cracked Panel

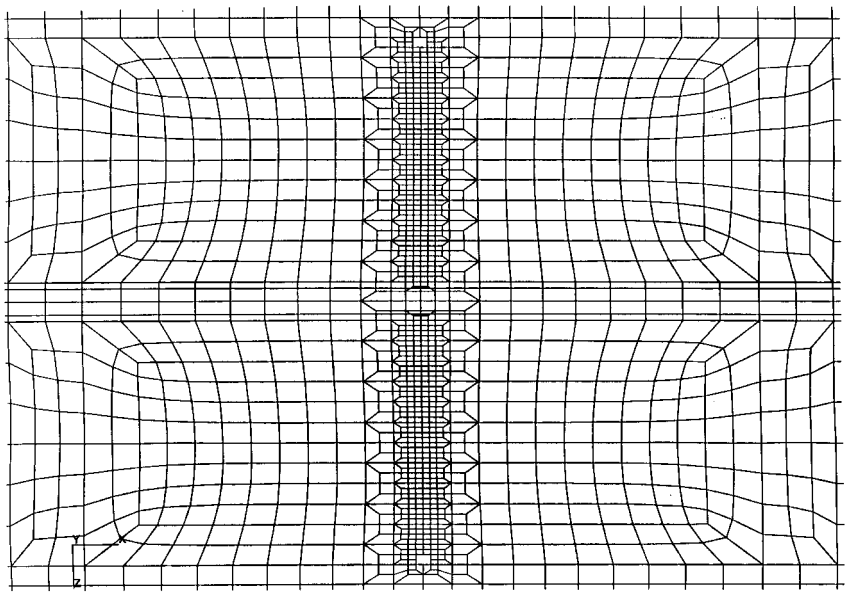

Figure 61. Close-up of Mesh in Vicinity of Crack

Linear elastic analysis results in straight-line plots of load vs. K_I at various crack lengths, as shown in Figure 62. The projected intercept with the vertical axis is the stress intensity factor due to the uniform surface pressure of 8.6 psi. Note that as the crack approaches the thickness discontinuity at the stiffener base at half-crack length, a=7.45, the stress intensity increases little with crack length. The analysis was also run with both NASTRAN and STAGS for a half crack length of 8 inches, corresponding to a crack extending midway through the stiffener base on each side, with results shown in Figure 63. Excellent agreement was found between the two codes.

As previously discussed, the most complete R-curve of 7050-T7451 plate material (machined to a thickness of 0.060 inches) gave a critical stress intensity value of 108 ksi-in$^{1/2}$in the L-T orientation. Based on the thickness transition analysis and test data [21], the point of maximum strength should lie at the thickness interface (a=7.45). While no further refinement of the model was done to more accurately evaluate the stress intensity in the vicinity of the thickness interface, we can obtain a conservative estimate of the residual strength from Figure 62 with a half-crack length of 7.306 inches. For a fracture toughness of 108 ksi-in$^{1/2}$, the residual strength is estimated at about 110 kips.

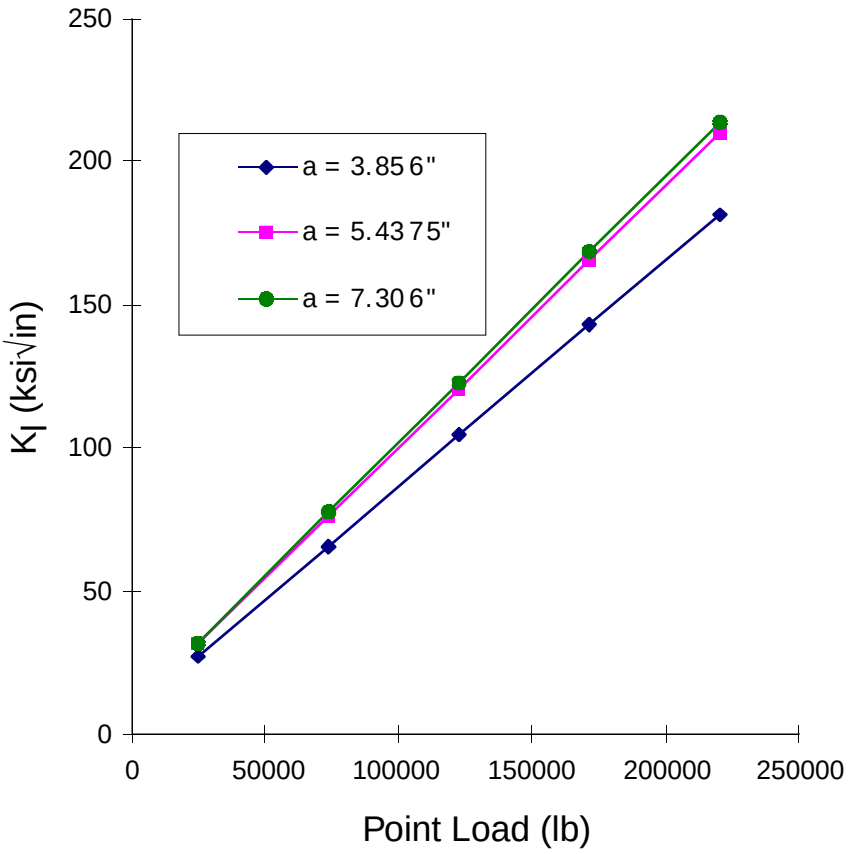

Figure 62. NASTRAN Load/Stress Intensity Plots for the Circumferentially Cracked Fuselage Panel Model, Various Crack Lengths, Applied Internal Pressure 8.6 psi.

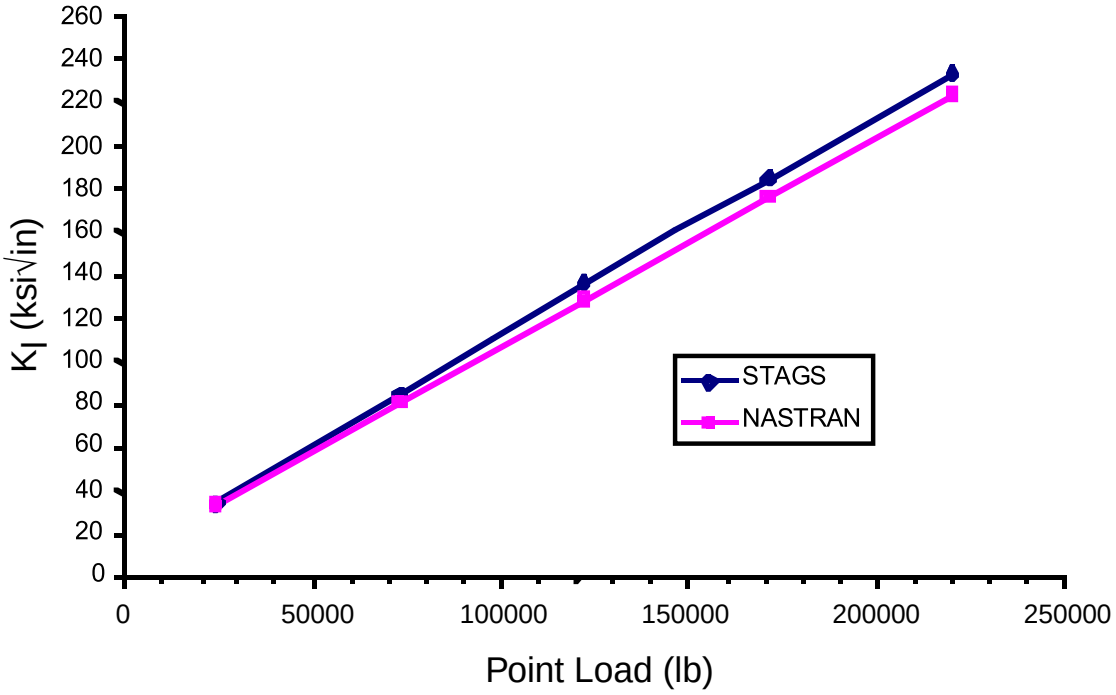

Figure 63. Load/Stress Intensity Plots for the Circumferentially Cracked Fuselage Panel Model, a=8.0 Inches, Applied Internal Pressure 8.6 psi, Comparing Stags and NASTRAN Results.

5.5.4 Longitudinal Crack Panel

The Longitudinal Crack Panel was designed, built and tested in the Tulalip wide-body pressure test fixture. The detail design followed the basic structural concept illustrated in Figure 15, which was designed for equal weight and structural performance to baseline panels tested under an earlier program [18]. The purpose of the test was to evaluate the ability of an integral pressurized fuselage concept to arrest a two-bay crack, including observation of fatigue crack growth and the potential for crack turning.

Complete documentation of this test is forthcoming in the Boeing Seattle IAS Final Report [21]. In brief, the panel sustained a residual strength 9.89 psi with the crack extending two bays, and arrested at the integral tear strap (the thickened region under the frame) at each end. This was a small improvement over the conventional construction of the baseline panels, which failed at 9.4 psi.

Only a very small amount of crack turning occurred, but the modeling capability for a crack turning analysis using the 2nd order theory is only now becoming available, thus no theoretical correlation has been obtained to date.

6.0 CONCLUSIONS AND RECOMMENDED FUTURE WORK

In this section, a brief summary of what has been learned, and a discussion of potential follow-on work relevant to integral structures will be undertaken. The purpose of the IAS program has been to develop structural concepts that cost significantly less than current practice, and to validate to the degree possible both the reduction in cost, and the structural performance of the new design concepts. In the following discussion, the proposed follow-on work will thus be divided between manufacturing development, and efforts to improve our ability to predict structural behaviors relevant to integral structure.

6.1 Manufacturing Development

In the process of fabricating test specimens, the IAS program validated the ability to produce plate hogouts bump formed to simple contours representative in size and configuration to constant-section fuselage panels. Similar efforts using large, near-net extrusions were not successful due to substantial dimensional variation in the extruded panels, due largely to unsatisfactory prototype practices for straightening and flattening of the extruded product. Also, the fracture orthotropy observed in extrusion is not beneficial from a structural standpoint.

Future work could improve both the properties and dimensional integrity of large extrusions. It has been suggested that the dimensional aspect of the problem could be averted by starting with non-near-net shapes, as has been done by Lockheed for wing planks for many years. However, results of the cost study [3] indicate that even near-net extrusions, if they were adequate from a dimensional and material property standpoint, would likely result in higher-cost structure than high-speed machined plate hogouts, due to the expected high raw material cost of large extrusions. Nevertheless, improvement in large extrusion technology—both to reduce the cost, and to improve the dimensional and mechanical properties--would likely benefit certain applications, and is worth doing.

Doubly curved structure, such as the demo panel not completed under this phase of the program, was not demonstrated for either plate hogout or extruded structure. Age creep forming was identified as a likely candidate processes, and the foremost material of choice, 7475-T7351, for plate hogouts is thought to be age-creep formable. However, the process needs to be demonstrated with a panel of representative size, and the cost needs to be evaluated. This is not a large program, but should be undertaken.

Looking out in the more distant future, major cost reductions can be obtained by doing one of two things. Either we develop lower cost process, such as precision assembly or automation, to build airplanes using more or less current structural technology, or we eliminate processes by developing technology which eventually yields large, highly complex net shapes with high dimensional accuracy and excellent material properties—at low cost.

Admittedly the second approach is a tall order, but may hold the highest payoff. Large extrusions and high-speed machined plate hogouts are a small step in this direction. Castings and stereolithography (or solid printing in general) allow successively greater dimensional complexity (which could allow integration of frames and other details), but the material properties, costs, and scale-up are successively less viable at the current level of technology. Research to improve such processes could eventually yield truly revolutionary results (in multiple industries). Regardless of the technology used, it appears that process elimination will eventually lead to integral structure, and thus many of the design and damage tolerance issues discussed earlier in this report will still be applicable.

6.2 Structural Mechanics

In the present work, significant strides have been made with regard to the ability to predict the residual strength of integral structure. Prior to this program it was not generally thought possible to design an integral structure with equal weight and equal static and 2-bay crack residual strength. It has now been demonstrated. Nevertheless, there is much work yet remaining.

The thickness transition test data demonstrated to a certain extent that linear elastic fracture mechanics can be used to predict residual strength for a crack arrested at an integral tear strap. However, if the tear strap were thoroughly yielded (which can happen in practice), it would seem that at some point this ceases to be true. Thus, an elastic plastic approach needs to be developed. Methods such as the critical Crack Tip Opening Displacement (CTOD) approach could be correlated with data developed under the IAS program, and specimens modified to exaggerate the presence of plasticity could be tested if necessary.

Crack turning behavior was identified as a potentially important phenomenon for crack arrest in integral structure, but did not play a significant role in the arrest of the longitudinal crack panel. Crack turning theory was improved to include both fracture orthotropy and the effect of the T-stress in the course of this program, and related programs in the academia. Tools are just becoming available (a modified version of the Cornell code, FRANC3D) to apply this technology to complex structures, such as the longitudinal crack test, but these analyses have yet to be performed, and test correlation obtained. Also, various deficiencies remain in the theory. Methods to determine the material properties relevant to crack turning are still lacking, and the effects of shell bending and plasticity on crack turning are little understood. Perhaps with better understanding, these phenomena could be better used to our advantage in integral structure (or even conventional structure).

Lastly, a philosophy for reducing the threat of MSD has been briefly introduced in Section 3.1, and some attempt made to reduce the threat of MSD in the structural concepts developed under this program to levels below the MSD threat of conventional structure. Specifically, the joints were designed for very long fatigue life by integrally reinforcing the joint regions, in hopes that some less MSD critical

feature of the structure might become fatigue life limiting. Unfortunately, validation of this design objective was not possible under the present phase of the program, because it requires cycling a large piece of fuselage structure to failure. Nevertheless, it is proposed that a research effort be directed toward design of MSD tolerant structures (whether or not they are integral).

7.0 REFERENCES

1. Boeing *Current Market Outlook*, www.boeing.com/news/cmo, May 1988.

2. Airbus *Global Market Forecast*, www.airbus.com/gmf97, May 1988.

3. Metschan, S. *IAS Validated Feasibility Study of Integrally Stiffened Metallic Fuselage Panels for Reducing Manufacturing Cost—Cost Assessment of Manufacturing/Design Concepts*, NASA/CR-2000-209343.

4. T. Swift, “Application of Damage Tolerance Technology to Type Certification”, SAE Paper #811062, Aerospace Congress and Exp., Anaheim, CA October 1981.

5. H. F. Hardrath et al, NACA Tech Note #3856, 1956.

6. C. C. Poe, “Crack Propagation in Stiffened Panels”, ASTM STP 486, 1971.

7. T. Swift, “The Applications of Fracture Mechanics in the Development of the DC-10 Fuselage”, in *Fracture Mechanics of Aircraft Structures* , AGARD-AG-176 by H. Liebowitz, Neuilly sur Seine, France, pp. 226-287, 1974.

8. T. Swift, “Damage Tolerance in Pressurized Fuselage”, 11th Plantema Memorial Lecture, 14th Symposium of the ICAF, *New Materials and Fatigue Resistant Aircraft*, Ottawa, Canada, June 1987 (also Douglas Paper 7768).

9. J. Maclin, “Performance of Fuselage Pressure Structure”, *1991 International Conference on Aging Aircraft and Structural Airworthiness*, Washington D.C., November 19-21, 1991, NASA Conference Pub 3160 (1992).

10. M. Miller, K. Kaelber, and R. E. Worden, “Finite Element Analysis of Pressure Vessel Panels”, *Durability of Metal Aircraft Structures*: Proc. of International Workshop on Structural Integrity of Aging Airplanes, Atlanta Technology Publications, Atlanta, GA, pp. 337-339, 1992.

11. National Transportation Safety Board Aircraft Accident Report, Aloha Airlines Flight 243, Boeing 737-200, N73711, Near Maui, Hawaii, April 28, 1988, NTSB/AAR-89/03, 1989.

12. M. Kosai, A. S. Kobayashi, M. Ramulu, “Tear Straps in Aircraft Fuselage”, *Durability of Metal Aircraft Structures*: Proc. of International Workshop on Structural Integrity of Aging Airplanes, Atlanta Technology Publications, Atlanta, GA, pp. 443-457, 1992.

13. D. O. Potyondy, Discrete Crack Growth Analysis Methodology for Cracks in Pressurized Fuselage Structures”, FAA/NASA Symposium on Advanced Structural Integrity Methods for Airframe Durability and Damage Tolerance, NASA Conference Publication 3274, Part 2, pp. 581-601, 1994.

14. M. Kosai, A. Shimamoto, C. T. Yu, S. I. Walker, A. S. Kobayashi, and P. Tan; Axial Crack Propagation and Arrest in Pressurized Fuselage”, FAA/NASA Symposium on Advanced Structural Integrity Methods for Airframe Durability and Damage Tolerance, NASA Conference Pub. 3274, Part 1, pp. 375-392, 1994.

15. B. Knops, *Numerical Simulation of Crack Growth in Pressurized Fuselages*, Ph.D. Thesis, Delft University of Technology, September, 1994.

16. R. G. Pettit, J. C. Newman, M. S. Domack, *Crack Turning Damage Tolerance Approach for Integrally Stiffened Structure*, 19th ICAF Symposium, Edinburg, June 1997.

17. Mil-Hdbk-5G, *Metallic Materials and Elements for Aerospace Vehicle Structures*, U.S. Department of Defense, November, 1994.

18. M. L. Gruber, C. J. Mazur, K. E. Wilkins, R. E. Worden, *Investigation of Fuselage Structure Subject to Widespread Fatigue Damage*, Final Report, Federal Aviation Administration Contract DTFA03-94-C-00065, Report Number DOT/FAA/AR-95/97, October, 1995.

19. R. E. Adkisson, G.V. Deneff*, Analytical Investigation of Medium STOL Transport Structural Concepts*, USAF Contractor Interim Report C75-11906 Vol. 1, 1974.

20. L. J. Hart-Smith, *Interface Control, the Secret to Making DFMA Succeed*, SAE Aerospace Manufacturing Technology Conference & Expo (McDonnell Douglas Paper MDC 96K0132), Seattle, June 2-5, 1997.

21. J. Munroe, K. Wilkins, M. Gruber *Integral Airframe Structure (IAS) Validated Feasibility Study of Integrally Stiffened Metallic Fuselage Panels for Reducing Manufacturing Cost—Final Report*, NASA/CR-2000-209337.

22. Cho, David J*., C-17 Metallic Materials Design Properties*, MDC K0327, May 1988.

23. J. Schijve, A. M. Vlutters, J. C. Kluit, “Crack Growth in Aluminum Alloy Sheet Material Under Flight-Simulation Loading”, *International Journal of Fatigue*, Vol. 7, No. 3 (1985), pp. 127-136.

24. L. J. Hart-Smith, *Mechanically-Fastened Joints for Advanced Composites--Phenomenological Considerations and Simple Analyses*, (Douglas Paper 6748A) Fourth Conference on Fibrous Composites in Structural Design, San Diego, November 1978.

25. W. D. Nelson, B. L. Bunin, L.J. Hart-Smith*, Critical Joints in Large Composite Aircraft Structure*, (Douglas Paper #7266) Sixth Conference on Fibrous Composites in Structural Design, New Orleans, January, 1983.

26. T. R. Logan, *Master Planning and Control Document*, Integrated Airframe Structure, Contract NAS1-20268, Task 15, McDonnell Douglas Corp.,

27. R. G. Pettit, *Crack Turning and Damage Tolerance of Integrally Stiffened Fuselage Structure,* McDonnell Douglas IRAD Technical Report, 1996.

28. K. Zaal, *A Survey of Crack Path Stability Criteria and Their Application to Crack Flapping Phenomena in Stiffened Structures*, Report LR-681, TU Delft, Faculty of Aerospace Engineering, The Netherlands, September, 1992.

29. M. Shirmohamadi, *Stable Crack Growth Trajectories and Fracture Due to Interacting Cracks*, Ph.D. Dissertation, University of California at Berkeley, 1995.

30. M. L. Williams, “On the Stress Distribution at the Base of a Stationary Crack”, ASME Transactions, *Journal of Applied Mechanics*, Vol. 24, 1957.

31. F. Erdogan, G. C. Sih; “On the Extension of Plates under Plane Loading and Transverse Shear”, *Journal of Basic Engineering*, Vol. 85D, No. 4, pp. 519-527, 1963.

32. J. G. Williams, P. D. Ewing, “Fracture Under Complex Stress--The Angled Crack Problem” , *International Journal of Fracture Mechanics*, Vol. 8, pp. 441-446, 1972.

33. I. Finnie, A. Saith, “A Note on the Angled Crack Problem and the Directional Stability of Cracks”, *International Journal of Fracture* , Vol.9, pp.484-486,1973.

34. M. Kosai, A. S. Kobayashi, M. Ramulu, “Tear Straps in Aircraft Fuselage”, *Durability of Metal Aircraft Structures*: Proc. of International Workshop on Structural Integrity of Aging Airplanes, Atlanta Technology Publications, Atlanta, GA, pp. 443-457, 1992.

35. 12. B. Cotterel, J. R. Rice, “Slightly Curved or Kinked Cracks”, *International Journal of Fracture*, Vol. 16, pp. 155-169, 1980.

36. M. B. Buczek , C. T. Herakovich, “A Normal Stress Criterion for Crack Extension Direction in Orthotropic Composite Materials”, J. Composite Materials, Vol. 19, pp. 544-553, 1985.

37. T. J. Boone, P. A. Wawrzynek, and A. R. Ingraffea, *Engineering Fracture Mech.*, Vol. 26, No. 2, pp. 185-201, 1987.

38. C.F. Shih, “Small Scale Yielding Analysis of Mixed Mode Plane-Strain Crack Problems”, *Fracture Analysis*, ASTM STP 560, American Society for Testing and Materials, 1974, pp. 187-210.

39. A. M. Al-Ani, J. W. Hancock, “J-Dominance of Short Cracks in Tension and Bending”, *J. Mech. Phys. Solids* , Vol. 39, No. 1, pp. 23-43, 1991.

40. P. S. Leevers, J. C. Radon, “Inherent Stress Biaxiality in Various Fracture Specimen Geometries”, *International Journal of Fracture*, Vol. 19, pp. 311-325, 1982.

41. G. E. Cardew, M.R. Goldthorpe, I. C. Howard, A. P. Kfouri, Fundamentals of Deformation and Fracture, Proceedings of the Eshelby Memorial Symposium, Sheffield (April 1984), Cambridge University Press, 1985.

42. A. P. Kfouri, “Some Evaluations of the Elastic T-Term Using Eshelby’s Method”, *International Journal of Fracture*, Vol. 30, pp. 301-315, 1986.

43. C. S. Chen, R. Krause, L. Banks-Sills, R. G. Pettit, A. R. Ingraffea, P. A. Wawrzynek, *Numerical Assessment of T-Stress Computation*, (in preparation).

44. M. S. Domack, *Fatigue Crack Growth Rate and Fracture Toughness Testing at NASA Langley Research Center*, IAS Workshop, NASA LaRC, April 29-30, 1998 (work-in-progress presentation, likely to be published in subsequent NASA technical reports).

45. B. Gross and J.E. Srawley, “Stress Intensity Factors for Single-Edge Notch Specimens Subjected to Splitting Forces”, NASA TN D-3295 (1966).

46. R.M.L. Foote and V. T. Buchwald, “An Exact Expression for the Stress Intensity Factor for a Double Cantilever Beam”, Int. Journ. of Fract. 29 (1985), pp. 125-134.

47. R. K. Bird, *Basic Stiffener Fatigue Testing of 7050 Aluminum at Langley Research Center*, IAS Workshop, NASA LaRC, April 29-30, 1998 (work-in-progress presentation, likely to be published in subsequent NASA technical reports).

A.0 APPENDIX

A.1 Description of Analysis Methods for EXCEL Panel Optimizer

(Reference: Bruhn, *Analysis and Design of Flight Vehicle Structures*, Jacobs Publishing, 1973, pages noted)

Tension:

Allowable Tensile Load/in = $(\Sigma\, Kn_i Ftu_i A_i)/d_{st}$

Where Kn_i = *Notch factor for* i^{th} *material*
(material dependent, .88 used for soft materials,
Ftu_i = *Ultimate tensile strength for* i^{th} *material*
A_i = *Area per bay of* i^{th} *material (skin fully effective in tension)*
dst = Stiffener spacing

Shear: Only the thickness of the skin, *tsk* is assumed effective in shear

Allowable Shear load/in = $.34\, Ftu_{sk} tsk\, dst$

The factor, .34, is derived from Bruhn, p. C11.53, assuming fully developed diagonal tension. It is a conservative value, used in the absence of shear panel test data. Stiffener failure modes were not analyzed for shear in the trade study because the panel was also required to satisfy realistic and substantial compressive load requirements.

Compression:

Euler/Johnson Allowable Compressive Load/in = $(A_{eff}+A_{fillet})\, Fc/dst$
A_{eff} is as defined below. A_{fillet} is the fillet cross-sectional area per bay, and may be negative (for bent sheet)--it was neglected in the trade study, but included in the design of the longitudinal crack panel geometry.

$$Fc=Fcc-Fcc^2/(4Fcr)$$

$$Fcc= (\Sigma A_i Fcc_i)/\Sigma A_i$$

summed for each stiffener element and effective skin

For skin, $Fcc_{skin} = Fcy\, w_{eff}\, tsk$ (w_{eff} defined below)

For stiffener elements,

$$Fcci=MIN\{Fcy, J\, Fcy/[(Fcy/Ec)^{1/2}\, b_i/t_i]^{.812}\}$$

where b_i , t_i are the length and thickness of each segment (defined so that the segment areas add up to the overall cross sectional area), and J=.565 for upper and lower caps, and 1.427 for stiffener web (based on Marshall Space Flight Center Structures Manual crippling charts).

$$Fcr=\pi^2 Ec/(L'/rho)^2$$

$$L'= d_{frame}/\sqrt{c}$$

where the end fixity, c = 2.0 for trade study, test correlation
1.5 for longitudinal crack panel design

(Note: A spot check of the data confirmed that the outcome of the trade study was not sensitive to the end fixity assumed within this range, as long as the same end fixity was assumed for all configurations).

$$Rho = (I/A_{eff})^{1/2}$$

Where I, A_{eff} are calculated for the stiffener area, Ast, plus effective skin

$$Ask_{eff} = t\ W_{eff}$$

$$W_{eff} = 1.7\ tsk\ (Ec/Fcy)^{1/2} \qquad \text{(Bruhn, p. C7.11)}$$

The Excel Solver Optimizer was utilized to minimize weight while satisfying the load requirements for shear, tension, and compression.

A.2 Lot Release Data for 7050-T7451 Plate

1.5 Inch Plate, Sheet 1/1

PECHINEY
RHENALU
USINE D'ISSOIRE
LABORATOIRE ET CONTROLE

CERTIFICAT DE RECEPTION

INSPECTION CERTIFICATE / ABNAHMEPRUFZEUGNIS

EN. 10204 3.1.B / DIN 50049 3.1.B

B.P. 42 - 63.02 IS
TEL. 73 66 50 60 - TELECOP
TELEX 99
PUY-DE-DO

NUMERO - Number - Nummer : 345095

COMMANDE CLIENT - Customer Order - Kundenbestellung
910 SE SUNSHINE
METALS PO 32902
PWT USA INC.

DESTINATAIRE - Consignee - Empfanger
SUNSHINE METALS
120 37TH N.E.
AUBURN, WASHINGTON 98002
USA

COMMANDE PECHINEY N°
75394/01

AVIS D'EXPEDITION - Dispatch Note -
76592B DU 05/07/

TOLE AERO 7050 T7451
AMS.4050.IND.E (RCP:SANS.TENACITE/
USI:BAC.5439.3.ED.11.02.87./
MIL.STD.2154.ED.09.82/A/
CONF1:DMS.2233.IND.C/
CONF2:MMS.1420.REV.D+ADD./REV.H)
DIM 1231,90 /3670,30 /38,10

DIM.48"50X144"50X1"500 PV COMPLET
LIVRAISON HUILE COLIS 2722 KG BRUT

1 UI

CAISSE Case Kiste	LOT ORIGINE Heat lot Los	PRODUIT Product Produkt	PLATEAU Slab Walzlafel	ETAT Temper Zustand	SENS Direction Richtung	ESSAIS DE TRACTION Tensile Tests Zugversuche Rt Tensile Strength KSI	Rt 0,2 Yield Strength KSI	A % Elongation %	AUTRES ES Other te Andere Pr
119548	75394/011	651912 A	098452/07	T7451	LL	77,4	68,0	13	
					TL	76,9	68,3	12	

SUNSHINE METALS
SOLD TO Douglas Aircraft Mulberry
P.O. # 6XY0355594
MATERIAL 7050 T7451
SIZE 1.5x48.5x144.5
SPEC. AMS4050
QUANTITY 3
LOT # 75394/011

9/25/96

TRACER# 005826

COULEE - Castings Schmelze	COMPOSITION CHIMIQUE - Chemical Composition - Zusammensetzung SI	FE	CU	MN	MG	CR	NI	ZN	TI	ZR	PB	NA	
098452	0,05	0,11	2,17	0,01	2,27	0,02	65*	6,10	0,04	0,09	18*	1*	* e

CONDUCTIVITY IACS : 40,2/41,7

We certify that subject to the exceptions and engineering departures above mentioned the present supply has been manufactured to the technical specifications of custome contract, order or sub-order, and that after completion of all inspections and tests, it complies in EVERY ASPECT with the particular specifications which are there attached with the drawings and all the relative standards and regulations in force.

ISO 9002
AFAQ

P.O. M. BARTHOMEUF
Conclusion de chef de contrôle
Conclusion of chief inspector
Entscheidung des Leiters der Abteilung Kontrolle

B. SCHAFFHAU
08/07/96

OBSERVATIONS DE LA SURVEILLANCE
Remarks of official inspector
Bemerkungen von der Beaufsichtigung

PECHINEY RHENALU

USINE D'ISSOIRE
LABORATOIRE ET CONTROLE

CERTIFICAT DE RECEPTION

INSPECTION CERTIFICATE / ABNAHMEPRUFZEUGNIS

EN. 10204 3.1.B / DIN 50049 3.1.B

B.P. 42 - 63502 ISSOIRE
TEL. 73 55 50 50 - TELECOPIE 73
TELEX RHUIS
PUY-DE-DOME

NUMERO - Number - Nummer : 345111

COMMANDE CLIENT - Customer Order - Kundenbestellung:
913 SE SUNSHINE
METALS PO 32904
PWT USA INC.

DESTINATAIRE - Consignee - Empfanger:
SUNSHINE METALS
120 37TH N.E.
AUBURN, WASHINGTON 98002
USA

COMMANDE PECHINEY RHENALU: 75436/01

AVIS D'EXPEDITION - Dispatch Note - Liefers: 76593B DU 05/07/96

TOLE AERO 7050 T7451
BMS.7323B.TYPE.1 REV.12.05.95
(RCP:K1C.L-T,T-L,S-L/
USI:BAC.5439.3.ED.11.02.87./
MIL.STD.2154.ED.09.82/A/
CONF1:AMS.4050.IND.E/
CONF2:DMS.2233.IND.C/

CONF3:MMS.1420.REV.D+ADD./REV.H)
DIM 1231,90 /3670,30 /63,52
DIM.48"50X144"50X2"501 PV
EN10204.31B
LIVRAISON HUILE COLIS 2722 KG BRU

8 UNI

CAISSE Case Kiste	LOT ORIGINE Heat lot Los	PRODUIT Product Produckt	PLATEAU Slab Walzlafel	ETAT Temper Zustand	SENS Direction Richtung	ESSAIS DE TRACTION Tensile Tests Zugversuche			AUTRES ESSAI Other tests Andere Prob
						R Tensile Strength KSI	R 0,2 Yield Strength KSI	A % Elongation %	K1C KSI VI
119475	75436/011	651889 A B	098449/02	T7451	LL	75,1	66,6	10	33,3
					LL	75,1	66,7	10	
					ST	72,8	62,2	7,3	26,9
					ST	73,4	62,5	7,4	
					TL	75,8	66,7	9	27,9
					TL	76,1	66,7	10	
		651892 B	098449/08		LL	74,8	66,1	13	
					LL	74,5	65,7	11	
					ST	72,4	62,2	7,4	
					ST	73,1	63,1	7,2	
					TL	76,0	66,7	9	
					TL	75,7	66,4	9	
119476		651890 B	098449/09		LL	74,7	65,7	12	
					LL	75,3	66,8	11	
					ST	72,6	62,6	7,5	
					ST	73,5	63,8	7,5	
					TL	75,3	65,5	10	

COULEE - Castings Schmelze	COMPOSITION CHIMIQUE - Chemical Composition - Zusammensetzung												
	SI	FE	CU	MN	MG	CR	NI	ZN	TI	ZR	PB	NA	
098449	0,05	0,10	2,17	0,02	2,25	0,02	60*	6,15	0,03	0,10	16*	1*	

* en

CONDUCTIVITY IACS : 39,8/41,4

We certify that subject to the exceptions and engineering departures above mentioned the present supply has been manufactured to the technical specifications of customer contract, order or sub-order, and that after completion of all inspections and tests, it complies in EVERY ASPECT with the particular specifications which are there attached with the drawings and all the relative standards and regulations in force.

P.O. M. BARTHOMEUF

DECISION DU CHEF DE CONTROLE
Conclusion of chief inspector
Entscheidung des Leiters der Abteilung Kontrolle

B. SCHAFFHAUSI

08/07/96

OBSERVATIONS DE LA SURVEILLANCE
Remarks of

ISO 9002

AFQ

PECHINEY RHENALU

USINE D'ISSOIRE
LABORATOIRE ET CONTROLE

CERTIFICAT DE RECEPTION

INSPECTION CERTIFICATE / ABNAHMEPRUFZEUGNIS

EN. 10204 3.1.B / DIN 50049 3.1.B

B.P. 42 - 63502 ISSOIRE
TEL. 73 55 60 50 - TELECOPIE 73
TELEX RHENUS 9
PUY-DE-DOME -

NUMERO - Number - Nummer : 345111

COMMANDE CLIENT - Customer Order - Kundenbestellung
913 SE SUNSHINE
METALS PO 32904
PWT USA INC.

DESTINATAIRE - Consignee - Empfanger
SUNSHINE METALS
120 37TH N.E.
AUBURN, WASHINGTON 98002
USA

COMMANDE PECHINEY RHENALU
75436/01

AVIS D'EXPEDITION - Dispatch Note - Liefer
76593B DU 05/07/96

TOLE AERO 7050 T7451
BMS.7323B.TYPE.1 REV.12.05.95
(RCP:K1C.L-T,T-L,S-L/
USI:BAC.5439.3.ED.11.02.87./
MIL.STD.2154.ED.09.82/A/
CONF1:AMS.4050.IND.E/
CONF2:DMS.2233.IND.C/

CONF3:MMS.1420.REV.D+ADD./REV.H)
DIM 1231,90 /3670,30 /63,52
DIM.48"50X144"50X2"501 PV
EN10204.31B
LIVRAISON HUILE COLIS 2722 KG BRU

CAISSE Case Kiste	LOT ORIGINE Heat lot Los	PRODUIT Product Produckt	PLATEAU Slab Walztafel	ETAT Temper Zustand	SENS Direction Richtung	ESSAIS DE TRACTION Tensile Tests Zugversuche R Tensile Strength KSI	R 0,2 Yield Strength KSI	A % Elongation %	AUTRES ESSA Other tests Andere Probe KIC KSI VI
119476	75436/011	651890	098449/09	T7451	TL	75,8	66,0	10	
		651891 B	098449/03		LL	74,2	65,3	12	
					LL	74,5	66,0	12	
					ST	72,6	62,4	7,7	
					ST	73,4	63,7	7,3	
					TL	75,0	65,4	9	
					TL	76,0	66,4	11	
		651892 A	098449/08		LL	74,8	66,1	13	
					LL	74,5	65,7	11	
					ST	72,4	62,2	7,4	
					ST	73,1	63,1	7,2	
					TL	76,0	66,7	9	
					TL	75,7	66,4	9	
119477		651890 A	098449/09		LL	74,7	65,7	12	
					LL	75,3	66,8	11	
					ST	72,6	62,6	7,5	
					ST	73,5	63,8	7,5	

COMPOSITION CHIMIQUE - Chemical Composition - Zusammensetzung

COULEE - Castings Schmelze	SI	FE	CU	MN	MG	CR	NI	ZN	TI	ZR	PB	NA	
098449	0,05	0,10	2,17	0,02	2,25	0,02	60*	6,15	0,03	0,10	16*	1*	

* en

CONDUCTIVITY IACS : 39,8/41,4

We certify that subject to the exceptions and engineering departures above mentioned the present supply has been manufactured to the technical specifications of customer contract, order or sub order, and that after completion of all inspections and tests, it complies in EVERY ASPECT with the particular specifications which are there attached with the drawings and all the relative standards and regulations in force.

P.O. M. BARTHOMEUF

DECISION DU CHEF DE CONTROLE
Conclusion of chief inspector
Entscheidung des Leiters der Abteilung Kontrolle

B. SCHAFFHAUS

08/07/96

OBSERVATIONS DE LA SURVEILLANCE
Remarks of official inspector

ISO 9002

AFAQ

2.5 Inch Plate, Sheet 3/3

PECHINEY RHENALU

USINE D'ISSOIRE
LABORATOIRE ET CONTROLE

CERTIFICAT DE RECEPTION

INSPECTION CERTIFICATE / ABNAHMEPRUFZEUGNIS

EN. 10204 3.1.B / DIN 50049 3.1.B

B.P. 42 - 63502 ISSOIRE
TEL. 73 55 50 50 - TELECOPIE 73
TELEX RHUIS F
PUY-DE-DOME

NUMERO - Number - Nummer: 345111

COMMANDE CLIENT - Customer Order - Kundenbestellung:
913 SE SUNSHINE
METALS PO 32904
PWT USA INC.

DESTINATAIRE - Consignee - Empfanger:
SUNSHINE METALS
120 37TH N.E.
AUBURN, WASHINGTON 98002
USA

COMMANDE PECHINEY RHENALU: 75436/01

AVIS D'EXPEDITION - Dispatch Note - Lieferschein: 76593B DU 05/07/96

TOLE AERO 7050 T7451
BMS.7323B.TYPE.1 REV.12.05.95
(RCP:K1C.L-T,T-L,S-L/
USI:BAC.5439.3.ED.11.02.87./
MIL.STD.2154.ED.09.82/A/
CONF1:AMS.4050.IND.E/
CONF2:DMS.2233.IND.C/

CONF3:MMS.1420.REV.D+ADD./REV.H)
DIM 1231,90 /3670,30 /63,52
DIM.48"50X144"50X2"501 PV
EN10204.31B
LIVRAISON HUILE COLIS 2722 KG BRU

CAISSE Case Kiste	LOT ORIGINE Heat lot Los	PRODUIT Product Produckt	PLATEAU Slab Walztafel	ETAT Temper Zustand	SENS Direction Richtung	ESSAIS DE TRACTION Tensile Tests Zugversuche: R Tensile Strength KSI	R 0,2 Yield Strength KSI	A % Elongation %	AUTRES ESSAIS Other tests Andere Proben: KIC KSI VI
119477	75436/011	651890	098449/09	T7451	TL	75,3	65,5	10	
					TL	75,8	66,0	10	
		651891 A	098449/03		LL	74,2	65,3	12	
					LL	74,5	66,0	12	
					ST	72,6	62,4	7,7	
					ST	73,4	63,7	7,3	
					TL	75,0	65,4	9	
					LL	76,0	66,4	11	

QC 5 (stamp: SUNSHINE METALS)

9/25/96

SUNSHINE METALS
SOLD TO Douglas Aircraft Military
P.O. # 6K0355549-9
MATERIAL 7050 T7451
SIZE 2.5x48.5x144.5
SPEC. AMS4050

QUANTITY 3
LOT # 75436/011

TRACER# 005823

COULEE - Castings Schmelze	COMPOSITION CHIMIQUE - Chemical Composition - Zusammensetzung: SI	FE	CU	MN	MG	CR	NI	ZN	TI	ZR	PB	NA
098449	0,05	0,10	2,17	0,02	2,25	0,02	60*	6,15	0,03	0,10	16*	1*

* en

CONDUCTIVITY IACS : 39,8/41,4

We certify that subject to the exceptions and engineering departures above mentioned the present supply has been manufactured to the technical specifications of customer contract, order of sub-order, and that after completion of all inspections and tests, it complies in EVERY ASPECT with the particular specifications which are there attached with the drawings and all the relative standards and regulations in force.

ISO 9002 AFAQ

DECISION DU CHEF DE SERVICE - Conclusion of chief inspector - Entscheidung des Leiters der Abteilung Kontrolle: P.O. M. BARTHOMEUF

B. SCHAFFHAUSER 08/07/96

OBSERVATIONS DE LA SURVEILLANCE - Remarks of official inspector

A.3 R-Curve Data Reduction Using DCB Specimen Results

In investigating the phenomenon of crack turning in double cantilever beam (DCB) specimens the following method was used to calculate R-Curves (Stress intensity vs. effective change in crack length) in those specimens which did not turn immediately following the precrack.

Specimens had an aspect ratio of h/w = .2 (Figure 29), and were prepared and tested a manner comparable to ASTM E561. The initial crack length was put into the specimens with an EDM or saw cut, followed by fatigue precracking. Specimens were then loaded quasi-statically to failure (without back modulus loops), with data acquisition for load and crack opening displacement using an extensometer mounted adjacent to the crack flanks directly between the load points (head movement was also recorded, but was not used). A normalized compliance value (CEB) was calculated for each set of load/crack opening displacement data.

$$CEB = (2Vo\ E\ t)/P \qquad (A.3.1)$$

Where Vo is the half crack opening displacement at the crack flanks between the load points (note that the extensometer deflection is equal to 2Vo), E is Young's modulus, t is the panel thickness, and P is the applied load.

In order to calculate the effective crack length, a_{eff}, one must obtain a theoretical solution for the given aspect ratio. A finite element model was developed for a crack in a specimen with an aspect ratio of 0.2. The analysis determined the crack opening displacement for a unit load at various crack lengths, which was normalized to obtain the CEB ratio for each crack length. A quartic curve fit was then produced to match the CEB values calculated from the FEM within 0.4 percent for $0.83<a/W<3.13$. This defines the theoretical CEB value, or CEBt as

$$CEBt = 19.9264\ (a/h) + 6.38254\ (a/h)^2 + 12.1794\ (a/h)^3 - .608207\ (a/h)^4 \qquad (A.3.2)$$

For each specimen, actual dimensions for h and t were used to evaluate equations (A.3.1) and (A.3.2). In order to compute the R-curve, load values below the precrack load were neglected. Per ASTM guidelines, the compliance calibration ratio (CEB ratio) was calculated at the first load/deflection data point above the maximum precrack load, assuming the crack length equal to the measured crack length after precracking.

$$CEB\ ratio = CEBt / CEB \qquad (A.3.3)$$

Following ASTM guidelines, this value should be within ± 10 percent of unity. Actual values fell well within the ASTM criteria and generally were within $\pm$ 3 percent. The correction ratio was considered constant thereafter, thus allowing an effective CEBt to be calculated from the observed CEB at each load point by

$$CEBt = CEB * CEB\ ratio \qquad (A.3.4)$$

Equation (A.3.2) can then be solved for the quartic root h/a corresponding to the effective CEBt value calculated using equation (A.3.4) to attain a_{eff} for a given load and deflection. By taking each effective crack length and subtracting the precrack we can attain a value for the change in effective crack length (Δa_{eff}). The stress intensity factor may be calculated at a_{eff} using Equation (5.3.3.1.1).

A.4 Mechanical Joint Specimen Drawings

(See following pages)

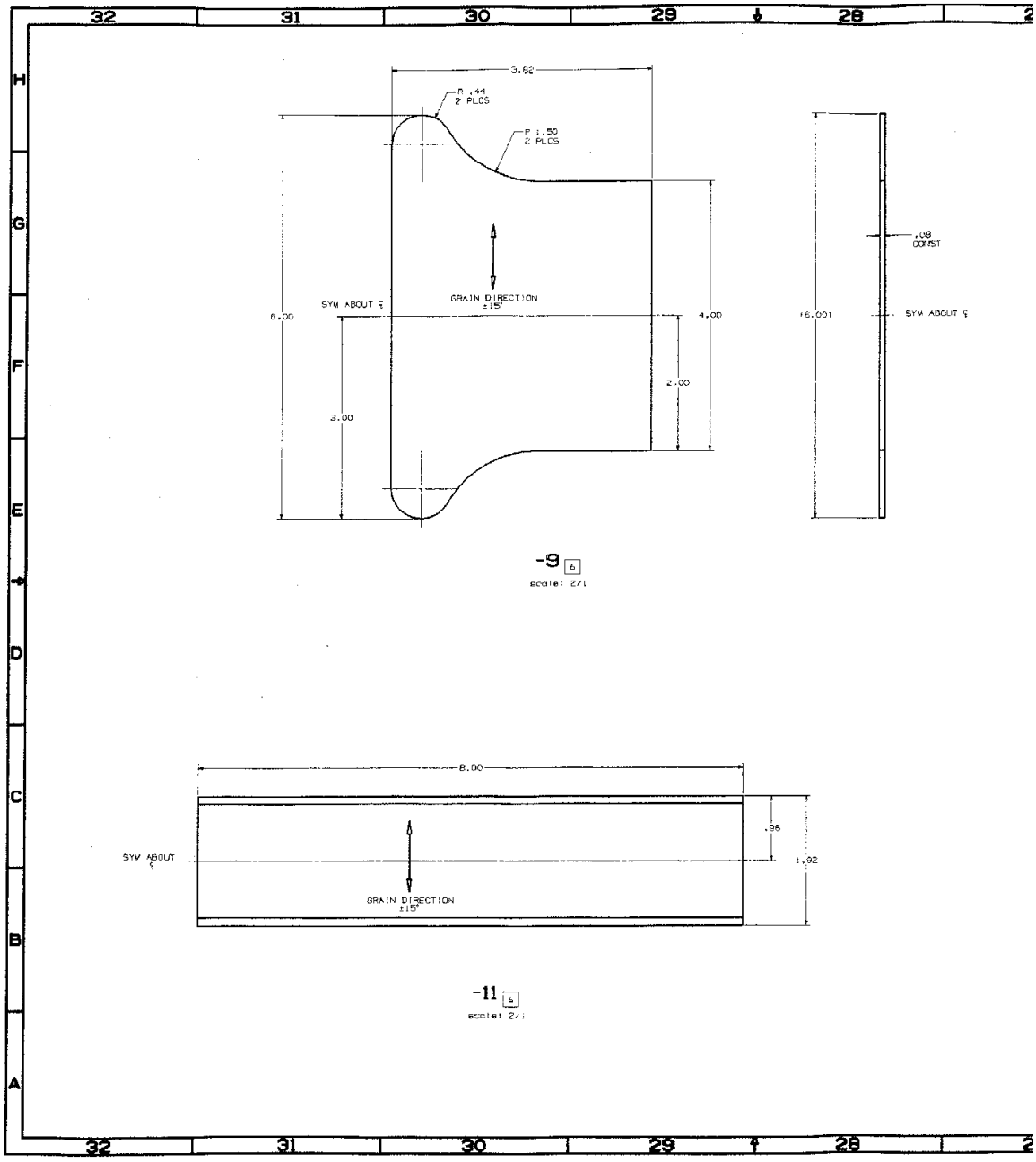
32
31
30
29
28
H
G
F
E
D
C
B
A
3.62
R .44
2 PLCS
R 1.50
2 PLCS
GRAIN DIRECTION
±15°
SYM ABOUT ℄
6.00
4.00
2.00
3.00
.08
CONST
16.001
SYM ABOUT ℄
-9 6
scale: 2/1
8.00
.08
1.92
SYM ABOUT ℄
GRAIN DIRECTION
±15°
-11 6
scale 2/1

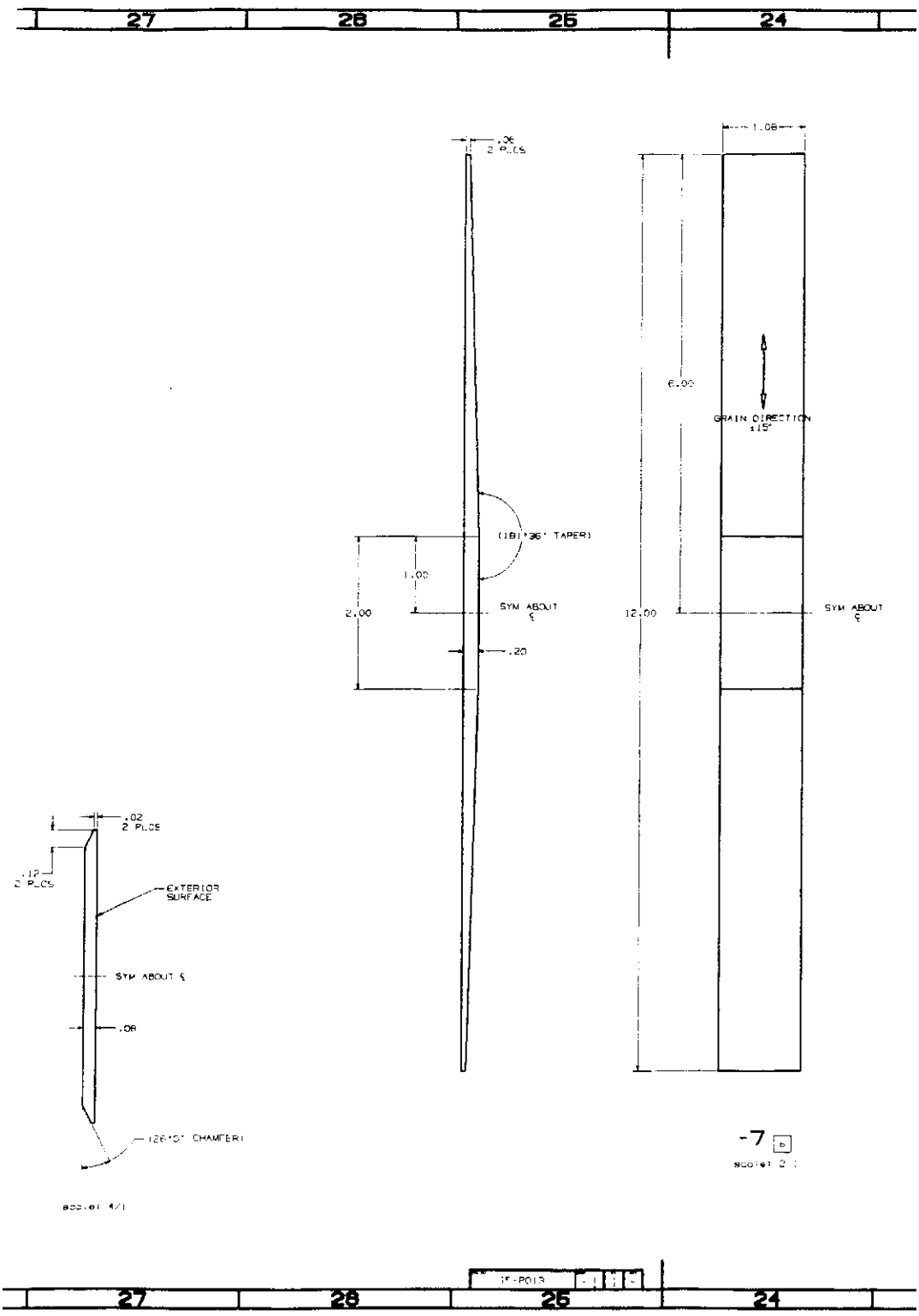
27
26
25
24
.06
2 PLCS
1.08
6.00
GRAIN DIRECTION
±15°
(18) 36° TAPER
1.00
2.00
SYM ABOUT
℄
.20
12.00
SYM ABOUT
℄
.02
2 PLCS
.12
2 PLCS
EXTERIOR
SURFACE
SYM ABOUT ℄
.08
(26) 10° CHAMFER
-7
b
27
26
25
24

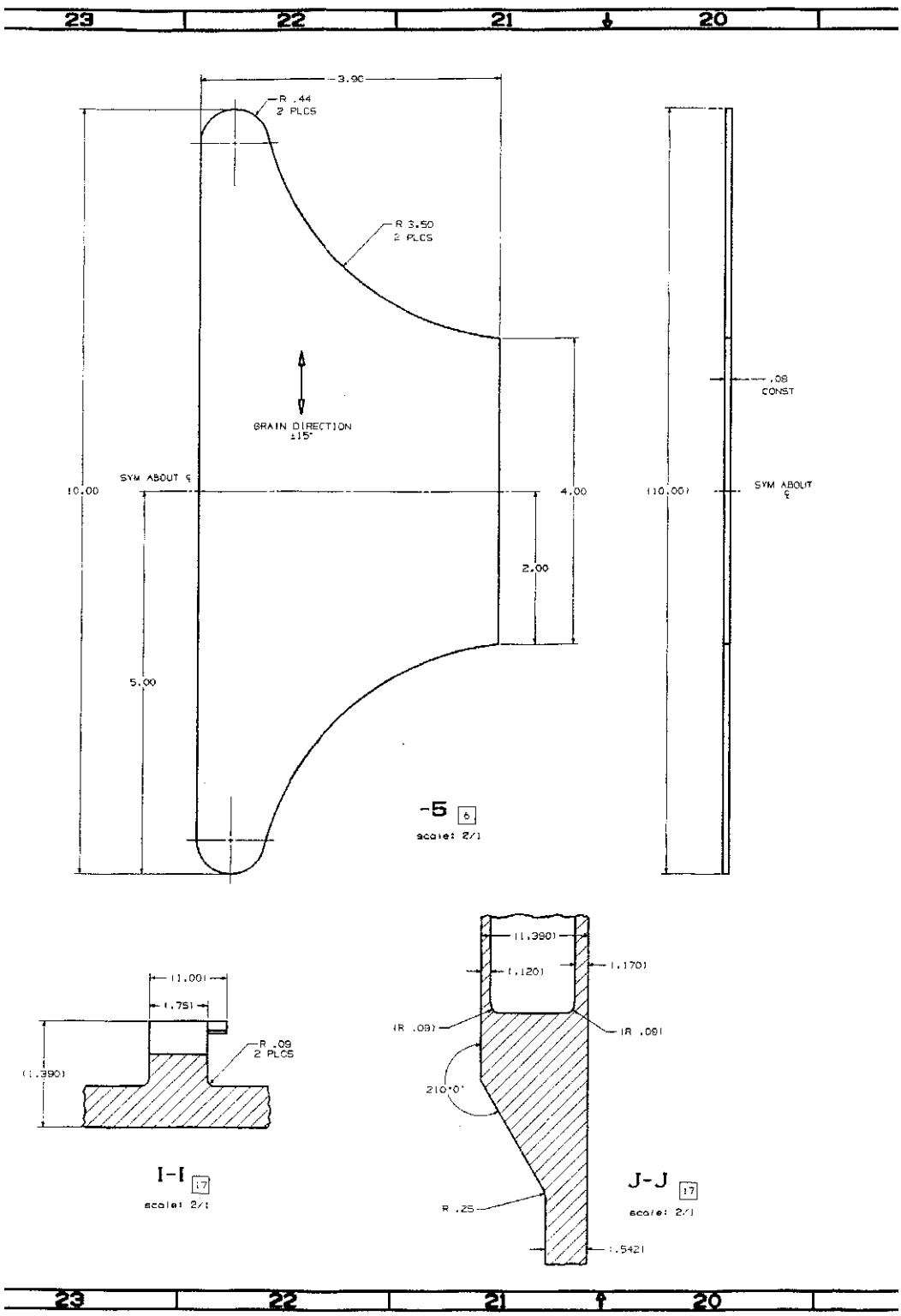
23
22
21
20
3.90
R .44
2 PLCS
R 3.50
2 PLCS
GRAIN DIRECTION
±15°
SYM ABOUT ℄
10.00
4.00
2.00
5.00
.08
CONST
(10.00)
SYM ABOUT
℄
-5 6
scale: 2/1
(1.000)
(.75)
R .09
2 PLCS
(1.390)
I-I 17
scale: 2/1
(1.390)
(.120)
(1.170)
(R .09)
(R .09)
210°0'
R .25
(.542)
J-J 17
scale: 2/1
23
22
21
20

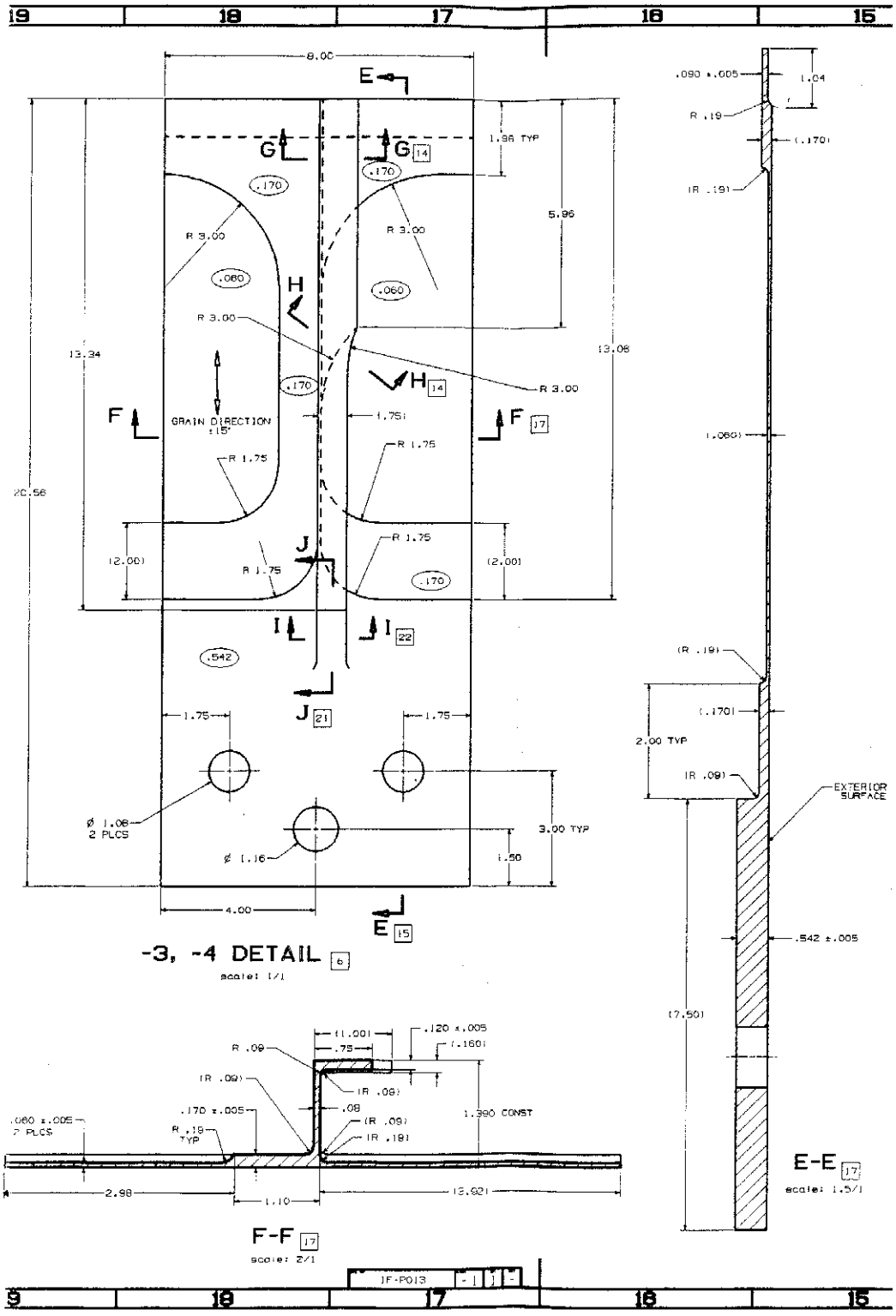
19
18
17
16
15
8.00
E
G
G 14
.170
1.96 TYP
5.96
R 3.00
.060
H
H 14
13.34
13.08
F
GRAIN DIRECTION ±15°
F 17
R 1.75
20.56
(2.00)
J
I
I 22
.542
J 21
1.75
ø 1.08
2 PLCS
3.00 TYP
1.50
4.00
E 15
-3, -4 DETAIL 6
scale: 1/1
.090 ±.005
1.04
R .19
(.170)
(R .19)
(.060)
(R .19)
(.170)
2.00 TYP
(R .09)
EXTERIOR SURFACE
.542 ±.005
(7.50)
E-E 17
scale: 1.5/1
(1.00)
.75
.120 ±.005
(.160)
R .09
(R .09)
(R .09)
.09
(R .09)
(R .18)
1.390 CONST
.060 ±.005
2 PLCS
.170 ±.005
R .18
TYP
2.98
1.10
12.92
F-F 17
scale: 2/1
JF-P013

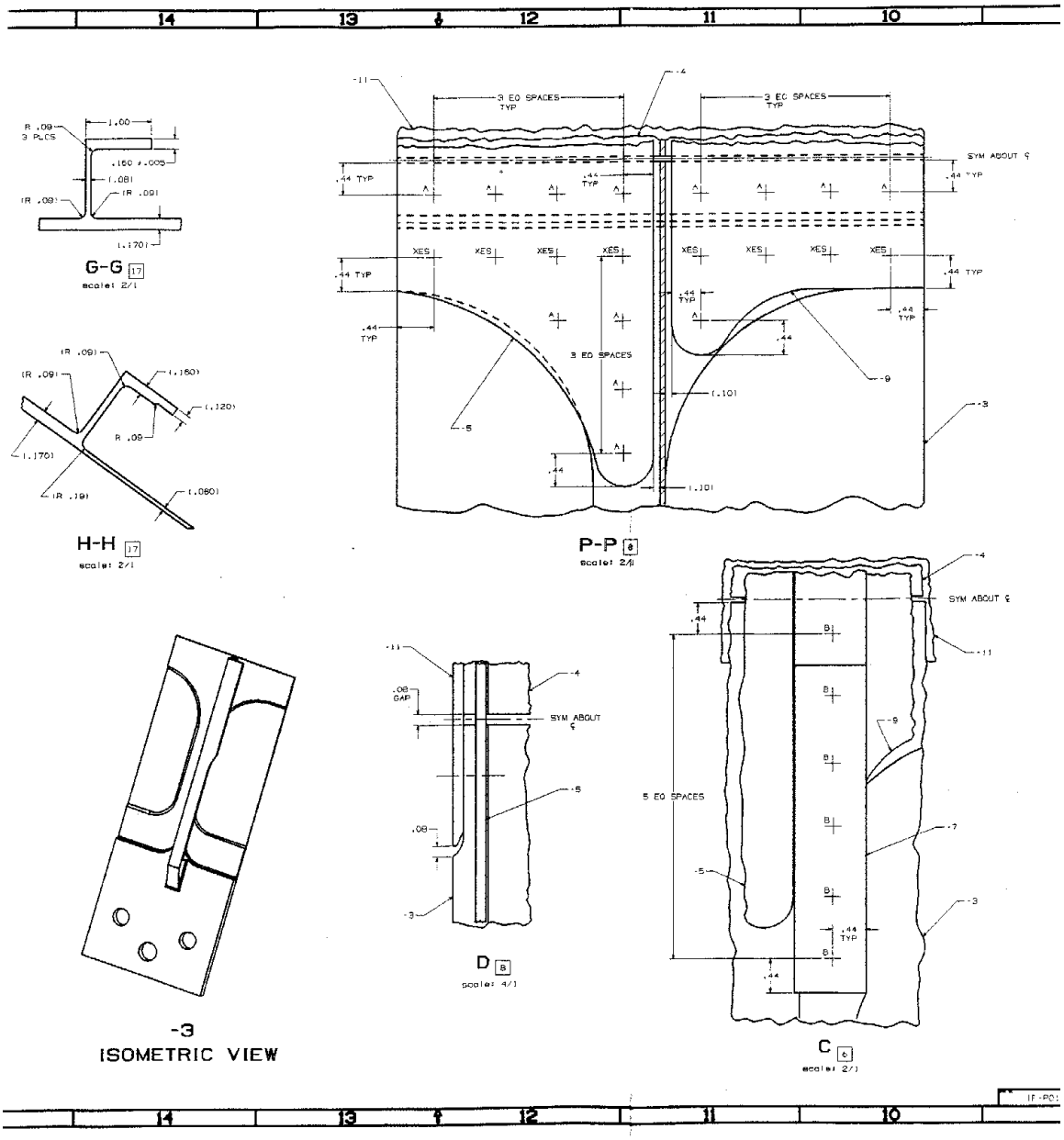
14
13
12
11
10
G-G 17
scale 2/1
H-H 17
scale 2/1
P-P 8
scale 2/1
D 8
scale 4/1
C 6
scale 2/1
-3
ISOMETRIC VIEW
3 EQ SPACES TYP
SYM ABOUT ℄
.44 TYP
XES
5 EQ SPACES
.08 GAP

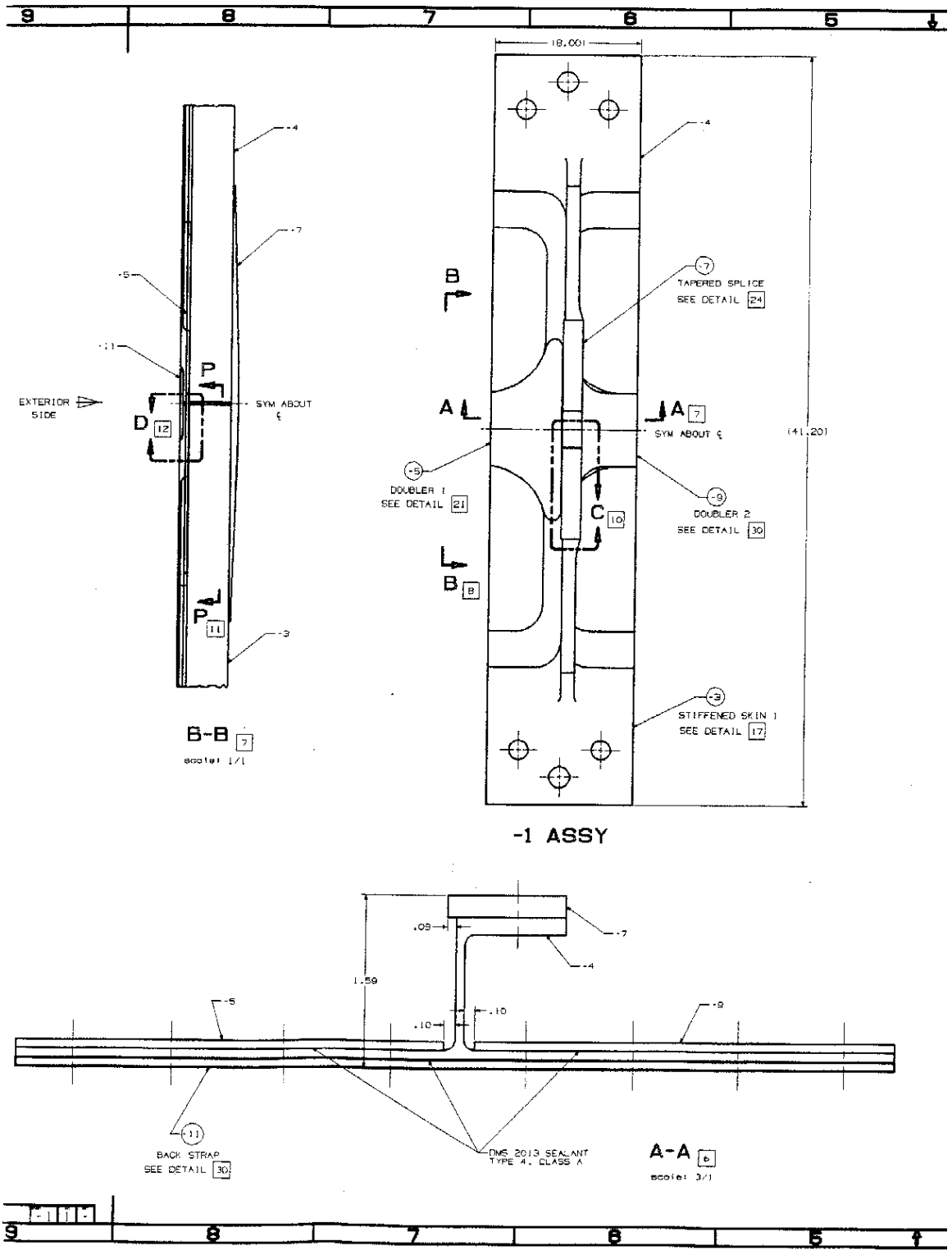
9
8
7
6
5
18.001
-4
-7
-5
-11
P
EXTERIOR SIDE
SYM ABOUT ℄
D 12
P 11
-3
B-B 7
scale: 1/1
B
A
A 7
SYM ABOUT ℄
(41.20)
-7
TAPERED SPLICE
SEE DETAIL 24
-5
DOUBLER 1
SEE DETAIL 21
C 10
-9
DOUBLER 2
SEE DETAIL 30
B 8
-3
STIFFENED SKIN 1
SEE DETAIL 17
-1 ASSY
.09
1.59
.10
.10
-11
BACK STRAP
SEE DETAIL 30
DMS 2013 SEALANT
TYPE 4, CLASS A
A-A 6
scale: 3/1

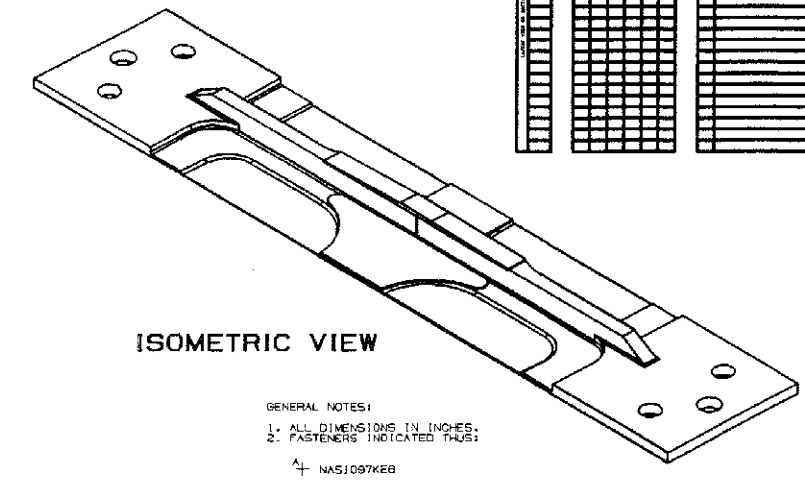

ISOMETRIC VIEW

GENERAL NOTES:

1. ALL DIMENSIONS IN INCHES.
2. FASTENERS INDICATED THUS:

   A — NAS1097KE8

   B — MS20470E6

   XES — S4931919

3. SURFACE FINISH 125√ RMS PER ANSI B46.1.
4. ALL SPECIMEN SURFACES SHALL BE FREE OF NICKS AND SCRATCHES.
5. FR PRIME PER DPS 4.50-36. DO NOT PRIME EXTERIOR SURFACES OF -3, -4, AND -11.
6. INSTALL FASTENERS PER DPS 2.50.
7. APPLY SEALANT ON FAYING SURFACES PER DMS 2.30 AS NOTED.
8. ⬭ ENCLOSED VALUE INDICATES THICKNESS.
9. MAX MISMATCH OF CUTS .015
10. CC COAT ALL DETAIL PARTS PER DPS 9.45.
11. BREAK ALL SHARP EDGES TO .03 MAX EDGE RADII PER DPS 4.710-1.

QUANTITY PER DASH NUMBER	PART ID NUMBER	NOMENCLATURE	STOCK SIZE	MATERIAL DESCRIPTION	MATERIAL SPECIFICATION (OR SUPPLIER)	ZONE
DRAWING PARTS LIST						
AR	NAS1252-10L	WASHER		7075-T6	QQ-A-283 TEMP T6	
AR	MS21042L3	NUT		STEEL	MIL-N-25027	
AR	S4931918-8-5	PIN		TI-6AL-4V	AMS4967	
AR	DMS 2013	SEALANT				
AR	MS20470E6	RIVET				
AR	NAS1097KE8	RIVET				
1	-11	BACK STRAP	0.08 X 3.0 X 9.0	7075-T6		B30
1	-9	DOUBLER 2	0.08 X 5.0 X 7.0	7075-T6		E30
1	-7	TAPERED SPLICE	0.20 X 2.0 X 13.0	7075-T6		B24
1	-5	DOUBLER 1	0.08 X 5.0 X 11.0	7075-T6		D22
1	-4	STIFFENED SKIN 2	1.50 X 8.5 X 22.0	7050-T7451		C17
1	-3	STIFFENED SKIN 1	1.50 X 8.5 X 22.0	7050-T7451		C17

NAS1-20014

TRANSVERSE JOINT SPECIMEN

EPD DRAWING

J 88277 IF-P013 -1

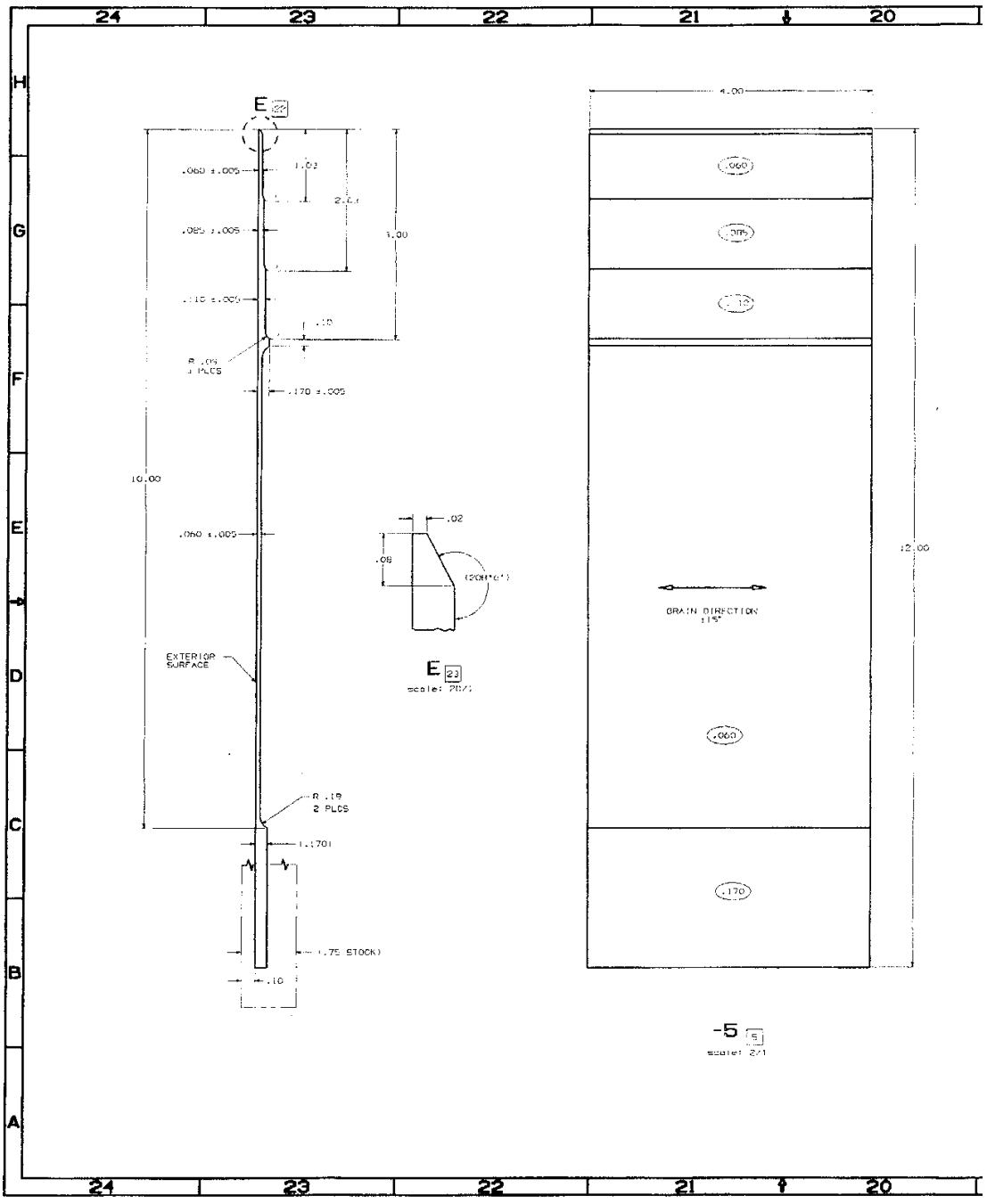
24
23
22
21
20
H
G
F
E
D
C
B
A
E 22
.060 ±.005
.085 ±.005
.110 ±.005
.170 ±.005
1.00
.10
R .05
3 PLCS
10.00
EXTERIOR SURFACE
R .18
2 PLCS
1.1701
1.75 STOCK)
.10
.02
.08
(208°C)
E 23
scale: 2/1
4.00
12.00
.060
.085
.110
.060
.170
GRAIN DIRECTION
±15°
-5 5
scale: 2/1

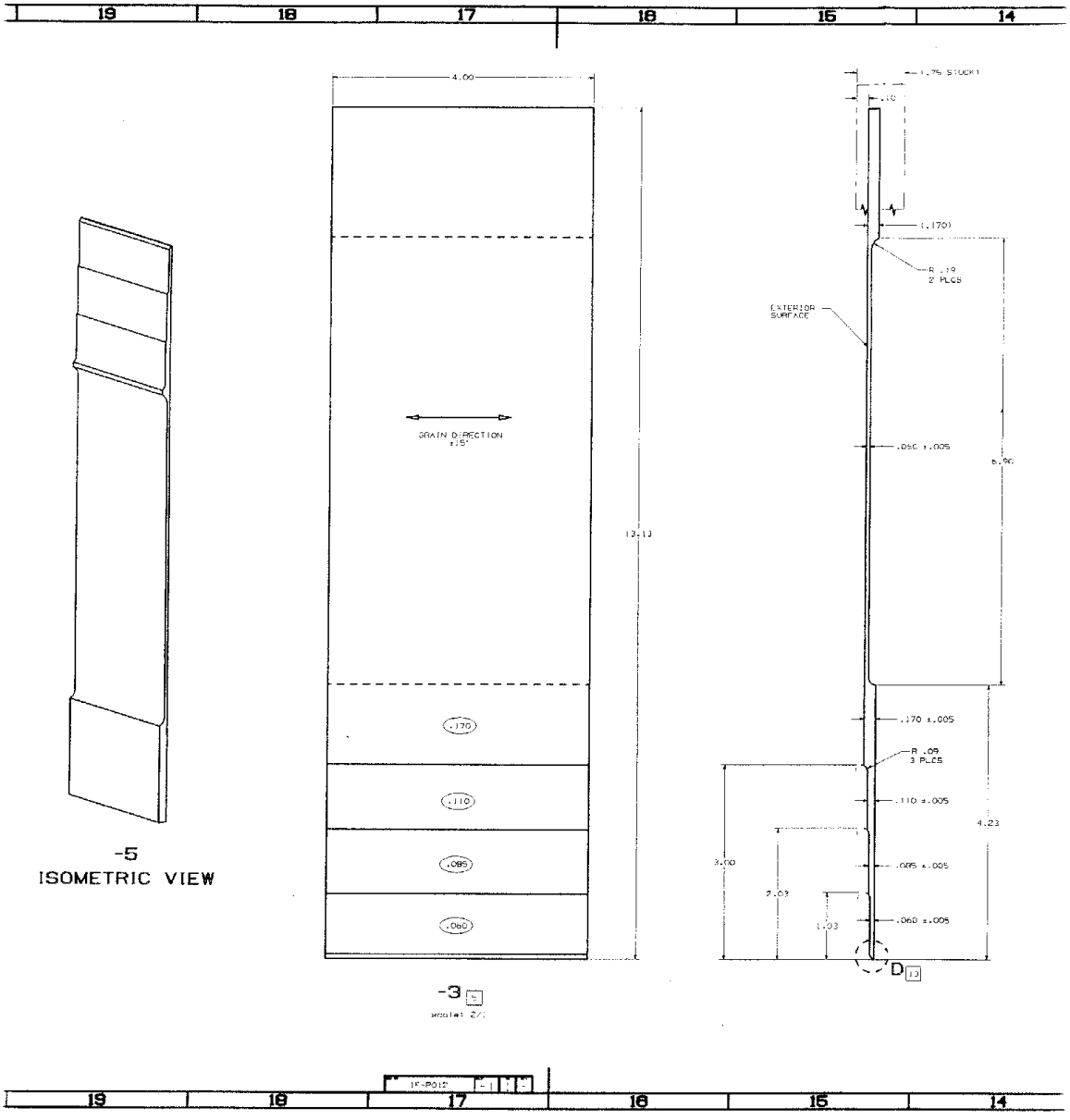
19
18
17
16
15
14
4.00
13.13
GRAIN DIRECTION
.170
.110
.085
.060
1.75 STOCK
.110
(.170)
R .19
2 PLCS
EXTERIOR
SURFACE
.060 ±.005
6.90
.170 ±.005
R .09
3 PLCS
.110 ±.005
4.23
3.00
2.03
1.03
.085 ±.005
.060 ±.005
D
-5
ISOMETRIC VIEW
-3

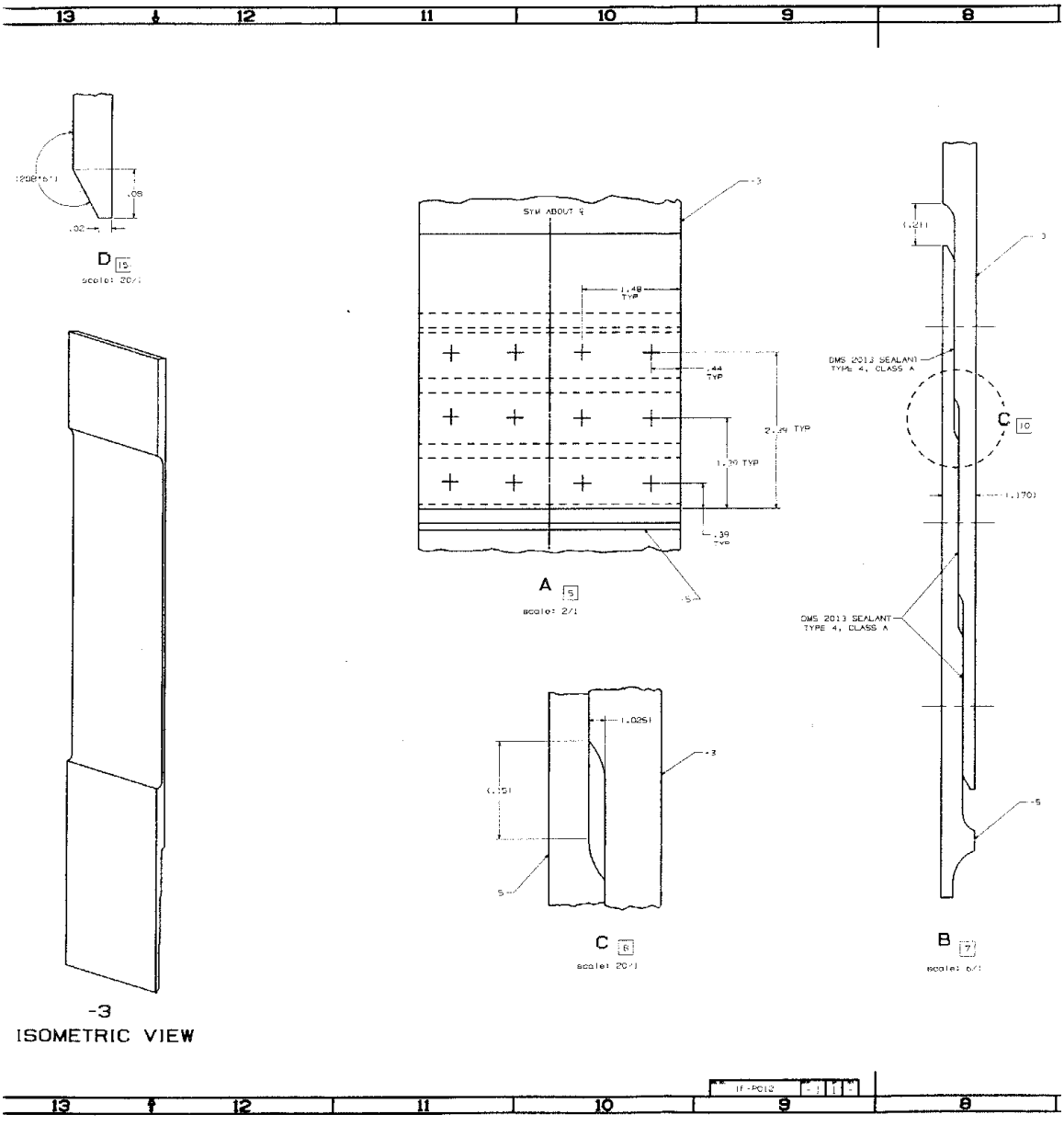
13
12
11
10
9
8
.08
.02
D
scale: 20/1
SYM ABOUT ℄
1.48 TYP
.44 TYP
2.64 TYP
1.32 TYP
.39 TYP
A
scale: 2/1
DMS 2013 SEALANT TYPE 4, CLASS A
C
DMS 2013 SEALANT TYPE 4, CLASS A
B
scale: 6/1
1.025
C
scale: 20/1
-3
ISOMETRIC VIEW

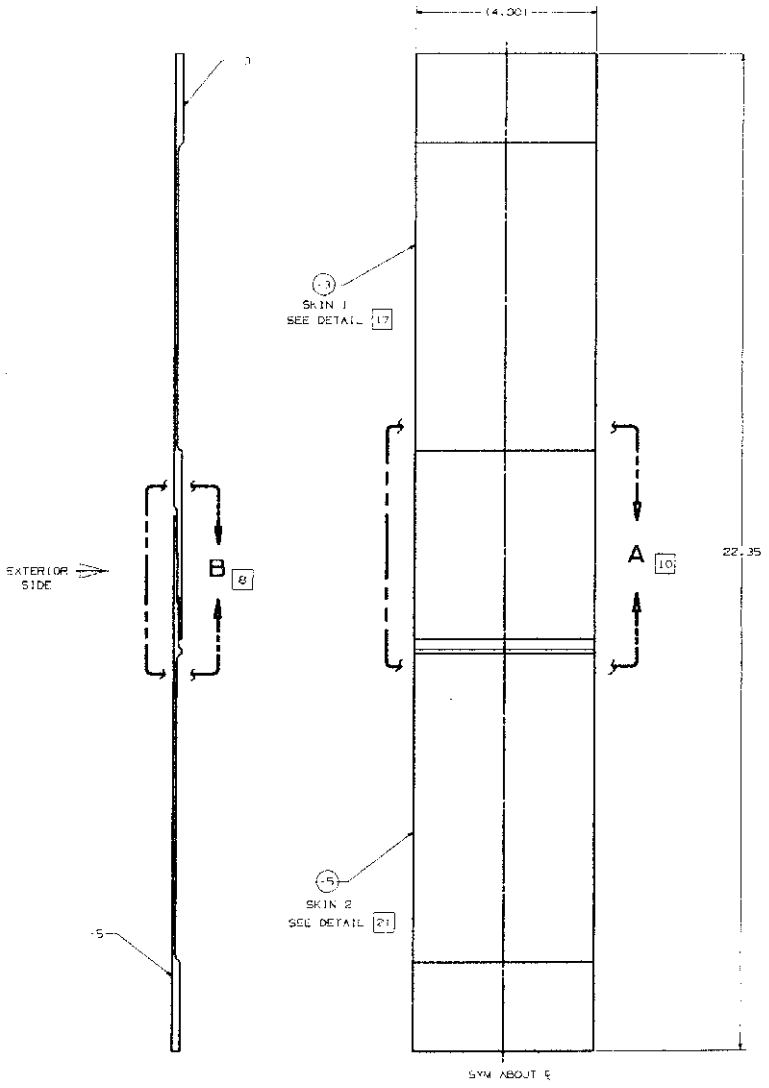
(4.00)
-3
SKIN 1
SEE DETAIL 17
EXTERIOR
SIDE
B 8
A 10
22.35
-5
SKIN 2
SEE DETAIL 21
SYM ABOUT ℄

-1 ASSY

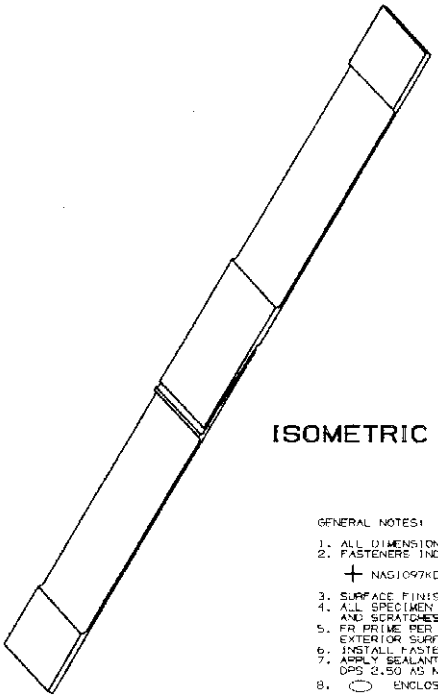

ISOMETRIC VIEW

GENERAL NOTES:

1. ALL DIMENSIONS IN INCHES.
2. FASTENERS INDICATED THUS:
   + NAS1097KD6 RIVET
3. SURFACE FINISH 125√ RMS PER ANSI B46.1.
4. ALL SPECIMEN SURFACES SHALL BE FREE OF NICKS AND SCRATCHES.
5. FR PRIME PER DPS 4.50-36. DO NOT PRIME EXTERIOR SURFACES OF -3 AND -5.
6. INSTALL FASTENERS PER DPS 2.50.
7. APPLY SEALANT ON FAYING SURFACES PER DPS 2.50 AS NOTED.
8. ⬭ ENCLOSED VALUE INDICATES THICKNESS.
9. CC COAT ALL DETAIL PARTS PER DPS 9.45.
10. BREAK ALL SHARP EDGES TO .03 MAX EDGE RADII PER DPS 4.710-J.

QUANTITY PER DASH NUMBER	PART ID NUMBER	NOMENCLATURE	STOCK SIZE	MATERIAL DESCRIPTION	MATERIAL SPECIFICATION (OR SUPPLIER)	ZONE
	DRAWING PARTS LIST					
- 1						
1	-5	SKIN 2	0.75 X 5.00 X 15.80	7050-T7451		
1	-3	SKIN 1	0.75 X 5.00 X 15.80	7050-T7451		
AR	NAS1097KE6	RIVET				
AR	DMS 2013	SEALANT				

NAS1-20014

LONGITUDINAL JOINT SPECIMEN

SPEC DRAWING

J 88277 1F-P012 -1

REPORT DOCUMENTATION PAGE

Form Approved
OMB No. 0704-0188

1. AGENCY USE ONLY *(Leave blank)*	2. REPORT DATE	3. REPORT TYPE AND DATES COVERED
	May 2000	Contractor Report

4. TITLE AND SUBTITLE
Validated Feasibility Study of Integrally Stiffened Metallic Fuselage Panels for Reducing Manufacturing Costs

5. FUNDING NUMBERS
C NAS1-20014, Task 34

522-12-51-01

6. AUTHOR(S)
R. G. Pettit, J. J. Wang, and C. Toh

7. PERFORMING ORGANIZATION NAME(S) AND ADDRESS(ES)
The Boeing Company
2401 E. Wardlow Road
Long Beach, CA 90807-5309

8. PERFORMING ORGANIZATION REPORT NUMBER

9. SPONSORING/MONITORING AGENCY NAME(S) AND ADDRESS(ES)
National Aeronautics and Space Administration
Langley Research Center
Hampton, VA 23681-2199

10. SPONSORING/MONITORING AGENCY REPORT NUMBER
NASA/CR-2000-209342

11. SUPPLEMENTARY NOTES
Langley Technical Monitor: Marcia S. Domack
Final Report

12a. DISTRIBUTION/AVAILABILITY STATEMENT
Unclassified–Unlimited
Subject Category 26 Distribution: Standard
Availability: NASA CASI (301) 621-0390

12b. DISTRIBUTION CODE

13. ABSTRACT ***(Maximum 200 words)***

The continual need to reduce airframe cost and the emergence of high speed machining and other manufacturing technologies has brought about a renewed interest in large-scale integral structures for aircraft applications. Applications have been inhibited, however, because of the need to demonstrate damage tolerance, and by cost and manufacturing risks associated with the size and complexity of the parts. The Integral Airframe Structures (IAS) Program identified a feasible integrally stiffened fuselage concept and evaluated performance and manufacturing cost compared to conventional designs. An integral skin/stiffener concept was produced both by plate hog-out and near-net extrusion. Alloys evaluated included 7050-T7451 plate, 7050-T74511 extrusion, 6013-T6511 extrusion, and 7475-T7351 plate. Mechanical properties, structural details, and joint performance were evaluated as well as repair, static compression, and two-bay crack residual strength panels. Crack turning behavior was characterized through panel tests and improved methods for predicting crack turning were developed. Manufacturing cost was evaluated using COSTRAN. A hybrid design, made from high-speed machined extruded frames that are mechanically fastened to high-speed machined plate skin/stringer panels, was identified as the most cost-effective manufacturing solution. Recurring labor and material costs of the hybrid design are up to 61 percent less than the current technology baseline.

14. SUBJECT TERMS
Integrally stiffened structure; Damage tolerance; Cost analysis; Crack turning; Extrusion; Manufacturing technology

15. NUMBER OF PAGES
132

16. PRICE CODE
A07

17. SECURITY CLASSIFICATION OF REPORT	18. SECURITY CLASSIFICATION OF THIS PAGE	19. SECURITY CLASSIFICATION OF ABSTRACT	20. LIMITATION OF ABSTRACT
Unclassified	Unclassified	Unclassified	UL